Interplay of DNA replication, repair and chromatin under radiation stress

Zusammenspiel von DNA Replikation, Reparatur und Chromatin unter Stress durch Bestrahlung

Dem Fachbereich Biologie der Technischen Universität Darmstadt zur Erlangung des akademischen Grades eines Doctor rerum naturalium vorgelegte Dissertation von

M.Sc. Annina Scholl aus Hardheim

1. Gutachten: Prof. Dr. M. Cristina Cardoso
2. Gutachten: Prof. Dr. Bodo Laube

Interplay of DNA replication, repair and chromatin under radiation stress

Vom Fachbereich Biologie der Technischen Universität Darmstadt

zur

Erlangung des akademischen Grades

eines Doctor rerum naturalium

genehmigte

Dissertation von

M.Sc. Annina Scholl

aus Hardheim

1. Referent/ Referentin: Prof. Dr. M. Cristina Cardoso

2. Referent/Referentin: Prof. Dr. Bodo Laube

Tag der Einreichung: 15.05.2017

Tag der mündlichen Prüfung: 12.07.2017

Darmstadt 2017

D 17

Ehrenwörtliche Erklärung:

Ich erkläre hiermit ehrenwörtlich, dass ich die vorliegende Arbeit entsprechend den Regeln guter wissenschaftlicher Praxis selbstständig und ohne unzulässige Hilfe Dritter angefertigt habe.

Sämtliche aus fremden Quellen direkt oder indirekt übernommenen Gedanken sowie sämtliche von Anderen direkt oder indirekt übernommenen Daten, Techniken und Materialien sind als solche kenntlich gemacht. Die Arbeit wurde bisher bei keiner anderen Hochschule zu Prüfungszwecken eingereicht.

Darmstadt, den

.....
Annina Scholl

Contents

1. Summary

The human genome contains around 1.2% protein coding sequences and over 50% repetitive elements. Within the nucleus, it is packed together with proteins and RNAs and is highly organized as chromatin. The lowest organization level is the DNA double helix wrapped around the core histones to form the nucleosome, multiple nucleosomes form the beads on a string. Higher order chromatin structures on the Mbp range have been termed the 1 Mbp domain or topologically associated domains (TADs), but what lies in between the beads on a string and the higher order structures is not fully understood. DNA maintenance processes like DNA replication and repair are dictated by many features of chromatin organization, including structural organization, compaction level and epigenetics. DNA replication and repair structures, such as the phosphorylated form of the histone variant H2AX, have been associated with forms of structural chromatin organization. In the first part of the thesis, DNA replication and repair were utilized to identify a possible basic unit of structural chromatin organization using super-resolution microscopy. Therefore, single replicons were labeled by nucleotide incorporation and the cells irradiated with X-ray radiation and stained for γH2AX. Both replicons and repair (nano)foci are compared, considering their DNA content, size and localization. Despite their independent distribution and the accompanied low probability of colocalization we were able to identify a surprisingly high number of colocalizing replicons and repair (nano)foci. These were assumed to be most comparable, since they are likely localized on the same chromatin structure. Direct comparison revealed that the majority of foci exhibited an astonishing similarity, suggesting that replicons and repair (nano)foci might indeed be based on the same basic unit of chromatin structure. This chromatin structure shows sizes between 27.5-91.2 kbp for human and 61.6-118.6 kbp for murine cells. With a possible formation of chromatin loops, this structure can be ranked between the beads on a string and higher order chromatin structures like TADs or the 1 Mbp domain. The sizes are consistent with microscopy based data (40-160 kbp) and comparable to Hi-C data (185 kbp) of chromatin structures.

Repetitive elements can be divided into interspersed elements, like the Alu and LINE1 elements, and tandemly repeated DNA like satellite III. While Alu is associated with euchromatin, LINE1 and satellite III are (predominantly) heterochromatic, with satellite III being located in pericentromeric heterochromatin. The second part of the thesis focusses on the replication timing and repair kinetics of these elements. Alu is replicated during early S-phase as expected for a euchromatic element, LINE1 is replicated throughout S-phase, with the majority at the early to mid S-phase transition, while satellite III is replicated exclusively during the mid to late S-phase transition. The repair kinetics of Alu and LINE1 were similar to global DNA repair kinetics, while damage in satellite III persists longer. All of this is compatible with replication and repair kinetics of the respective chromatin types and suggests that repetitive elements are well integrated into the genome, despite their reputation as “junk” DNA.

2. Zusammenfassung

Das menschliche Genom besteht zu ca. 1,2% aus Protein-codierenden Sequenzen und zu mehr als 50% aus repetitiven Elementen. Innerhalb des Nukleus ist DNA dicht verpackt mit Proteinen und RNAs und als Chromatin hoch organisiert. Das unterste Organisationslevel ist die DNA Doppelhelix, die sich um ein Histon-Oktamer wickelt und das Nukleosom bildet. Mehrere aneinander gekettete Nukleosomen bilden eine Art Perlenschnur, die *beads on a string*. Höhere Formen von Chromatin-Struktur wurden beschrieben als 1 Mbp Domäne oder Kontakt-Domänen (TADs) in der Größenordnung von Mbp, aber was zwischen den *beads on a string* und der 1 Mbp Domäne oder TADs liegt ist bis heute nicht vollständig klar. DNA Replikation und DNA Reparatur werden durch z. B. Chromatin-Organisation, Verdichtung und Epigenetik reguliert. Außerdem wurden Strukturen beider Prozesse, z. B. die phosphorylierte Form der Histon-Variante H2AX, in Verbindung mit struktureller Chromatin-Organisation gebracht. Im ersten Teil dieser Thesis werden Replikation und Reparatur genutzt um eine gemeinsame mögliche Grundeinheit der Chromatin-Struktur zu identifizieren. Dazu wurden einzelne Replikons durch Nukleotid-Inkorporation markiert und Zellen bestrahlt um γH2AX zu färben. Trotz ihrer unabhängigen Verteilung und der damit verbundenen geringen Co-lokalisations-Wahrscheinlichkeit waren wir dazu in der Lage eine überraschend hohe Anzahl co-lokalisierender Foci zu identifizieren. Diese sollten am besten miteinander vergleichbar sein, da sie wahrscheinlich auf der gleichen Chromatin-Struktur positioniert sind. Im direkten Vergleich sind sich der größte Teil an Replikons und Reparatur (Nano)Foci erstaunlich ähnlich, was darauf hindeutet, dass beide scheinbar wirklich auf der selben Grundeinheit der Chromatin-Organisation basieren. Diese Grundeinheit hat eine Größe von 27,5-91,2 kbp für menschliche und 61,6-118,6 kbp für murine Zellen, ist möglicherweise in Form von Schlaufen (*loops*) organisiert und ist zwischen den *beads on a string* und der 1 Mbp Domäne bzw. TADs anzusiedeln. Die Größen sind konsistent mit bereits beschriebenen Mikroskopie-basierenden (40-160 kbp) und vergleichbar mit Hi-C-basierenden Daten (185 kbp).

Repetitive Elemente können in eingestreute (*interspersed*), wie Alu und LINE1 Elemente, und hintereinander-wiederholte Elemente (*tandem repeats*), wie Satellit III, unterteilt werden. Alu ist euchromatisch, LINE1 und Satellit III (mehrheitlich) heterochromatisch, wobei es sich bei Satellit III um perizentrisches Heterochromatin handelt. Im zweiten Teil dieser Arbeit wird der Replikations-Zeitpunkt und die Reparatur-Kinetik dieser Elemente untersucht. Alu wird während der frühen, LINE1 während der gesamten S-phase repliziert, wobei der Großteil im Übergang zwischen früher und mittlerer S-phase repliziert wird. Satellit III wird ausschließlich im Übergang zwischen mittlerer und später S-phase repliziert. Die Reparatur-Kinetiken von Alu und LINE1 sind der globalen Reparatur-Kinetik ähnlich, während Schäden in Satellit III länger bestehen bleiben. Diese Beobachtungen sind vereinbar mit denen für die entsprechenden Chromatin-Typen, was darauf hindeutet, dass repetitive Elemente, trotz ihrem Ruf als „Schrott-DNA“, gut in das Genom integriert sind.

3. Preface

This thesis will address how chromatin organization influences processes like DNA replication and DNA repair. For this, two separate projects were designed, the first one focusses on structural chromatin organization based on replication and repair whereas the second one is about replication and repair kinetics of repetitive elements, a major feature of the human genome. Therefore, there is a general introduction about the common aspects, before the two projects are addressed separately. Each of the two parts has an additional introduction, that aims to provide all information necessary for the understanding of the individual projects. Each project will be discussed in its own chapter before a general conclusion and outlook is given at the end of this thesis.

4. General introduction

4.1. Chromatin organization

Genetic material, the DNA, is not naked within the cell nucleus. In fact, it is packed with proteins and RNA, forming what is referred to as chromatin. Chromatin is folded in different organizational levels beginning with the DNA double helix wrapped around the core histones forming the nucleosome. Each nucleosome contains 8 histones, 2 copies of H2A, H2B, H3 and H4 plus ~147 base pairs (bp) of DNA (Luger et al., 1997). Multiple nucleosomes with linker DNA in between form the "beads on a string" structure, also referred to as the first order structure or 11 nm fiber. The linker histone H1, which is not part of the nucleosome core particle, stabilizes the nucleosomes and the 11 nm fiber is assumed to be further packed into the controversial 30 nm fiber. How exactly chromatin is folded to form the 30 nm fiber is unclear. There have been suggestions for different chromatin conformations and H1 seems to play an important role (Li and Zhu, 2015). It is also possible that several conformations might exist simultaneously within a cell, reflecting different chromatin compaction levels in presence or absence of H1 (Li and Reinberg, 2011). Chromatin folding beyond the 30 nm fiber seems highly variable. Contact domains for example between promoters and transcriptional enhancers have been described to form chromatin loops of sizes ranging from a few kbp and several Mbp. These contacts can be mediated by architectural proteins such as cohesin or the CCCTC-binding factor CTCF (Tark-Dame et al., 2011). However, chromatin loop organization remains elusive. The highest organization level of chromatin is reached in the form of highly condensed metaphase chromosomes. Every chromosome exhibits different characteristics such as size, symmetry and banding patterns. The banding patterns can be visualized by different methods such as Giemsa staining, resulting in a "striped" pattern on chromosomes (G-banding, Francke, 1994). Staining of some repetitive elements such as LINEs and SINEs also results in banding patterns individual for all chromosomes (Korenberg and Rykowski, 1988). The organization of chromosomes is dependent on the cell cycle phase, as chromatin is compacted into what is observed as "metaphase chromosomes" only for mitosis. During interphase, chromatin is less condensed but still spatially organized as chromosomes are restricted to certain volumes within the nucleus – the chromosome territories (Bolzer et al., 2005, Cremer and Cremer, 2010).

Chromatin can be subdivided into eu- and heterochromatin. While euchromatin is in general transcriptionally active chromatin, which is regularly transcribed, heterochromatin is largely inactive. Heterochromatin can be subdivided into facultative and constitutive heterochromatin. Facultative heterochromatin contains genes that need to be inactivated during development, and is therefore cell type specific (Trojer and Reinberg, 2007).

Structural organization of chromatin and epigenetic marks, such as DNA methylation, histone methylation or acetylation, mainly of histones H3 and H4, are closely related and influence chromatin

function. DNA methylation, tri-methylation of H3K27 and H3K9 are silencing marks and associated with heterochromatin, H3K27me3 however is a feature of facultative heterochromatin, such as the inactive X chromosome (Lachner et al., 2003, Plath et al., 2003, Silva et al., 2003). H3/H4 acetylation and H3K4me3 are linked to active gene expression and are therefore associated with euchromatin (Berger, 2007, Santos-Rosa et al., 2002). Additionally, epigenetic marks are also able to influence chromatin compaction for example by recruitment of chromatin remodeling factors (Bannister and Kouzarides, 2011).

4.2. DNA replication

Every time a cell divides, it is essential that all genetic material (DNA) is completely, correctly and only once duplicated. This process of duplication is called DNA replication and takes place during the S-phase of the cell cycle. It is a highly organized process involving many factors and demanding precise coordination.

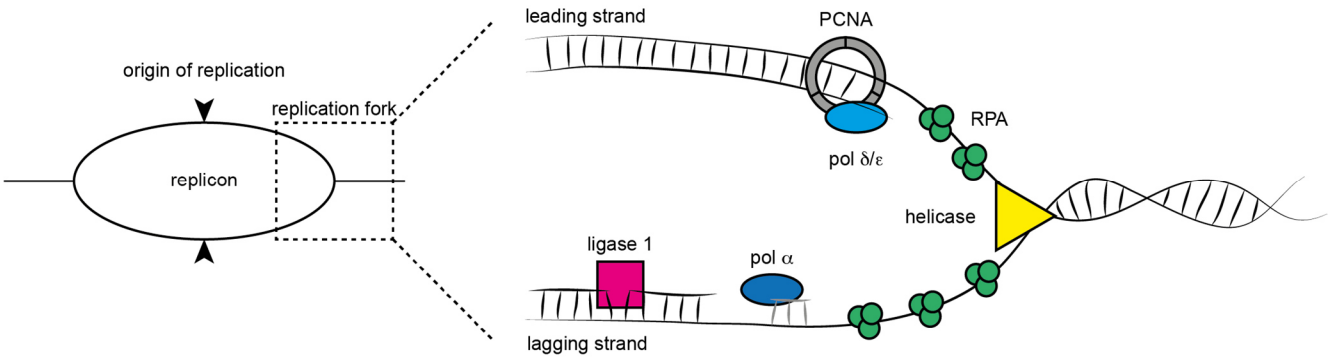

Figure 1: Definition of commonly used DNA replication terms and scheme of a replication fork with the DNA replication machinery.

DNA replication begins at so called origins of replication. Starting from each origin two replication forks progress in a bidirectional manner (Huberman and Riggs, 1968), their replication machineries (replisomes) duplicate a section of DNA (replicon). In bacteria, origins can be mapped and characterized as they are well defined by sequence motives (Meijer et al., 1979, Fuller et al., 1984). In eukaryotes replication origins are more elusive, especially in higher eukaryotes, the features of an origin are rather unclear (Gilbert, 2001, Robinson and Bell, 2005, Dellino et al., 2013). The replisome – on a molecular level - consists of a variety of factors, that are responsible for DNA replication. During the replication process itself (Figure 1), DNA needs to be unwound by a helicase (mini chromosome maintenance complex, MCM2-7, Bochman and Schwacha, 2009) and the single strand regions are covered by a single strand binding protein (replication protein A, RPA, Fanning et al., 2006) for stabilization and stimulation of further unwinding. A DNA polymerase (polymerase α, a primase) is then recruited to start DNA synthesis by producing RNA-DNA primers, polymerase α is later replaced by the more processive polymerase δ and ε (Hubscher et al., 2002). The proliferating cell nuclear

antigen (PCNA) serves as a loading platform for the polymerases to enhance their processivity (Jonsson and Hubscher, 1997). Synthesis on the leading strand can be performed continuously, while on the lagging strand further unwinding of the double helix takes place in the opposite direction of the polymerase activity. This leads to discontinuous synthesis and the generation of so called Okazaki fragments (Okazaki et al., 1968). These fragments are later ligated by a DNA ligase (DNA ligase 1, Howes and Tomkinson, 2012).

DNA replication can be followed *in vivo* by observing replication factors such as PCNA, coupled to a fluorescent protein (Leonhardt et al., 2000). In situ DNA replication can be visualized by immuno-detection of replication factors themselves or incubation of cells with thymidine analogues such as BrdU or EdU, which are then detected by antibodies or chemical reactions (Gratzner, 1982, Nakamura et al., 1986, Salic and Mitchison, 2008). Both ways result in the observation of replication patterns, which have a spatio-temporal chronology and are associated with different chromatin types. The first pattern, also referred to as early S-phase pattern, is characterized by a large number of foci distributed throughout the nucleus except the nucleoli and the nuclear periphery. During this S-phase stage mostly euchromatin is replicated. During mid S-phase facultative heterochromatin is replicated, which is located in the nuclear and nucleolar periphery whereas the late S-phase pattern is characterized by larger and fewer foci in the nucleus, that are associated with constitutive heterochromatin (Okeefe et al., 1992). The three replication patterns can be observed from cell cycle to cell cycle, in different cell types and in different species. Furthermore, replication sites, that are active during the S-phase of one cell cycle will, to some degree, maintain their replication timing in the following S-phase of the next cell cycle (Sadoni et al., 2004). Additionally new replication sites will appear close to previously active sites, suggesting the activation of neighboring origins in close proximity in a domino-like manner (Sporbert et al., 2002).

But how is replication timing coordinated? Many factors have been suggested to contribute to this process for example epigenetic composition, chromatin conformation and/or structural organization. It has been suggested that euchromatin is replicated first due to its more open structure and higher transcriptional activity, although the chromatin structure is probably more essential (Chagin et al., 2010; Donaldson, 2005). These features might provide easier access to the replication machinery, hence it is replicated early. In contrast, heterochromatin is more compact and less accessible to the replication machinery making it less likely that replication initiates in this chromatin type. Epigenetic marks have also been suggested to play a role in replication timing. As the epigenetic modifications seldom come alone and influence each other, it can be challenging to identify which one of them essentially influences DNA replication timing (Casas-Delucchi and Cardoso, 2011). A good example and study object is the inactive X chromosome (Xi) in female cells, which is inactivated for dosage compensation by the long non-coding RNA Xist (Xi specific transcript) during embryonic development

(Brockdorff et al., 1991; Clemson et al., 1996). The Xi has a complex epigenetic make up of DNA methylation, H3K27me3 and histone hypoacetylation (Norris et al., 1991, Plath et al., 2003; Silva et al., 2003, Jeppesen and Turner, 1993). It is replicated in a certain time-frame during mid S-phase, while the active X (Xa) is replicated throughout S-phase (Morishima et al., 1962). It has been shown that disruption of Xist leads to lower levels of H3K27me3. Disruption of H3K27me3 in turn leads to higher acetylation levels. Increasing the overall acetylation levels however does not have an effect on H3K27me3 levels but affects the replication timing of the Xi, making histone hypoacetylation the major regulator of the Xi replication timing (Casas-Delucchi et al., 2011).

4.3. DNA repair

Throughout life every organism is exposed to a multitude of damage inducing factors such as (UV-) light, oxidative stress or ionizing radiation (for example X-ray for medicinal purposes). All of these factors can induce DNA damage, the type and severity depends on exposure time and energy. If not properly repaired, these types of damage can lead to mutations, cancer and in the worst case to (cell)death. However, during evolution organisms learned to cope with DNA damage and developed various repair mechanisms. These mechanisms involve many different proteins and are specialized to specific types of damages.

If a cell encounters damage such as DNA double strand breaks (DSBs) it activates a whole signaling cascade to recruit the repair machinery. The damage is recognized by kinases, mainly ATM (Ataxia Telangiectasia Mutated) and DNA-PKcs (DNA-dependent protein kinase catalytic subunit), which will phosphorylate the core histone H2A variant H2AX at the serine residue 139 within minutes (Burma et al., 2001, Paull et al., 2000), which is then called γH2AX. Histone H2AX substitutes between 2 and 25% of the total H2A (core) population, depending on the cell type. The phosphorylation of H2AX is thought to spread approximately 2 Mbp around a DSB and represents a central step in in DNA damage response (Rogakou et al., 1998, Kinner et al., 2008).

There are two major pathways to repair DNA double strand breaks (Figure 2), which are (non-homologous) end joining (NHEJ) and homologous recombination (HR), but NHEJ seems to be the main DSB repair pathway (Rothkamm et al., 2003) throughout the cell cycle. During (canonical) NHEJ the free DNA ends are bound by the DNA-PK holoenzyme (Ku70/80/DNA-PKcs), which is important for DNA end protection, coordination, facilitation of end resection and ligation (Gottlieb and Jackson, 1993; Liang and Jasin, 1996, Smith and Jackson, 1999). In case of simple, blunt end breaks the ends can be ligated by the XRCC4/Ligase 4/XLF complex (Grawunder et al., 1997, Nick McElhinny et al., 2000). If the ends contain overhangs or other damage types are in close proximity the ends need processing by the nuclease Artemis before ligation. This processing can lead to loss of DNA by end resection (Mahaney et al., 2009). For repair by HR the MRN complex (Mre11/Rad50/Xrs2) is

recruited to the DSB to keep the DNA ends in close proximity. The MRN complex is also involved in resection of the ends together with CtIP (C-terminal binding protein-interacting protein) (D'Amours and Jackson, 2002; Sartori et al., 2007). The single stranded regions are initially covered by RPA for stabilization (Fanning et al., 2006). RPA is later replaced by Rad51, leading to a Rad51 covered nucleoprotein filament. The filament finds the homologous sequence and invades the strand of the sister chromatid forming a complex called holliday junction, where both resected ends anneal with the homologous sequences (Baumann and West, 1998, Sung et al., 2003). In this formation, DNA polymerases synthesize the missing sequences (Sneeden et al., 2013). Dissolving the holliday junction is a highly complex process. Depending on the dissolving strategy homologous parts of the sister chromatids can be exchanged (Matos and West, 2014).

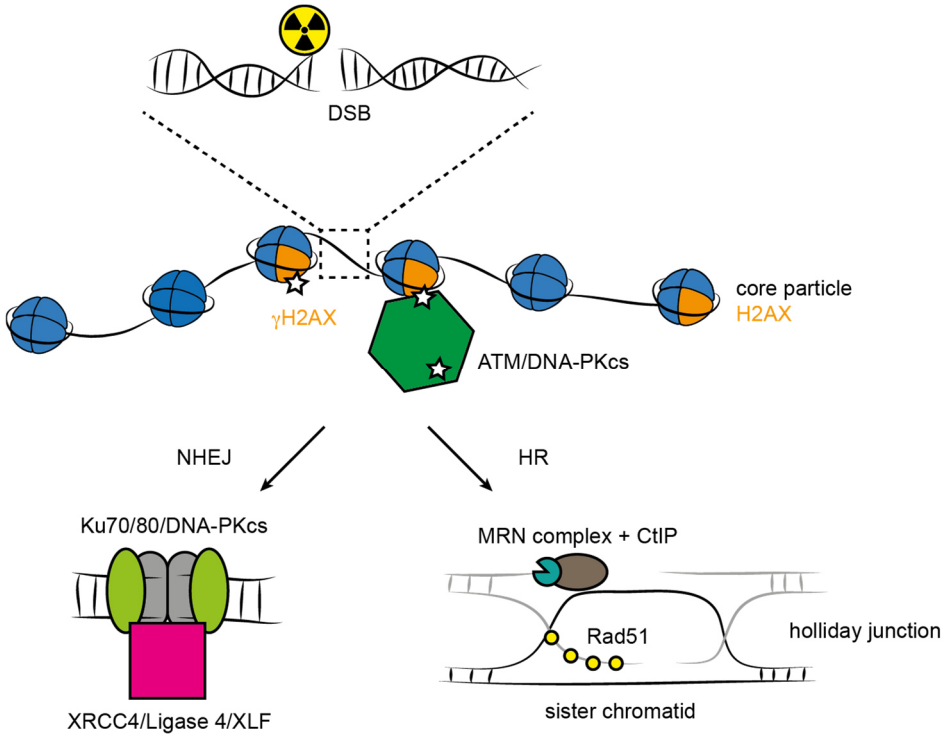

Figure 2: DNA damage signaling upon detection of a DSB and the two main DSB repair pathways non-homologous end joining (NHEJ) and homologous recombination (HR).

Because of their mechanistical differences the two repair pathways have different properties. The rather straight forward NHEJ pathway is error prone due to the lack of a repair template, while during HR the sister chromatids are used as a template to repair the damage in an error-free way. However, due to its mechanism HR can only be utilized during late S-phase and G2, when the homologous sequences from the sister chromatid are available (Rothkamm et al., 2003, Jackson and Bartek, 2009). DNA repair can be monitored by observing factors involved in signaling or the repair mechanisms themselves. γH2AX is a widely used damage marker, as it is thought to cover regions in the Mbp range, making it an “easy-to-spot” target, to represent 1 DSB in 1 γH2AX focus and to be dephosphorylated after the damage is successfully repaired (Rothkamm et al., 2003, Riballo et al., 1999, Rogakou et al.,

1999). Monitoring the kinetics of DSB repair leads to the observation that the repair includes a fast and a slow component. The fast component is assumed to represent repair by NHEJ, while the pathway of the slow component depends on the cell cycle phase. In G2 it is represented by HR while in G1 it is represented by an altered pathway of the canonical NHEJ. Both slow components have in common that the DNA ends need resection and that they are dependent on the nuclease Artemis and the kinase ATM, suggesting that the slow component might represent the repair of more complicated DSBs (DiBiase et al., 2000, Riballo et al., 2004, Beucher et al., 2009, Biehs et al., 2017). Moreover, euchromatic regions seem to be repaired faster than heterochromatic regions. Potential reasons for this could the more condensed state of heterochromatin, making it less accessible to the repair machinery, higher damage complexity or repair pathway choice (Cowell et al., 2007, Goodarzi et al., 2008, Natale et al., 2017, in press).

Taken together, chromatin organization and maintenance are all conserved and highly complex processes. DNA replication and repair mechanisms and kinetics seem to be dictated by the underlying chromatin features such as structure, compaction level and epigenetic marks. Although scientists have answered many questions towards DNA replication, repair and chromatin organization over the years, a full understanding is yet to be gained. How is chromatin organized between the beads on a string and higher order structures in the Mbp range? What determines replication and repair dynamics and kinetics? Are repetitive elements, which represent a large part of the genome, dominated by the chromatin type they are associated with or do they follow an independent replication and repair timing?

4.4. Aim of this thesis

This thesis aims to answer some of the above-mentioned questions and therefore contributes to our view and understanding of the interplay between chromatin, DNA replication and DNA repair. The thesis will focus on chromatin organization and genome maintenance. Two main processes, DNA replication and DNA repair, which are key keepers of the genome, will be analyzed. In the first part both processes will be utilized to get new insights into high resolution chromatin organization using super-resolution microscopy. The second part will focus on genome maintenance especially on DNA replication timing and DNA repair kinetics of repetitive elements via immuno-FISH and microscopic analysis.

5. Correlating DNA replication & repair structures as elementary units of chromatin organization

5.1. Introduction

5.1.1. Chromatin structure

In the past decades, new methods have become available, which allow more detailed studies of chromatin organization. Such techniques are for example 3C (chromatin conformation capture) and its extensions. They are based on the isolation of chromatin contact domains, can involve sequencing techniques (for example Hi-C) and allow to analyze if two or more pieces of chromatin are in contact with each other. Using Hi-C a higher level of chromatin organization has been identified as so called topological (ly associated) domains (TDs, TADs). These are areas of chromatin that, in the scale of Mbp, interact with each other (Dixon et al., 2012) and are conserved among species and in many cases bordered by the architectural protein CTCF. Chromatin organized within one TAD has the same replication timing (Pope et al., 2014). Furthermore, active genes seem to be clustered with other active genes and contact domains often exhibit the same epigenetic marks (Lieberman-Aiden et al., 2009, Rao et al., 2014). While the concept of TADs is relatively new, other concepts of higher order chromatin organization were described before. One of them is the 1 Mbp domain, which is based on the observation of focal DNA replication structures, labeled by nucleotide incorporation (Nakamura et al., 1986, Nakayasu and Berezney, 1989). These structures contain ~1 Mbp of DNA, are spatially stable over several cell cycles and are thought to represent chromatin structures. It has also been suggested that the 1 Mbp domain consists of aggregates of several 100 kbp domains/loops (Jackson and Pombo, 1998, Ma et al., 1998, Berezney and Wei, 1998, Zink et al., 1999, Cremer et al., 2000). TADs and the 1 Mbp domain are not mutually exclusive and might describe the same chromatin structure.

The concept of loop formation is based on the concept that two chromatin regions come into contact with each other and that the chromatin between those two regions is then looped out (Schleif, 1992). Higher resolution Hi-C studies revealed thousands of previously undetected contacts, forming loops of ~ 185 kbp (Rao et al., 2014), although also mega-domains of 3 Mbp were observed. Contact domains are often (but not always) accompanied by CTCF and/or cohesin component binding sites, suggesting that they regulate chromatin looping. The most obvious contact domains are probably regulators and promoters to facilitate gene expression. A prime example for active gene regulation is the β-globin locus, where a locus control region (LCR) stands in direct contact with the β-globin genes, which are 40-60 kbp apart, enhancing their expression. The region in between is looped out. In cells where the β-globin genes are not expressed, there is no contact between the LCR and the genes (Tolhuis et al., 2002). This is an example where the distance between the regulatory element and the genes is relatively short, but they can also be separated by more than 1 Mbp (Dekker and Misteli, 2015).

In summary, chromatin looping and formation of higher order structures like the 1 Mbp domain and TADs are the foundation of chromatin organization and are closely linked with chromatin function. Nevertheless, chromatin folding and looping is not fully understood and needs further investigation.

5.1.2. DNA replication and repair observed with super-resolution microscopy

Conventional light microscopy underlies the limit of resolution (diffraction limit, Abbe limit), which is roughly 200 nm, depending on the wavelength (Abbe, 1873, Rayleigh, 1896). In the past decades, new optical (super-resolution) microscopy techniques have been developed to overcome this limit. Examples are 3D structured illumination microscopy (3D-SIM, Gustafsson et al., 2008) with a resolution down to 100-130 nm in xy dimensions or stimulated emission depletion (STED, Schmidt et al., 2008) microscopy with a resolution of about 20-100 nm in xy dimensions (Schermelleh et al., 2010). Super-resolution microscopy opened new possibilities to investigate processes within the cell in more detail and has been used to study DNA replication and repair processes.

DNA replication foci have been studied using different microscopy techniques including 3D-SIM, revealing that with increasing resolution the number of replication foci also increased from ~1000 in confocal microscopy to over 5000 in 3D-SIM. These replication foci have an average diameter of 120 nm and represent single replicons, as calculations based on replication fork speed, genome size and S-phase duration reveal that around 5000 replicons need to be active at any given time to replicate the whole genome (Baddeley et al., 2010, Chagin et al., 2016). Additionally, replicons have been suggested to underlie the local organization of chromatin structure in the sense that per chromatin loop only one origin of replication is activated (Lob et al., 2016).

Using 3D-SIM γH2AX foci observed with conventional microscopy could be resolved into clusters of smaller γH2AX (nano or sub)foci of 100-200 nm in diameter, questioning if one γH2AX focus really represents one DSB (Lopez Perez et al., 2016, Natale et al., 2017, in press). The Ku protein complex has been suggested as a more reliable DSB marker as it is directly associated with the DSB ends (Britton et al., 2013). Co-staining with phospho-Ku70 and terminal desoxynucleotidyl transferase mediated dUTP nick end labeling (TUNEL) has revealed that multiple γH2AX (nano)foci, arranged in a cluster, are accompanied by single DSBs. This suggests that γH2AX (nano)foci and clusters represents different units of chromatin organization and that (nano)foci arise from discontinuous phosphorylation of H2AX within the clusters (Natale et al., 2017, press).

5.2. Aim of this study

Different levels of spatial chromatin organization have been shown from the DNA double helix wrapped around the core histones to form nucleosomes up to topologically associated domains in the range of Mbp. Chromatin folding in between has been described as loop formation but is not yet fully understood.

Both replicons and γH2AX (nano)foci have been associated with forms of local chromatin organization. Both structures show focal patterns of similar sizes in super-resolution microscopy, raising the question if they might be based on a common structural unit. We started an experiment based on both human and murine cells, co-stained replication and repair structures within the same nucleus and studied them using super-resolution imaging (3D-SIM) in order to investigate similarity between both structures and to possibly identify an elementary unit of chromatin organization.

5.3. Material & Methods

5.3.1. Cell culture

Cultures of C2C12 mouse myoblasts (ATCC CRL-1772), HeLa Kyoto (Erfle et al., 2007, a gift from Jan Ellenberg) and HeLa (ATCC CCL-2) cells were grown at 37 °C and 5% CO_2 in DMEM supplemented with 50 μg/ml gentamycin, 20 mM L-glutamine and 10% FCS for HeLa and HeLa Kyoto cells or 20% FCS for C2C12 cells. For experiments involving immunofluorescence stainings cells were grown on glass coverslips.

5.3.2. Irradiation

For X-ray irradiation cells were exposed to single doses of 2 and 5 Gy (90 kV, 33.7 mA) using a GE ISOVOLT Titan E X-ray machine.

5.3.3. Simultaneous visualization of replication and repair structures

Cells were pulse labeled with 10 μM CldU for 15 min, then grown for 10 hours without any treatment and irradiated with 2 or 5 Gy X-ray. At 30 min post irradiation cells were fixed with 3.7% formaldehyde/1x PBS for 15 min, then permeabilized with 0.7% Triton X-100/1x PBS and blocked with 1% BSA/1x PBS for 30 min. Incubation with the primary antibodies mouse anti histone H2AX phospho Ser139 (clone JBW301, 05-636, Upstate/Millipore, 1:800) and rabbit anti BrdU (600-401-C29, Rockland/Biomol, 1:500) was performed together with 50 U/ml DNaseI in 1x DNase buffer (30 mM Tris-HCl, pH 8, 33 mM $MgCl_2$, 1 mM β-mercaptoethanol) and 2% BSA at 37 °C for 1 h. Detection with the secondary antibodies, goat anti mouse IgG Alexa Fluor 488 (A11029, Invitrogen/Thermo Fisher Scientific, 1:800) and goat anti rabbit IgG Alexa Fluor 594 (111-585-144, Jackson ImmunoResearch, 1:500) followed in 1% BSA/1x PBS for 1 h at room temperature. DNA counterstaining was performed with DAPI (20 ng/ml) for 10 min and the coverslips mounted in VectaShield (Vector Laboratories) and sealed with nail polish.

5.3.4. Maximum colocalization control

Cells were irradiated with 2 or 5 Gy X-ray, 30 min post irradiation they were fixed with 3.7% formaldehyde/1x PBS for 15 min, then permeabilized with 0.7% Triton X-100/1x PBS and blocked with 1% BSA/1x PBS for 30 min. Incubation with the primary antibody mouse anti histone H2AX phospho Ser139 (clone JBW301, 05-636, Upstate/Millipore, 1:800) in 1% BSA/1x PBS was performed at room temperature for 1 h. Detection with the secondary antibodies (simultaneously) goat anti mouse IgG Alexa Fluor 488 (A11029, Invitrogen/Thermo Fisher Scientific, 1:800) and donkey anti mouse IgG Alexa Fluor 594 (715-585-151, Jackson ImmunoResearch, 1:800) followed in 1% BSA/1x PBS for 1 h at room temperature. DNA counterstaining was performed with DAPI

(20 ng/ml) for 10 min and the coverslips mounted in VectaShield (Vector Laboratories) and sealed with nail polish.

5.3.5. Microscopy

Super-resolution microscopy was performed with a DeltaVision OMX V3 (GE Healthcare) 3D structured illumination microscope using a 100x/1.4 immersion objective UPlanSApo (Olympus) and z-spacing of 125 nm.

Confocal imaging was performed using a Perkin Elmer VoX-1000 Spinning Disk microscope with a 60x/1.4 NA/oil CFI Apochromat TIRF objective.

5.3.6. Image analysis of super resolution images

For segmentation of replication foci, the protocol used was originally described by Chagin et al., 2015 and Chagin et al., 2016. In brief, the images were converted into 16bit images. Replication foci were thresholded in ImageJ with the autothreshold using the triangle method on the stack histogram, the thresholded image was combined with the original image via Image calculator (method: min) creating a new image that contains the intensities of the original image but only in the thresholded areas. This new image and the corresponding other channels were then imported into the image analysis software Perkin Elmer Volocity 6.3 and converted into volumes. The pixel dimensions of the images were set to the specifications of the 3D-SIM images (x/y: 0.039 μm and z: 0.125 μm). The following steps also include the segmentation of repair foci (described by Natale et al., 2017, in press): Find objects ("nucleus") using the DAPI channel, method "Intensity" (set manually to the optimal value), use fill holes in object/dilate/erode until the object optimally fits the nucleus, exclude objects by size <500 μm^3. Find objects ("replicons") using the 594 channel, method "Intensity" (lower limit: 1, upper limit: 65535), separate touching objects, exclude "replicons" not touching "nucleus". Find objects ("repair foci") using the 488 channel, method "SD" (lower limit: set to optimal value for all cells that are to be compared), separate touching objects (object size guide 0.00019 μm, filter population: volume > 0.00152 μm^3), exclude "repair foci" not touching "nucleus". For the distance/colocalization measurements the following steps were added to the protocol: Measure distances (from: "repair foci" to "replicons"), compartmentalize (divide "repair foci" between "replicons" where sub-populations are nearest by centroid, restrict to items within 0.1 μm). Example images are shown in Figure 3.

The DNA content of foci were determined via the DAPI intensities and the genome size was calculated as indicated in Figure 4.

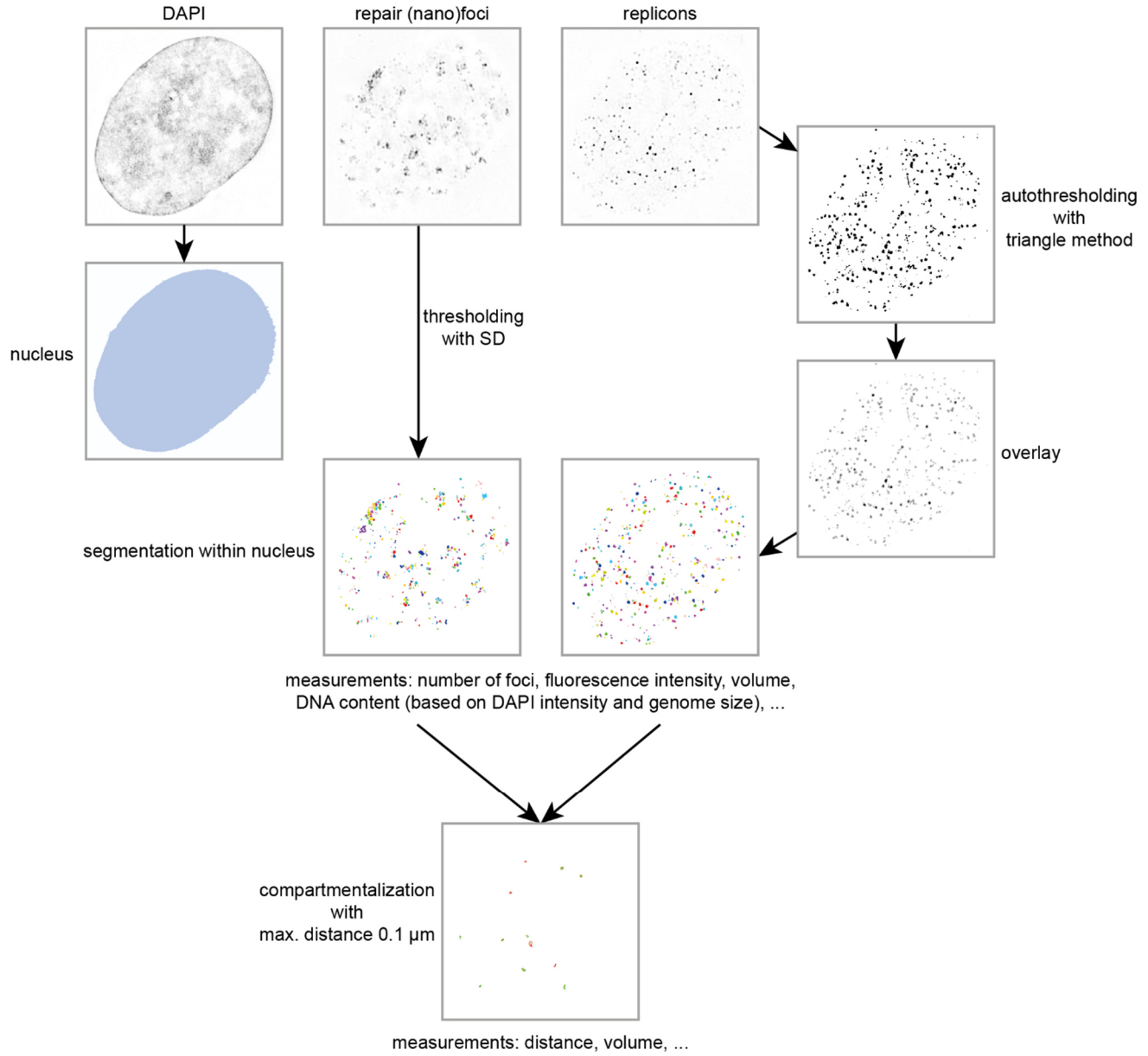

Figure 3: Segmentation of replicons and repair (nano)foci. Repair (nano)foci are segmented in Volocity using SD thresholding. Replicons are thresholded using ImageJ autothreshold, generating a "mask", that is then overlayed with the original intensities. The overlay is imported into Volocity for segmentation (different colors refer to different objects). Objects detected outside the nucleus will be excluded. To identify colocalizing replicons and repair (nano)foci, objects are compartmentalized with a maximum distance of 0.1 µm between centroids.

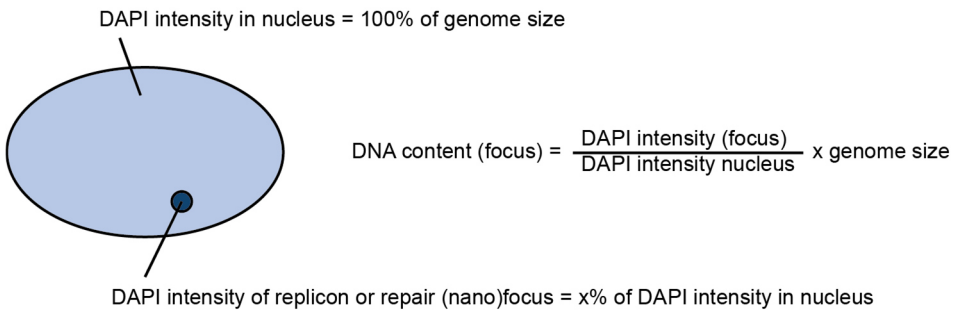

Figure 4: Calculation of focus DNA content based on the DAPI signal intensity and the genome size. The DNA content of the nucleus is equal to the (diploid) genome size of the cell line. The DNA content of a focus is then calculated as the fraction of the total DAPI intensity within a focus multiplied with the genome size. Adapted from Natale et al., 2017, in press.

5.3.7. Characterization of global X-ray repair kinetics

HeLa, HeLa Kyoto and C2C12 cells were exposed to 2, 5 or 10 Gy X-ray radiation, fixed 30 min, 3 h or 24 h after irradiation with 3.7% formaldehyde/1x PBS for 15 min and permeabilized with 0.7% Triton X-100/1x PBS for 15 min. After blocking with 1% BSA/1x PBS for 30 min, the cells were incubated with the primary antibody mouse anti histone H2AX phospho Ser139 (clone JBW301, 05-636, Upstate/Millipore, 1:800) in 1% BSA/1x PBS for 1 h and the secondary antibody donkey anti mouse IgG Cy5 (715-175-150, Jackson ImmunoResearch, 1:500) also in 1% BSA/1x PBS for 1 h. DNA counterstaining was performed with DAPI (1 μg/ml) for 10 min and the coverslips mounted in Mowiol 4-88/2.5% DABCO and allowed to harden at room temperature overnight.

5.3.8. High content imaging and image analysis for global X-ray kinetics

Samples were imaged using a high content imaging system (Perkin Elmer Operetta) with a 40x/0.95 NA air objective. Images were then analyzed using the Harmony Software (Perkin Elmer) with the following steps: Input image: individual planes, basic flatfield correction. Find nuclei: channel DAPI, method B (or C for C2C12). Select population: remove border objects from nuclei. Calculate morphology properties: area, roundness. Select population: filter nuclei by property, roundness >0.9, area >70 μm^2 (or roundness >0.8 for C2C12). Calculate intensity properties: channel DAPI. Calculate intensity properties: channel Cy5.

5.3.9. S-phase characterization and growth curve of HeLa cells

Human HeLa cells were seeded into p100 cell culture dishes with a cell number of $3*10^5$ per dish. During the next 4 days one dish per day was harvested by trypsinization and counted using a Neubauer chamber. For S-phase characterization cells were pulse labeled with CldU (100 μM) for 15 min, fixed with 3.7% formaldehyde/1x PBS for 15 min, then permeabilized with 0.7% Triton X-100/1x PBS for 15 min and blocked with 1% BSA/1x PBS for 30 min. Incubation with the primary rabbit anti BrdU (600-401-C29, Rockland/Biomol, 1:500) was performed together with 50 U/ml DNaseI (D5025, Sigma-Aldrich) in 1x DNase buffer (30 mM Tris-HCl, pH 8, 33 mM $MgCl_2$, 1 mM β-mercaptoethanol) and 2% BSA at 37 °C for 1 h. Detection with the secondary antibody goat anti rabbit IgG Alexa Fluor 594 (111-585-144, Jackson ImmunoResearch, 1:500) followed in 1% BSA/1x PBS for 1 h at room temperature. DNA counterstaining was performed with DAPI (1 μg/ml) for 10 min and the coverslips mounted in Mowiol 4-88/2.5% DABCO and allowed to harden at room temperature overnight.

5.3.10. High content imaging and image analysis for S-phase characterization

Samples were imaged using a high content imaging system (Perkin Elmer Operetta) with a 40x/0.95 NA air objective. Images were then analyzed using the Harmony Software (Perkin Elmer) with the following steps: Input image: maximum projection, basic flatfield correction. Find nuclei: channel DAPI, method C. Select population: remove border objects from nuclei. Calculate intensity properties: channel DAPI. Calculate morphology properties: area, roundness. Select population: filter nuclei by property, roundness >0.9, area >75 μm^2. Calculate intensity properties: channel Alexa Fluor 594. Select population (S-phase positive cells): filter by property, Alexa Fluor 594 intensity mean >350.

5.4. Results & Discussion

5.4.1. S-phase characteristics and DNA repair kinetics of HeLa, HeLa Kyoto and C2C12 cells

HeLa, HeLa Kyoto (both human, cervix, adeno carcinoma, female) and C2C12 (mouse, muscle, myoblast, female) are cell lines, which are in general well characterized. However, they have been used in different fields and we started our studies by summarizing and compiling published and unpublished data sets for DNA replication dynamics and DNA repair kinetics for the used cell lines.

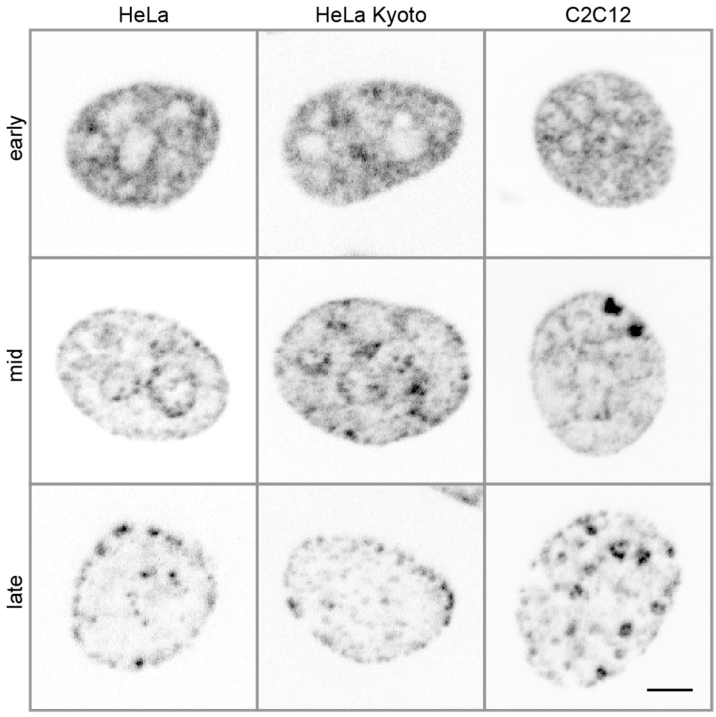

	HeLa	HeLa Kyoto	C2C12
Replication fork speed	?	1.65 kNtd/min	2.46 kNtd/min
Inter origin distance	?	188.7 kbp	161.7 kbp
S-Phase duration	10.5 h	9.5 h	9.4 h
Doubling time	23.3 h	22.6 h	22.6 h
Genome size	10.1 Gbp	9.7 Gbp	11.4 Gbp

Figure 5: S-phase characteristics of HeLa, HeLa Kyoto and C2C12 cells. Images show representative cells in early, mid or late S-phase (by nucleotide pulse labeling), scale bar 5 µm. Genome size of HeLa cells was determined by SKY analysis (data from Natale et al., 2017, in press). HeLa Kyoto and C2C12 genome size were generated using a high-resolution cytometer setup. All S-phase data for HeLa Kyoto and C2C12 cells from Chagin et al., 2016.

HeLa cells were marked for S-phase positive cells by nucleotide incorporation and subsequent immunofluorescent staining. In parallel doubling time was determined by growth curve analysis. Replication data of all three cell lines including genome size are summarized in Figure 5. Replication patterns of HeLa cells were as expected very similar to HeLa Kyoto, where the early S-phase pattern shows small foci distributed in the nucleus, except for the nucleolus, the mid S-phase pattern is concentrated in the nucle(ol)ar periphery and the late S-phase pattern shows fewer, but larger foci. S-

phase duration and doubling time were slightly longer than in HeLa Kyoto. Data for replication fork speed and inter origin distance of HeLa cells are not yet available, but are currently investigated. Mouse C2C12 cells show in principle the same replication patterns. During mid S-phase the inactive X (Xi) is replicated, which can be recognized by the large spots in the nuclear periphery. C2C12 cells are quasi tetraploid and therefore have two Xi (Casas-Delucchi et al., 2011). While these cells have a larger genome size, they have the same doubling time and almost the same S-phase duration as HeLa Kyoto, they seem to compensate by a lower inter origin distance and higher replication fork speed (Chagin et al., 2016).

To study DNA repair kinetics upon ionizing irradiation all three cell lines were irradiated with 2, 5 or 10 Gy X-ray, fixed after 0.5 h, 3 h or 24 h and then stained for the repair marker γH2AX. Slides were imaged and analyzed with a high content screening system. At 0.5 h post irradiation with all doses the γH2AX signal in C2C12 cells was characterized by a high number of foci everywhere in the nucleus (Figure 6A), at 3 h the number of foci decreased and at 24 h only few but distinct foci were visible. These observations are consistent with what could be observed for HeLa cells (Figure 6 and for example Barton et al., 2014). In unirradiated cells the γH2AX signal was found in a part of the population only. It was less intense and less structured in comparison to irradiated cells. This suggests that the γH2AX signal in unirradiated cells arises from S-phase, as previously published (Turinetto and Giachino, 2015). In C2C12 cells some signal was also found in the nucleolus, which is most likely and artefact from the immunofluorescence staining. Following the γH2AX signal intensity at the three increasing X-ray doses, it increased in all three cell lines. Over time the signal decreased constantly (Figure 6B, statistics of all data are summarized in Table S 1). At 3 h post irradiation with 2 Gy HeLa Kyoto cells show a change in signal, which would not be expected like this, as it was not observed in the higher doses. The signal for 3 h post irradiation is lower than at the 24 h time-point, but expected to be in between 0.5 h 24 h. In a repetition of the experiment (data not shown) we observed the expected trend, making the values shown here biological irregularities. We also studied the cell cycle distribution of all data sets by measuring DAPI intensity distribution and could observe that a part of the cell populations was arrested in G2 phase and that the higher the dose, the more cells were arrested in G2 (Figure 7A). We could observe that the size of nuclei at 24 h post irradiation was larger in comparison to the other time-points or unirradiated cells, which was especially pronounced after irradiation with 10 Gy and coincides with cell cycle arrest in G2 (Figure 7B). It has previously been suggested that the decondensation allows the DNA repair machinery to access damaged chromatin, supports damage signaling and promotes control for damage of the whole genome (Murga et al., 2007, Ziv et al., 2006). However, we observe that the DAPI intensity increases with increasing nucleus size, and that the increase of both properties exceeds that of unirradiated G2 cells (Figure 7C). Since the DNA content should not change from an unirradiated G2 cell to an irradiated G2 cell, the increase in

DAPI signal is unexpected. It is possible that DAPI can access DNA better in less condensed chromatin, which would result in an increase in DAPI intensity. However, during DNA repair, parts of the broken ends are resected and then newly assembled. The total DNA content could therefore exceed that of an unirradiated G2 cell, because the resected fragments are not yet abolished and new fragments are already present. If this change in DNA content is noticeable or if the increase in DAPI intensity is based on better DNA accessibility is unclear and should be further investigated.

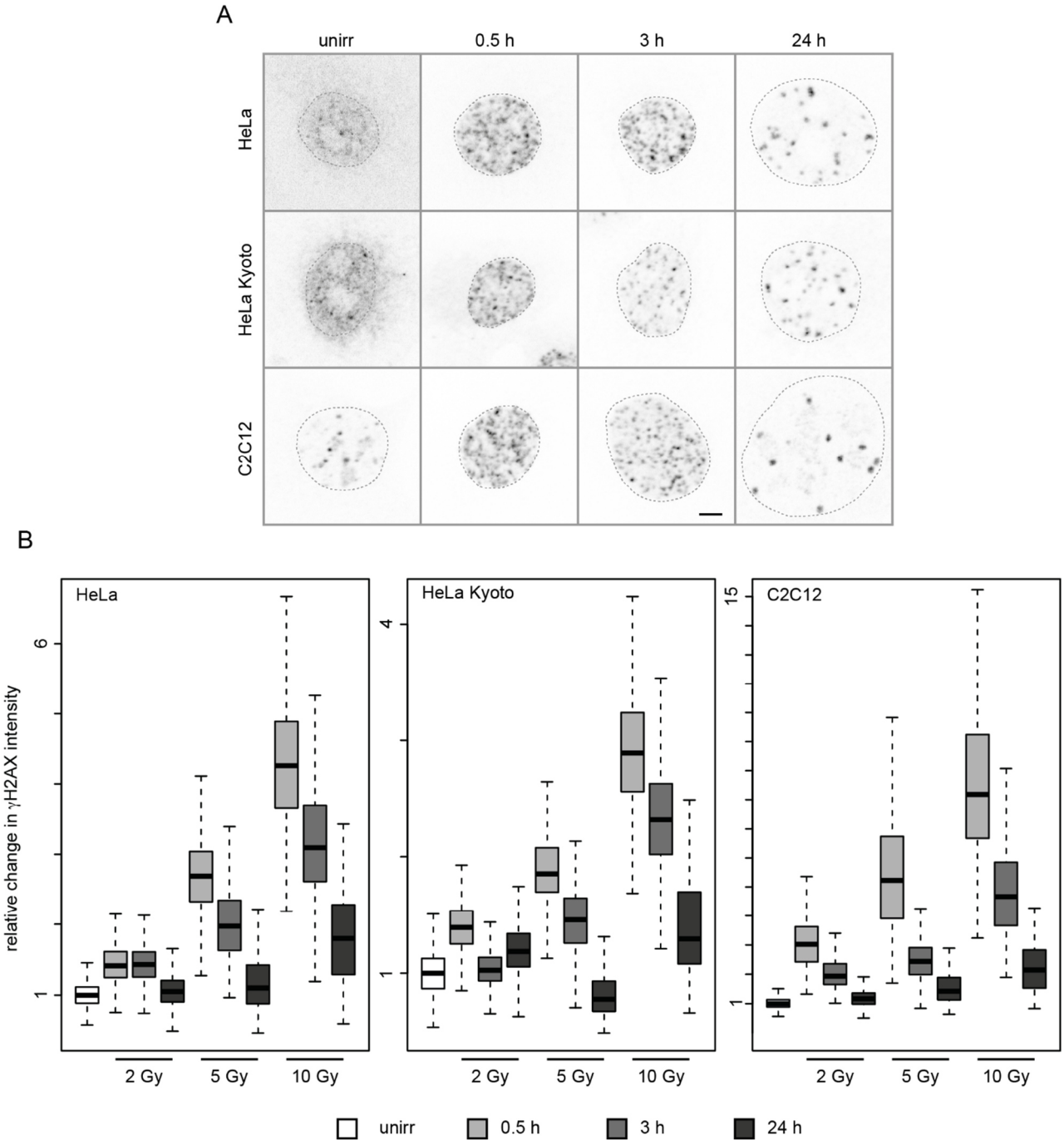

Figure 6: Repair kinetics of HeLa, HeLa Kyoto and C2C12 cells. Cells were irradiated with 2, 5 or 10 Gy X-ray, fixed after the times indicated, then stained for γH2AX and imaged and analyzed with a high content imaging system. A) representative images of cell irradiated with 2 Gy. Dashed line indicates the borders of the nuclei. Scale bar 5 µm B) Relative change in γH2AX fluorescence intensity. Data are normalized to the median of the unirradiated cells. For statistical analysis representation see Figure S 1. Data shown are from one experimental replicate, n = 764 on average (min = 212 cells for C2C12 5Gy 24h, max = 2015 cells for HeLa unirr).

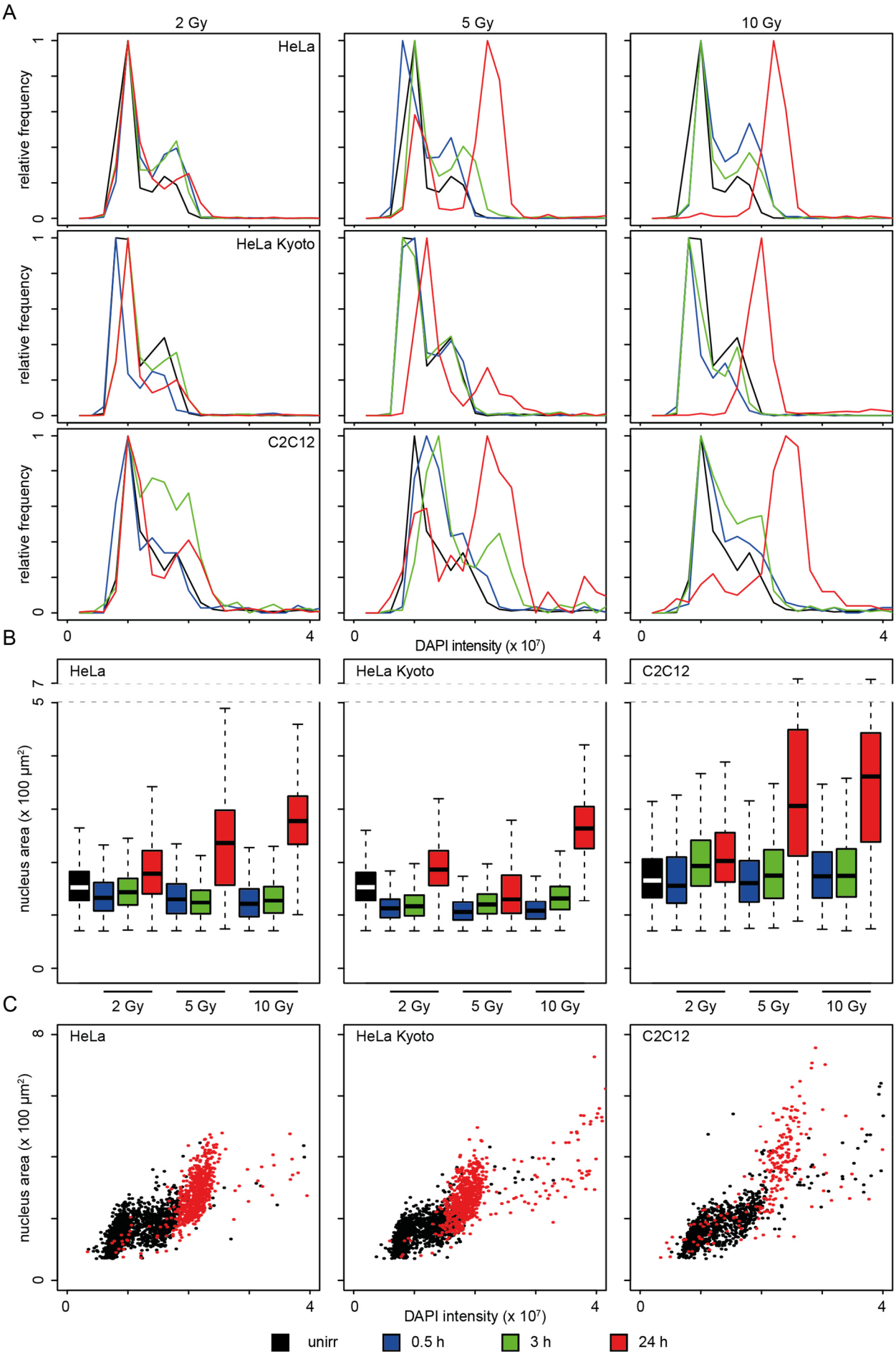
A
2 Gy
5 Gy
10 Gy
HeLa
HeLa Kyoto
C2C12
relative frequency
DAPI intensity (x 10⁷)
B
nucleus area (x 100 µm²)
C
unirr
0.5 h
3 h
24 h

Figure 7: Cell cycle analysis and size distribution of HeLa, HeLa Kyoto and C2C12 cells. Cells were irradiated with 2, 5 or 10 Gy X-ray, fixed after the times indicated, stained for γH2AX, imaged and analyzed with a high content imaging system. A) Cell cycle distribution by DAPI intensity. Data were normalized to the highest frequency value. B) Nucleus size distribution (μm²). Dashed line indicates where the y-axis was broken. C) DAPI intensity versus nucleus size (μm²) for cells 24 h post 10 Gy in comparison to unirradiated cells. Data from one experimental replicate are shown, n = 764 on average (min = 212 cells for C2C12 5Gy 24h, max = 2015 cells for HeLa unirr).

5.4.2. Replicons and repair (nano)foci analyzed by super-resolution microscopy

Both replication and repair structures have been associated with structural chromatin organization. In order to find out if they represent the same basic unit of chromatin organization we compared them within the same cell. Staining a single replication or repair factor is not enough for this approach since we are not interested in those factors but in chromatin. For DNA replication nucleotide incorporation and staining and for DNA repair structures γH2AX is the best option since both will cover large areas of chromatin and not only a single protein. To analyze chromatin labeled by replicons and repair (nano)foci within the same cell we designed the experiment in a way, that both structures were not influencing each other. It would be problematic for example if an active replication fork is hit by the irradiation leading to its collapse. Therefore, we labeled replication structures in the cells by nucleotide incorporation and allowed them to run out of S-phase by incubating them for 10 h before proceeding to irradiation. The time in between replication labeling and irradiation corresponds to the average S-phase length of HeLa Kyoto and C2C12 cells and allows us to ensure that the cells are not in the same (labeled) S-phase. Nevertheless, it is possible that cells labeled in mid or late S-phase had already proceeded to G1 during irradiation. We started our analysis by visually comparing replicons with repair (nano)foci. Imaging with 3D-SIM allowed the generation of images with different resolutions, from (pseudo) widefield to deconvolved, which is comparable to confocal resolution, and super-resolution (Figure 8A). We observed, that large focal structures in pseudo-widefield could be resolved into clusters of smaller structures, revealing thousands of foci for both replication and repair. Replicons and repair (nano)foci looked very similar in all three cell lines. Number of replicons per nucleus fluctuated between different S-phase stages. For HeLa cells 3300-5492, for HeLa Kyoto 4136-5368 and for C2C12 4275-5802 replicons were counted (Figure 8B and Table S 2). Numbers for late S-phase were always lower than in mid S-phase. Our results are in good agreement with the numbers described for C2C12 and HeLa Kyoto cells by Chagin et al., 2016. The number of repair (nano)foci is naturally highly dependent on the X-ray dose, with higher doses a higher number of DSBs are induced and therefore more H2AX is phosphorylated. For doses of 2 and 5 Gy 1260-2181 repair (nano)foci were counted for HeLa cells, 1701-2558 for HeLa Kyoto and 2443-3187 for C2C12 cells (Figure 8B and Table S 2). The number of repair (nano)foci from Natale et al., 2017 (in press) for HeLa cells irradiated with 2 or 5 Gy were higher, nevertheless our results are still within the same range. C2C12 cells had the highest number of repair (nano)foci, which is supported by the larger genome size of C2C12 cells in comparison to HeLa and HeLa Kyoto cells and by the fact that they accumulate the most

γH2AX signal in Figure 6, suggesting that these cells are more sensitive to X-ray irradiation although the comparison is difficult since they are from another species.

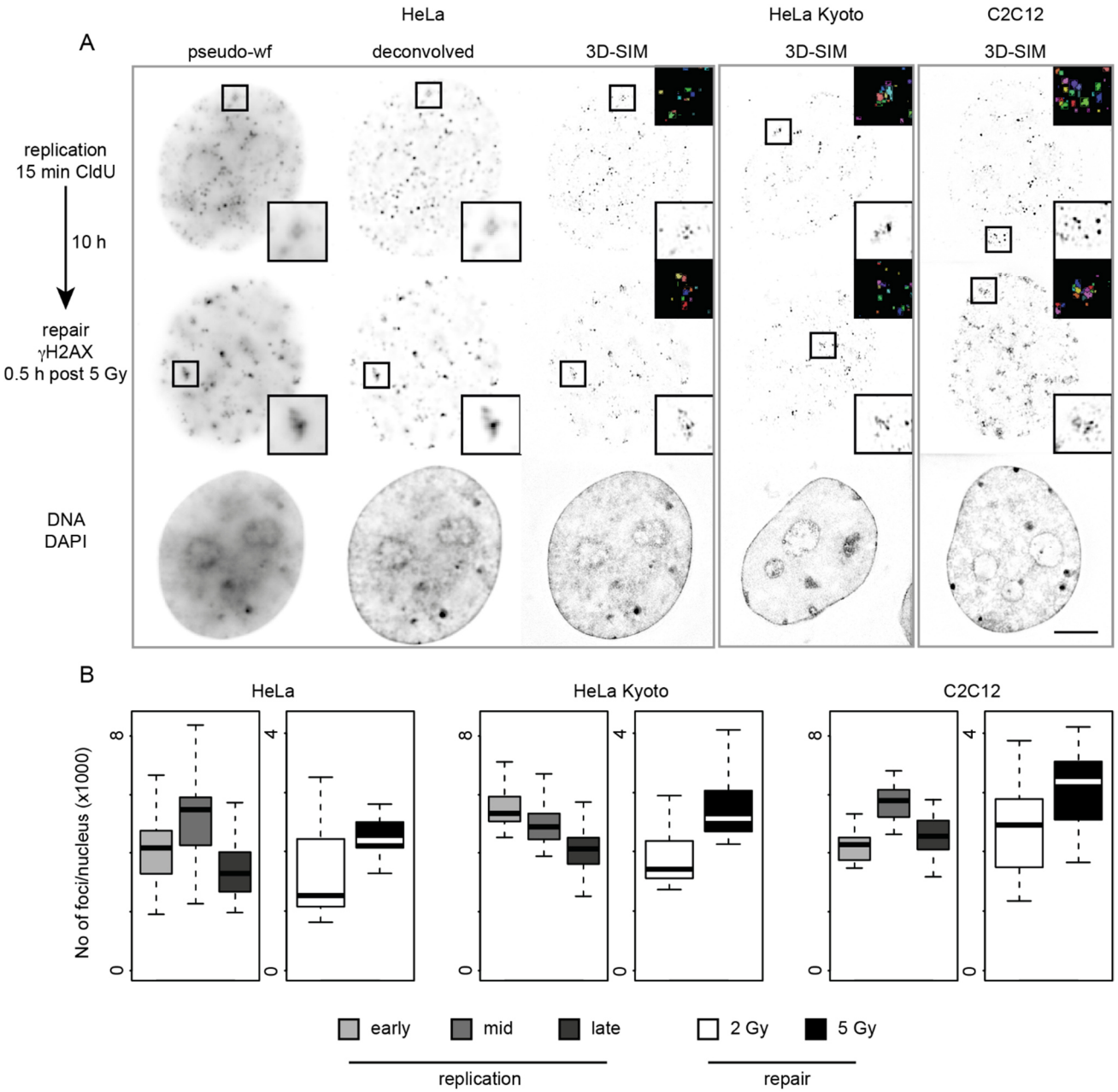

Figure 8: Replicons and repair (nano)foci of HeLa, HeLa Kyoto and C2C12 cells imaged with super resolution microscopy (3D-SIM). A) Experimental approach and replication and repair foci in three resolution levels. Cells in S-phase were labeled by nucleotide incorporation (CldU) for 15 min, washed, allowed to grow for 10 h, then irradiated with 2 or 5 Gy X-ray and fixed after 0.5 h followed by immunostaining for CldU and γH2AX. Pseudo-widefield and deconvolved images were generated from the 3D-SIM imaging data. Cropped regions show resolution increase in more detail and examples of the segmentation. Different colors refer to individual objects. Scale bar 5 µm. B) Number of replicons and repair (nano)foci per nucleus in super-resolution (3D-SIM). A summary of statistics is given in Table S 2.

5.4.3. Defining colocalization for 3D-SIM

The use of high resolution imaging systems challenges the definition of colocalization, because the higher the resolution, the more difficult it is to see two close structures actually colocalizing. It is therefore necessary to assess how colocalization is to be defined in those systems. Steric hindrance might be a reason for interruptions in signals of continuous structures, if the resolution is high enough and the molecules used for labeling are potentially too large (e. g. antibodies). This raises the question if the focal patterns observed in super-resolution images of for example γH2AX arise from the antigen being inaccessible to the antibody. Additionally, we wanted to know if other structures in close proximity to γH2AX foci are accessible to the respective antibody and if colocalization is at all possible in 3D-SIM. We therefore analyzed different staining combinations imaged with 3D-SIM and could observe that several factors such as the architectural protein CTCF, histone modifications (Natale et al., 2017, in press) and nucleotides incorporated during S-phase can be found close to γH2AX foci. They can be localized even within γH2AX focus clusters or overlapping/colocalizing with γH2AX. Example images for γH2AX co-stained with CTCF (kindly provided by Alexander Rapp) and γH2AX co-stained with a nucleotide from our experiments are shown in Figure 9.

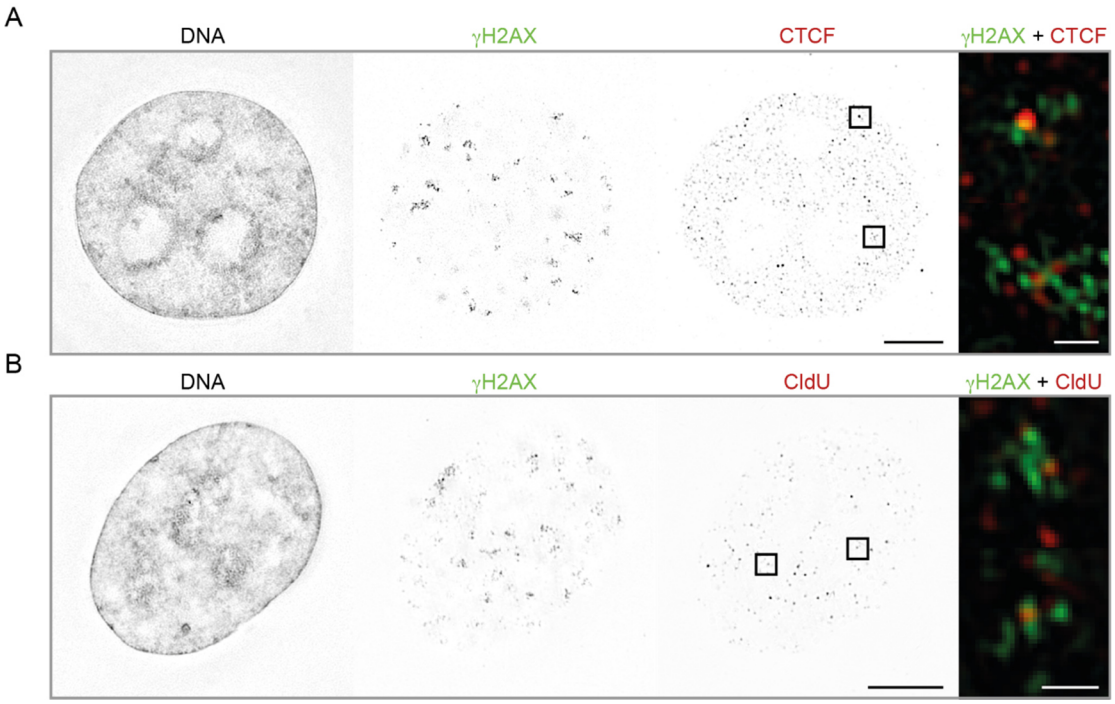

Figure 9: Antigen accessibility within γH2AX focus clusters in HeLa cells. A) γH2AX 24 h post 10 Gy X-ray irradiation and corresponding CTCF signal. Images were kindly provided by Alexander Rapp. B) γH2AX 0.5 h post 5 Gy X-ray irradiation, co-stained with the nucleotide CldU, incorporated 10 h before irradiation. Scale bar 5 µm in full images, 0.5 µm in cropped regions.

We conclude that antigen accessibility is given and that colocalization, at least to some degree, is possible in 3D-SIM imaging. To estimate the degree of colocalization we can expect using 3D-SIM, we designed a control that would give us structures as close to one another as possible. For this HeLa cells

were irradiated with 2 and 5 Gy X-ray and fixed after 0.5 h. The cells were incubated with a primary antibody specific for γH2AX and then with two differently labeled, polyclonal secondary antibodies, one red, one green, simultaneously. In this way, the primary antibody will be detected by a green and red labeled secondary antibody, which results in a staining of the same structures with two colors within the same cell (Figure 10A/B). We could observe that red and green repair (nano)foci overlapped quite well and that red and green structures correspond to one another. We assume that the slight difference between them may be a result of steric hindrance and competition of the two secondary antibodies. Since red and green signals correspond to each other, the number of red and green repair (nano)foci should be within the same range, although slight differences may be possible. Indeed, the number of repair (nano)foci was very similar and not significantly different for the two colors with 2076 (green) and 2014 (red) for 2 Gy and 2972 (green) and 3063 (red) for 5 Gy (Figure 10C and Table S 3). We also calculated the global Pearson´s correlation coefficient for red and green repair (nano)foci to quantify the degree of colocalization within the whole cell. This calculation revealed a high Pearson´s correlation coefficient of 0.75 for 2 Gy and 0.71 for 5 Gy, considering the resolution.

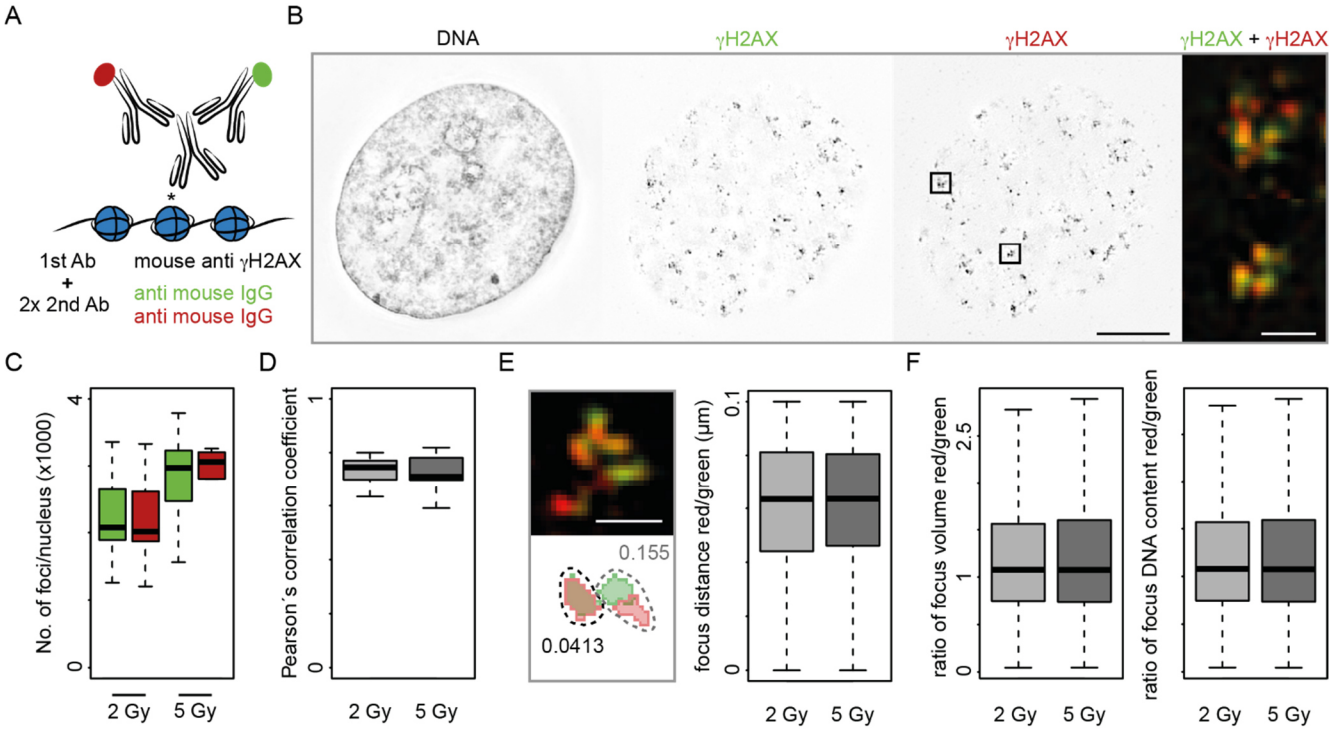

Figure 10: Control to define colocalization in 3D-SIM images. A) Experimental approach. HeLa cells were irradiated with 2 or 5 Gy X-ray, fixed after 0.5 h and stained for γH2AX. For detection of the primary antibody two secondary antibodies conjugated with different fluorophores were used simultaneously to label γH2AX in two distinct colors. B) Representative images of a cell irradiated with 5 Gy X-ray. Scale bar 5 µm in full images, 0.5 µm in cropped regions. C) Number of repair (nano)foci labeled in the respective colors. D) Global Pearson´s correlation coefficient calculated between green and red labeled repair (nano)foci. E) Distance between (compartmentalized) red and the corresponding green labeled repair (nano)foci. Images show examples for colocalizing (black) and non-colocalizing foci (grey) with the respective centroid to centroid distance in µm. F) Volume or DNA content of (compartmentalized) red foci divided by the volume or DNA content of the corresponding green labeled foci. A summary of statistics is given in Table S 3.

In order to identify colocalizing red and green foci, that correspond to the same structure, the segmented foci were compartmentalized with a maximum distance (centroid to centroid) of 0.1 μm, since foci with a greater distance were identified as clearly adjacent and not colocalizing (an example is shown in Figure 10E). Foci with a distance below 0.1 μm will be referred to as colocalizing foci. This value is below the resolution of 3D-SIM, but still valid due to the use of different fluorophores. The distance between colocalizing red and green foci was ~ 62 nm for both X-ray doses. To determine the similarity between colocalizing foci, we measured the volume and the DNA content by using the DAPI intensities and the genome size (for details on the calculation see Figure 4). Dividing the DNA content or volume of the red focus by the respective value of the corresponding green focus should result in a value of 1 for perfectly identical foci. We measured a volume ratio of 1.077 and a DNA content ratio of 1.076, indicating that the red foci are slightly larger than the green foci, which results in a slightly higher DNA content. This slight deviation might be a result of the optical differences of the fluorophore wavelengths.

The way of analysis and the observations served then as a maximum colocalization control for the identification and comparison of replicons with repair (nano)foci.

5.4.4. Replicons and repair (nano)foci as elementary units of chromatin organization

Next, we tested whether we could identify replicons and repair (nano)foci that colocalize in the same way as red and green repair (nano)foci in the maximum colocalization control. Calculations to determine how much of the genome is covered by replicons or repair (nano)foci (sum of DNA content of all foci in one nucleus divided by DNA content of the nucleus) revealed that for C2C12 cells maximally 7.53% were covered by replicons and 6.4% covered by repair (nano)foci (Table S 4), which is of course highly dependent on the X-ray dose. For the human cell lines the percentages were even lower, for HeLa cells 4.26% for replicons, 3.1% for repair(nano)foci and for HeLa Kyoto 6.29% for replicons and 3.54% for repair (nano)foci. Since both replication and repair structures are in our experiment more or less independent and the genome coverage is so low the probability of them colocalizing is likely not very high, which was confirmed by visual inspection, as only occasionally replicons would overlap with repair (nano)foci.

Before we started this kind of analysis we assumed we can observe one out of three options. 1) we would find replicons and repair (nano)foci in the same position and they would have the same size, 2) we would find them in the same position but their sizes would be completely different or 3) they would not colocalize and they would have different sizes. Visual inspection alone was not effective enough to identify colocalization. Since the compartmentalization approach with a maximum distance of < 0.1 μm gave accurate results for the maximum colocalization control, images with simultaneously stained replicons and repair (nano)foci were analyzed in the same way. Indeed, we could identify

colocalizing foci, defined by a maximum distance (centroid to centroid) of < 0.1 μm (Figure 11A). We then determined the fraction of replicons colocalizing with a repair (nano)focus. The fraction increased with increasing X-ray doses as expected and was 0.83-1.1% for HeLa cells irradiated with 2 Gy, 1.33-1.49% for HeLa cells irradiated with 5 Gy, for HeLa Kyoto 1.27-1.85% and 2.19-2.41% and for C2C12 cells 1.61-1.94% with 2 Gy and 1.93-2.79% with 5 Gy irradiation (Figure 11B). Even with the highest fraction in C2C12 cells only around 120 out of 4275 replicons colocalize with a repair (nano)focus in one cell.

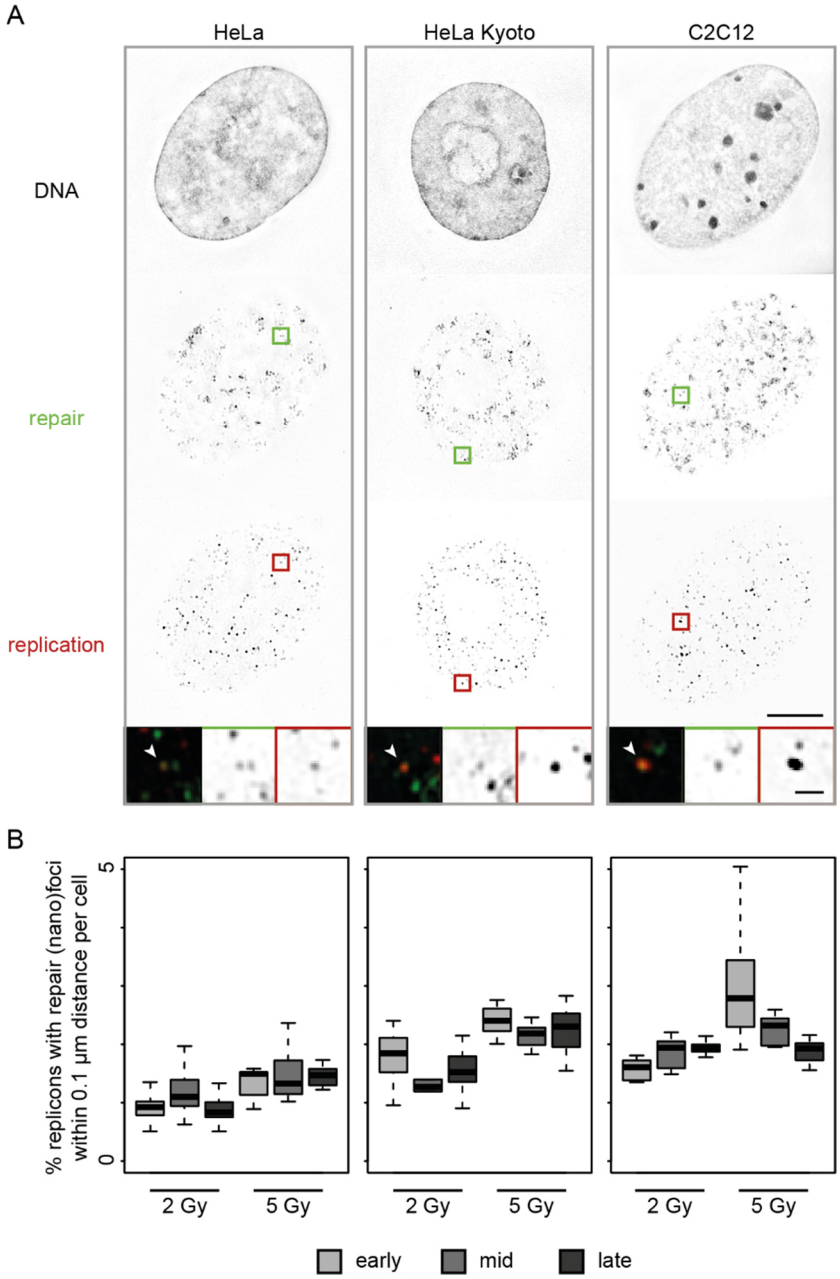

Figure 11: Replicons and repair (nano)foci can colocalize. A) Representative images of replicons and repair (nano)foci and colocalizing replicons and repair (nano)foci (cropped regions) in HeLa, HeLa Kyoto and C2C12 cells. Arrowheads point to colocalizing foci. Scale bar 5 µm in full images, 0.5 µm in cropped regions. B) Percentage of replicons that colocalize with repair (nano)foci, meaning replicons with a repair (nano)focus within 0.1 µm distance (centroid to centroid).

Nevertheless, almost all analyzed cells contained colocalizing foci and in total we could analyze a high number of colocalizing foci. As described for the maximum colocalization control we calculated the DNA content of all foci (Figure 12A, Table S 6). The DNA content of replicons was 27.5-38.2 kbp for HeLa cells, 39.4-55.4 for HeLa Kyoto and 61.6-106 kbp for C2C12 cells. The DNA content of repair (nano)foci was 71.2-91.2 kbp for HeLa cells, 83.3-85.8 kbp for HeLa Kyoto and 104.6-118.6 kbp for C2C12 cells. For the DNA content calculations, we use the genome size in G1, which would be double if the cells were in G2. In the worst case this means that our DNA content calculations are off by factor 2, if all cells were in G2. This however does not affect the comparison between replicons and repair (nano)foci since the same genome size was used to calculate their DNA content. The average inter-origin distance for HeLa Kyoto and C2C12 cells is between 160 and 190 kbp. A replicon should therefore have the same DNA amount, but our calculations give only around half of this size. The time a replicon needs to replicate the given DNA amount (lifetime) is estimated to be 33 to 57 min (mouse, human), based on inter-origin distance and replication fork speed (Chagin et al., 2016). Our labeling time by nucleotide incorporation was 15 min, which corresponds to less than half the time needed to replicate a full replicon. This might explain the difference between fiber data and super-resolution microscopy data. Besides this, the sizes measured from DNA fibers might well result in different DNA amounts from replicons in nuclei, since measurements on stretched fibers are likely more precise than on folded chromatin within the nucleus. The DNA dye used to estimate the DNA amount however does not influence the calculations negatively since we don´t observe a difference in DNA amount using different DNA dyes (Alexander Rapp, personal discussion). Despite these difficulties, the measurement of DNA content based on the intensity of the DNA dye, gives a good estimate within the same order of magnitude given by DNA fiber analysis. The DNA content of repair (nano)foci for HeLa cells irradiated with 10 Gy X-ray calculated by Natale et al., 2017 (in press) was around 40-160 kbp (median 75 kbp). Since we do not observe a massive difference between cells irradiated with 2 and 5 Gy X-ray doses, also not in their volume (Figure S 2), we can assume that the DNA content of individual repair (nano)foci is independent of the dose. Our data on HeLa cells are exactly within that range and the same applies to HeLa Kyoto and C2C12 cells. On a global level the DNA content of replicons seemed slightly smaller than that of repair (nano)foci but was nevertheless in the same order of magnitude.

Next, we looked only at colocalizing replicons and repair (nano)foci, since we expect those to be the most comparable in context of chromatin organization, if they are localized on the same basic chromatin structure. As described before we calculated the DNA content and divided the DNA content of replicons (red labeled) by that of repair (nano)foci (green labeled) (Figure 12B). For the maximum colocalization control the ratio was close to 1. The variation of values for colocalizing replicons and repair (nano)foci was higher, but the median values were 0.37-0.56 for HeLa, 0.81-1.2 for HeLa Kyoto and 0.42-1.02 for C2C12 cells. This fits to what we observed before, that the DNA content of replicons tends to be slightly smaller than that of repair (nano)foci. However, we find that the resemblance in

size between both structures too remarkable to be random. We also examined the volume of replicons and repair (nano)foci in the same way, this analysis gave similar results (Figure S 2).

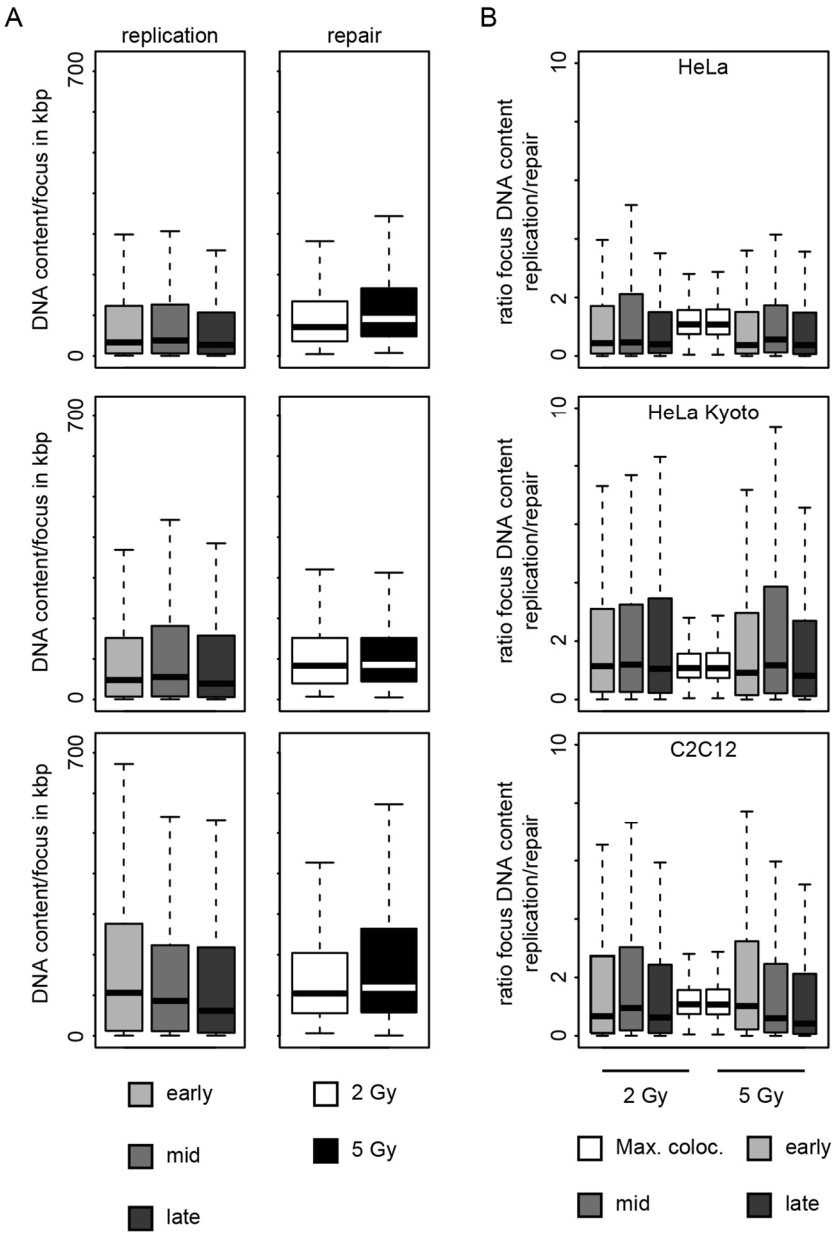

Figure 12: DNA content of replicons and repair (nano)foci. A) DNA content of replicons and repair (nano)foci in HeLa, HeLa Kyoto and C2C12 cells. Significant differences in DNA content between replicons from different S-phase stages and between repair (nano)foci from different X-ray doses were detected ($p < 0.05$) due to extremely high n numbers ($n > 58500$). B) Ratio of DNA content of replicons colocalizing with a repair (nano)focus in comparison to the maximum colocalization control shown in Figure 10. A summary of statistics is given in Table S 6.

Replicons labeled by nucleotide incorporation will always represent a mixture of longer and shorter stretches of chromatin since origins of replication do not all start at the same time. Some will have been already active before the nucleotide was added, so they are labeled completely for the duration of the labeling (unless they finish during the labeling time), others will start during the incubation time, which means they will be shorter. However, if the time for nucleotide incorporation is exceeded,

adjacent replicons are already activated leading to merging of neighboring replicons and artificially larger objects and replicon sizes. Thus, with the 15 min labeling time, we made a safe choice, which might lead to underestimation of the replicon size but more importantly we do not overestimate them. This would also explain the size difference between replicons and repair (nano) foci. Based on our observations we can assume that replicons and repair (nano)foci are based on the same chromatin structure, that dictates their sizes. Rao et al 2014 studied chromatin interaction using Hi-C and describe loops of sizes around 185 kbp which is higher than what we observe, but very close to the inter-origin distance (188.7 kbp for HeLa Kyoto and 161.7 kbp for C2C12 cells). Assuming that only one origin of replication per chromatin loop is activated, as suggested by Lob et al., 2016, the described loops in both studies might be the same. Using Hi-C to study chromatin contacts has the great advantage of a high resolution and knowing the "identity" of the sequence in contact but they investigate enriched and conserved peaks in a full cell population and not only single cells. It may be that loops in the smaller range are more dynamic and that larger loops are sub-divided into smaller, more dynamic loops. Both cannot be detected in Hi-C studies. Studying chromatin structures with super-resolution microscopy the way we do might be unconventional but has the advantage of not being limited to conserved chromatin structures in populations, since the images represent a "snap-shot" of single cells that allow to capture all chromatin structures – dynamic or conserved. DNA replication is the only process that regularly accesses all of the genome and can therefore label every chromatin segment during every cell cycle. Thus, it is likely that labeling DNA replication by nucleotide incorporation without exceeding the pulse length would allow to visualize chromatin organization in a microscopic approach. γH2AX may not be the best option to detect single double strand breaks in super resolution imaging, but for studying chromatin organization it is well suited. The single repair (nano)foci in a cluster have been proposed to be either single nucleosomes or clustered DNA damage due to the ion beam irradiation (Lopez Perez et al., 2016). Alternatively, they might be caused by γH2AX spreading being limited by the underlying chromatin structure, leading to discontinuous phosphorylation of H2AX around a single DSB (Natale et al., 2017, in press). Since we and Natale et al. used X-ray radiation to damage the cells, which is commonly accepted not to cause complex damage compared to ion beams, we assume to observe discontinuous phosphorylation. This is also supported by the afore mentioned TUNEL and phospho-Ku70 stainings by Natale et al.,2017 (in press) indicating that γH2AX (nano)foci cluster and not single(nano)foci correspond to single DSBs. If γH2AX spreading is limited by the underlying chromatin structure, and our observations suggest that progression of DNA replication underlies the same restriction, the question is what acts as a boundary. A potential candidate could be CTCF, as it is crucial for efficient γH2AX spreading/clustering and DNA damages response (Natale et al., 2017, in press). CTCF knockout is lethal during embryonic development (Moore et al., 2012). It has also been shown that interference with CTCF binding sites or

CTCF knockdown, especially in combination with knockdown of components of the cohesin complex, has severe effects on chromatin loop organization (Sanborn et al., 2015, Tark-Dame et al., 2014). These observations stress the importance of CTCF and cohesin as architectural proteins for chromatin function and organization. Not all of the contact domains identified by Rao et al., 2014 or Dixon et al., 2012 are accompanied by CTCF/cohesin binding sites, proposing that they are not always involved in chromatin loop formation and that other factors might play a role. New chromatin models suggest that cohesin and possibly CTCF bind chromatin and then extrude it until they encounter a boundary, which can be another cohesin complex or CTCF (Fudenberg et al., 2016, Sanborn et al., 2015, Dekker and Mirny, 2016). These models can recapitulate Hi-C maps, predict changes by altered CTCF binding sites and apparently work best with chromatin loops of sizes between 100-200 kbp. It has also been suggested that TADs are stable and conserved forms of chromatin organization, while loops within TADs are rather dynamic and temporary (Dekker and Mirny, 2016).

5.5. Conclusions

Predictions of inter-origin distances of 140-300 kbp made by Lob et al., 2016 reflect experimental data of 188.7 kbp in HeLa Kyoto perfectly. Hi-C data gave chromatin loops of ~ 185 kbp (Rao et al., 2014). The 1 Mbp domain is assumed to consist of clusters of 100 kbp sized domains or loops (Cremer et al., 2000). Microscopy data from Natale et al., 2017 (in press) result in 40-160 kbp sized elementary structural units of DNA repair and our data are in the same range for both replication and repair structures. All these predictions and observations strongly point to the existence of an elementary unit of chromatin organization in this order of magnitude. Taken together we propose that replicons and repair (nano)foci correspond to the same basic unit of chromatin structure. This unit is to be ranked between the beads on a string and higher order chromatin structures such as Mbp ranged TADs and could be present in cells in the form of loops with an architectural factor maintaining their shape and size (Figure 13).

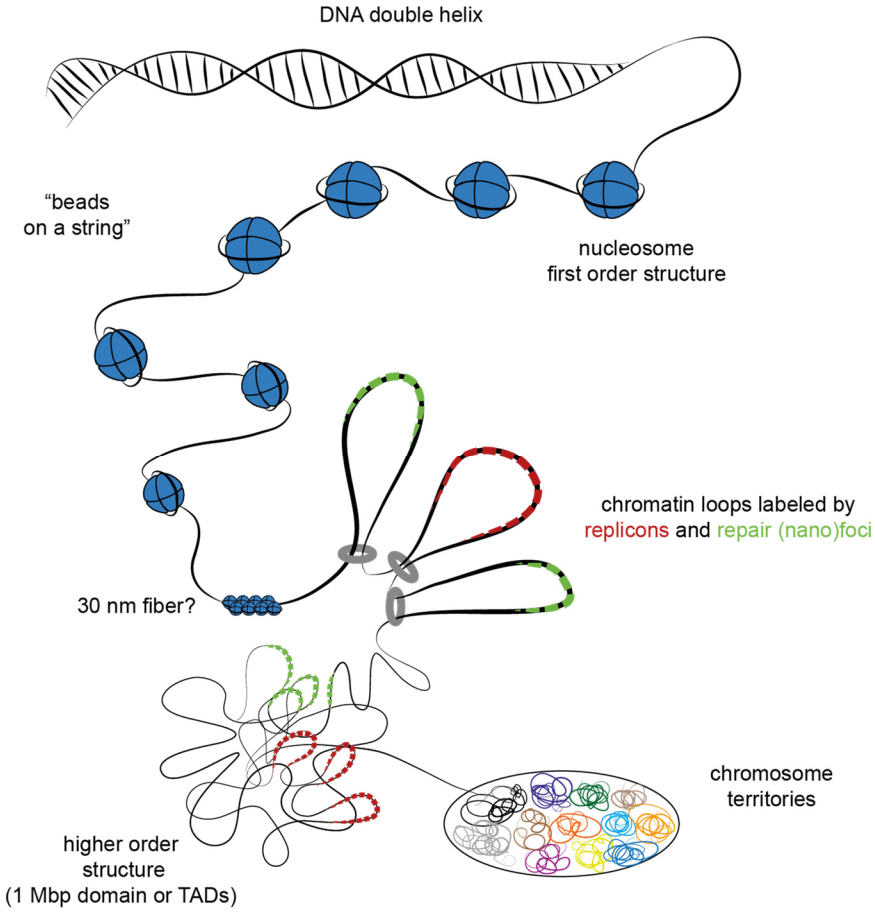

Figure 13: Model of chromatin organization from the DNA double helix to chromosome territories, with chromatin loops labeled by replicons and repair (nano)foci restricted by a structural protein like CTCF and/or cohesin.

Further controls would be to test whether the DNA content of replicons changes, when they are labeled by varying labeling times, for example 15, 30 or 60 min for human cells. A labeling time with 60 min corresponds to the replicon lifetime in HeLa Kyoto and might already lead to labeling of adjacent

replicons and therefore to larger objects if they merge. Depending on the outcome it might be interesting to repeat the whole experiment with simultaneous staining of replicons and repair (nano)foci within the same cell with a longer labeling time and a higher X-ray dose, for example 10 Gy, which increases the chances of colocalizing foci. This experimental design might result in even stronger similarity of replicons and repair (nano)foci, supporting the here described results and the existence of a common underlying chromatin structure.

6. DNA repair kinetics and replication timing of repetitive elements

6.1. Introduction

6.1.1. Repetitive elements in humans and mice

In many species, large parts of their genome are comprised of repetitive elements. For humans, the proportion is estimated to be more than 50%, which stands in contrast to only around 1.2% coding for proteins and for mice around 40% with 1.4% protein coding sequences (Shapiro and von Sternberg, 2005, Lander et al., 2001, Mouse Genome Sequencing et al., 2002). Despite their abundance, their function is not completely understood. The discussions about their usefulness have been going on for decades (for example Orgel and Crick, 1980, Doolittle and Sapienza, 1980), though more and more studies describe functions of repetitive elements (reviewed in Shapiro and von Sternberg, 2005). We will give examples thereof in the individual chapters of the repetitive elements.

There are different types of repetitive elements in the mammalian genome. Some are transposable elements like long interspersed nuclear elements (LINEs), short interspersed nuclear element (SINEs) or LTR retrotransposons, others are highly repetitive elements like satellites or telomeric repeats. These highly repetitive elements occur in tandem repeats, meaning a certain sequence unit is adjacently repeated for multiple times, which can result in DNA regions with the same sequence pattern in the order of Mbp, while LINEs and SINEs are scattered across the genome mostly as single copies (Vissel and Choo, 1989, Prak and Kazazian, 2000).

6.1.2. Satellite DNA

Satellite DNA is located in heterochromatic regions, such as the pericentromere and the centromere. Human satellite III and mouse major satellite are examples of pericentromeric heterochromatin while human α-satellite and mouse minor satellite can be found in centromeres (Jarmuz et al., 2007, Mouse Genome Sequencing et al., 2002, Guenatri et al., 2004, Wu and Manuelidis, 1980, Waye and Willard, 1986, Joseph et al., 1989, Wong and Rattner, 1988).

Mouse major satellite DNA reaches up to 8 Mbp with AT rich 234 bp units. It is localized in pericentromeric regions of all chromosomes, except for the Y chromosome. In interphase nuclei, major satellite DNA can be found colocalizing with "DAPI bright spots". These “spots” are called chromocenters, which consist of clusters of heterochromatic regions of several chromosomes (Mouse Genome Sequencing et al., 2002, Guenatri et al., 2004).

Satellite III in humans has a 5 bp unit size and its presence was shown in 7 autosomes (chromosomes 1, 9, 13, 14, 15, 21 and 22) and the Y chromosome (Jarmuz et al., 2007).

Despite their location in constitutive heterochromatin and the general assumption that this chromatin type is not transcriptionally active, pericentromeric satellites (and also centromeric) have been shown

to be transcribed in various instances (Saksouk et al., 2015), suggesting that there might be more to them than just “junk”.

Valgardsdottir et al., 2008 reported transcription of human satellite III in response to different stress factors, such as for example UV-C, DNA damaging chemicals, osmotic imbalance, oxidative stress and hypoxia. They discuss that next to a possible role in stabilizing pericentromeric chromatin regions (Jolly et al., 2004), satellite III transcripts might be involved in a general process to recover from stress including alternative splicing and modulation of gene expression of factors, that are important for stress response.

In early embryonic development of mice, major satellite DNA is transcribed during a restricted period of time (2-cell to 8-cell stage). This time-point coincides with the formation of chromocenters. Interference with this transcription leads to developmental arrest, suggesting that the transcripts are involved in the stabilization of heterochromatin (Probst et al., 2010).

6.1.3. Interspersed elements

LINEs and SINEs are retrotransposons. These are DNA elements that are distributed by a copy-and-paste mechanism, where the sequence is first transcribed into RNA, then converted to cDNA and integrated into a new position into the genome (Cordaux and Batzer, 2009).

LINEs are wide spread in many eukaryotic species. The only active member of the family, LINE1, is simultaneously the only autonomous retrotransposon in humans (Beck et al., 2011). It consists of a consensus sequence of around 6000 bp, including two open reading frames encoding for proteins that are necessary for retrotransposition (Feng et al., 1996, Mathias et al., 1991, Martin et al., 2003, Khazina et al., 2011). LINE1 alone makes up around 17% of the human genome and can be found in AT-rich and gene poor/heterochromatic regions. It is therefore associated with G banding and DAPI bright bands of metaphase chromosomes (Lander et al., 2001, Korenberg and Rykowski, 1988).

A member of the short interspersed nuclear element (SINE) family is the Alu element with a 280 bp consensus sequence. Alu is specific to primates but similar SINEs can be found in other organisms, such as B1 in rodents (Quentin, 1994). The Alu sequence, in contrast to LINE1, does not encode for proteins but contains a RNA Polymerase III promoter (Lander et al., 2001). Additionally Alus are thought to utilize the LINE1 derived proteins for retrotransposition (Dewannieux et al., 2003). Alus comprise with over 1 million copies around 10% of the human genome and can be found in gene-rich/euchromatic regions and correspond to R banding of metaphase chromosomes (Korenberg and Rykowski, 1988).

LINE1 and Alu activity is a double-edged sword. Due to their ability to “jump” into any position of the genome, LINE1 and Alu are a potential thread towards genome stability. By direct insertion of the transposable element into or close to a gene they can interfere with gene activity, disrupt exons and even influence splicing (Beck et al., 2011). Additionally, because they are so abundant, their sequences

may be used in homologues recombination in a non-allelic fashion, leading to insertions or deletions in the damaged region (Burwinkel and Kilimann, 1998, White et al., 2015). Both LINE1 and Alu (disruptive) insertions have been found in tumor suppressor genes in several cancer types (Lee et al., 2012).

On the other hand, there have been examples where Alu and LINE1 activity is beneficial or functional for the organism. While mostly silenced in somatic cells, LINE1 activity can occur and is required at specific times during early embryonic development (Beraldi et al., 2006). Untimely reactivation however can lead to severe defects such as male infertility (Barau et al., 2016).

Alu transcripts can be found in the nucleolus. Depletion of those transcripts leads to a disruption of the nucleolus and decreased rRNA transcription while enrichment leads to the formation of larger nucleoli accompanied by an increase in rRNA transcription. The authors suggest that the Alu transcripts play an important role in regulating the nucleolar function (Caudron-Herger et al., 2015).

The mobilization of LINEs and Alus can also lead to genomic diversity. The LINE1 derived proteins are able to transfer other sequences (not only LINEs and Alus) to new positions. These events can give rise to new proteins and protein functions. An impressive example for this is the combination of two genes, coding for the proteins CypA (Cyclophilin A) and TRIM5-α (tripartite motif-containing protein 5 α), in owl monkeys. TRIM5-α usually blocks HIV-1 (human immunodeficiency virus type 1) infection, whereas CypA is utilized by HIV-1 to prevent the host from blocking the infection. The fusion created a TRIM5-CypA fusion protein, which allows resistance towards HIV (Sayah et al., 2004).

In summary, repetitive elements make up a large part of the genome of many organisms. Although they have been previously described as “junk” DNA, more and more studies are published nowadays, that describe functions of repetitive elements. In fact, their importance might still be underestimated.

6.2. Aim of this study

Genome preservation by complete DNA duplication (DNA replication) prior to mitosis and by correct DNA repair (via various mechanisms) is of most importance for an organism and this includes the preservation of repetitive elements. While most studies on DNA repair or replication did not focus on repetitive elements, we tried to fill part of this gap by investigating DNA replication timing and DNA repair kinetics in a selection of repetitive elements (pericentromeric satellites, LINEs and SINEs). Depending on the associated chromatin type or the GC content there might be differences in both aspects. To analyze the DNA damage repair kinetics upon ionizing radiation we previously used γH2AX as a damage marker in a genome wide ChIP-Seq approach (Natale et al., 2017, in press). Our data suggested that γH2AX coverage in specific repetitive DNA elements changes over time. Since repetitive elements are not always well represented in genome wide sequencing data we were following a microscopic approach to investigate their replication and repair dynamics. The basis for this approach is the combination of a γH2AX immunofluorescence staining with fluorescence in situ hybridization (together immuno-FISH, for example Solovei and Cremer, 2010) to visualize DNA damage/replication sites and specific sequences simultaneously in the same cell.

6.3. Material & Methods

6.3.1. Cell culture

Cultures of C2C12 mouse myoblasts (ATCC CRL-1772) and HeLa cells (ATCC CCL-2) were grown at 37 °C and 5% CO_2 in DMEM supplemented with 50 μg/ml gentamycin, 20 mM L-glutamine and 10% FCS for HeLa cells or 20% FCS for C2C12 cells. For experiments involving immuno-stainings cells were grown on glass coverslips.

6.3.2. Irradiation

For X-ray irradiation cells were exposed to single doses of 2 Gy (90 kV, 33.7 mA) using a GE ISOVOLT Titan E X-ray machine.

6.3.3. Probe generation for fluorescence in situ hybridization

Probes for Alu elements were generated by first amplifying Alu elements from HeLa genomic DNA (gDNA) via PCR using specific Alu primers, followed by a labeling PCR with the same primers, biotin-labeled dUTP and the previous PCR product (diluted 1:50 in ddH_2O) as DNA template. The product of the labeling PCR was then purified with the QIAquick PCR Purification Kit (Qiagen). Mouse major satellite probes were generated by PCR using C2C12 genomic DNA and specific MaSat primers. All PCR reaction and cycling conditions are listed in Table 1 and Table 2.

AluF	GGATTACAGGYRTGAGCCA (Liu et al., 1993)
AluR	RCCAYTGCACTCCAGCCTG (Liu et al., 1993)
MaSatF	AAAATGAGAAACATCCACTTG (Frauer et al., 2011)
MaSatR	CCATGATTTTCAGTTTTCTT (Frauer et al., 2011)

Table 1: PCR reaction conditions for generation of FISH probes.

PCR reactions	Alu (template)	Alu (labeling)	MaSat
PCR buffer*	1x	1x	1x
dATP/dGTP/dCTP	0.2 mM each	0.2 mM each	0.4 mM each
dTTP	0.2 mM	0.15 mM	-
dUTP-biotin	-	0.05 mM	0.08 mM
primer F/R	1 μM each	1 μM each	0.2 μM each
Taq polymerase**	1.5 μl	1.5 μl	1 μl
DNA template	100 ng gDNA	1 μl 1:50 PCR product	100 ng gDNA
Final volume	to 50 μl	to 50 μl	to 50 μl

*10x PCR buffer: 100 mM Tris-HCl pH 8.3, 500 mM KCl, 15 mM $MgCl_2$

**Cardoso Lab, TU Darmstadt, Germany

Table 2: PCR cycling conditions for generation of FISH probes.

PCR cycling conditions	Alu	MaSat
Initial denaturation	94 °C for 4 min	98 °C for 10 min
1. Denaturation	94 °C for 1 min	98°C for 1 min
2. Annealing	*57 °C/65 °C for 1 min	56 °C for 1 min
3. Extension	72 °C for 3:30 min	72 °C for 2 min
No. of cycles steps 1. - 3.	35	35
Final extension	72 °C for 10 min	72 °C for 5 min

*temperature for template PCR/temperature for labeling PCR

The probes for LINE1 and for chromosome 1 specific satellite III were generated by nick-translation of plasmids containing the respective sequences: pLRE-eGFP (Garcia-Perez et al., 2010, a gift from John V. Moran, LRE wildtype LINE1 element) and pUC 1.77 (Cooke and Hindley, 1979, chromosome 1 specific satellite III). Both probes were labeled with biotin-labeled dUTP during nick translation. The nick translation reaction conditions were 50 mM Tris-HCl pH 8, 5 mM $MgCl_2$, 0.5 mg/ml BSA, 10 mM β-mercapto-ethanol, 0.04 mM dUTP-biotin, 0.05 mM each dATP/dGTP/dCTP, 0.32 U DNaseI (D5025, Sigma-Aldrich), 10 U Klenow fragment (M0210, New England BioLabs Inc.), 1 μg plasmid DNA in a total volume of 100 μl. The reaction was incubated for 90 min at 15 °C and stopped with 5 μl 0.5 M EDTA.

All probes were sheared with a Covaris S220 (according to the manufacturer's instructions: 150 bp program in microTUBEs, 520045, Covaris Inc.) in 50-65 μl aliquots, to reduce the fragment size. The probe amounts (see below) needed for FISH were then ethanol precipitated with sodium acetate, washed with 70% EtOH, air dried at room temperature, dissolved in hybridization solution with formamide (50-70% formamide, 2x SSC, 10% dextran sulfate, pH7) for Alu and LINE1 FISH on metaphase spreads or without formamide (10 mM Tris-HCl, 3 mM $MgCl_2$, 50 mM KCl, 10 μg/ml gelatin, 2x SSC, Celeda et al., 1992 and Celeda et al., 1994) for FISH on interphase nuclei and satellite III and MaSat FISH on metaphase spreads. The probe amounts needed per FISH sample were 250 ng LINE1 probe + 1 μg fish sperm DNA, 200 ng Alu probe + 1 μg fish sperm DNA, 50 ng satellite III probe or 5 μl MaSat PCR reaction + 1 μg fish sperm DNA per sample. For FISH on interphase nuclei the probes were dissolved in 15 μl hybridization solution and for metaphase spreads in 30 μl hybridization solution. After dissolving the probes, they were denatured at 80 °C for 5 min.

6.3.4. Preparation of metaphase spreads

For the preparation of metaphase spreads, HeLa and C2C12 cells were treated with 0.1 μg/ml colcemid for 2 h. Cells were harvested by trypsinization and incubated with 75 mM KCl (hypotonic shock) for 20 min at RT. Fixation followed in drop-wise added ice-cold methanol:acetic acid (ratio 3:1) and incubation for 30 min on ice. This step was repeated 2 times. For chromosome spreading, the cell suspension was dropped onto a wet microscopy slide from a height of approximately 25 cm. The slide was then air dried overnight. For metaphase FISH the slides were rehydrated in ddH_2O for 10 min, digested with 0.005% pepsin (165 U/ml, P6887, Sigma-Aldrich) in 0.01 M HCl for 10 min at 37 °C, then dehydrated in 70 and 100 % ethanol for 5 min each and again air dried overnight.

6.3.5. Fluorescence in situ hybridization on metaphase chromosomes

Equilibration of metaphase spreads was performed with the respective hybridization solution (with formamide for Alu and LINE1 probes, without formamide for chromosome 1 specific satellite III and mouse major satellite probes, composition described above) at room temperature for 30 min. The solution was removed before combining probes with the metaphase spreads in a humid chamber, denaturation was performed at 70-80 °C in a water bath for 5 min and the hybridization followed overnight at 37-42 °C. Post hybridization washing steps were done with 2x SSC and 0.1x SSC at 42 °C. Slides were blocked with 1% BSA/4x SSC for 30 min and FISH probes detected with streptavidin Alexa Fluor 488 (S11223, Molecular Probes/Thermo Fisher Scientific, 1:800) in 1% BSA/4x SSC for 30 min. DNA counterstaining was performed with DAPI (1 μg/ml) for 10 min and the coverslips mounted in Mowiol 4-88/2.5% DABCO and allowed to harden at room temperature overnight.

6.3.6. Combination of replication staining (EdU Click reaction) or immunofluorescence staining of γH2AX with fluorescence in situ hybridization

Cells were pulse labeled with 10 μM EdU for 15 min or irradiated with 2 Gy X-ray radiation. For replication stainings fixation with 3.7% formaldehyde/1x PBS followed directly after the pulse labeling and for irradiated cells 30 min, 3 h or 24 h post irradiation. The cells were permeabilized and pre-denatured with 0.5% Triton X-100 in 1x PBS for 15 min, 0.1 M HCl for 15 min and 0.5% Triton X-100/1x PBS for 15 min.

EdU was detected as described in the supplier's instructions using the EdU Click-594 ROTI kit (7776.1, Carl Roth) for imaging. The dye azide was used in final dilution of 1:2000.

For immuno-staining of γH2AX, irradiated cells were blocked with 1% BSA/1x PBS for 30 min, incubated with the primary antibody mouse anti histone H2AX phospho Ser139 (clone JBW301, 05-636, Upstate/Millipore, 1:200) in 1% BSA/1x PBS for 1 h and incubated with the secondary antibody donkey anti mouse IgG Cy5 (715-175-150, Jackson ImmunoResearch, 1:250) in 1% BSA in 1x PBS for

1 h. Both stainings were post-fixed with 1% formaldehyde/1x PBS for 10 min before proceeding with FISH.

The cells were equilibrated with hybridization solution without formamide (composition as described above) at room temperature for 30 min. The solution was removed before combining the probes with the cells in a humid chamber, samples were denatured at 80 °C in a water bath for 5 min and hybridized overnight at 42 °C. Post hybridization washing steps were done with 2x SSC and 0.1x SSC at 42 °C. FISH probes were detected with streptavidin Alexa Fluor 488 (S11223, Molecular Probes/Thermo Fisher Scientific, 1:800) in 1% BSA/4x SSC for 30 min. DNA counterstaining was performed with DAPI (1 μg/ml) for 10 min and the coverslips mounted in Mowiol 4-88/2.5% DABCO and allowed to harden at room temperature overnight.

6.3.7. Microscopy

Confocal imaging was performed using a Perkin Elmer VoX-1000 Spinning Disk microscope with a 60x/1.4 NA/oil CFI Apochromat TIRF objective or using a Zeiss Axiovert 200 with a 100x/1.4/oil NA Plan-Apochromat objective (metaphase spreads).

6.3.8. Image analysis for repair kinetics of repetitive elements

Image analysis was performed using the image analysis software Perkin Elmer Volocity 6.3. The following steps in the measurements tab were used to segment γH2AX foci and satellite regions (see also Figure 14B):

Find objects ("nucleus") using the DAPI channel (method "automatic", minimum object size: 400 μm^3), fill holes in object, dilate with 2 numbers of iterations, fill holes in object. Find objects ("repair foci") using the Cy5 channel, method "SD"(lower limit: set to optimal value for all cells within one condition", minimum object size: 0.3 μm^3), remove noise from objects with fine filter, separate touching objects (object size guide: 0.3 μm, filter population: volume > 0.3 μm^3), exclude "repair foci" not touching "nucleus". In case of satellite images: Find objects ("satellite") using the 488 channel, method "SD" (lower limit: set to optimal value for all cells within one condition", minimum object size 0.3 μm^3), remove noise from objects with fine filter, separate touching objects (object size guide: 1 μm, filter population: volume > 0.3 μm^3), exclude "satellite" not touching "nucleus".

6.3.9. Colocalization analysis for replication timing of repetitive elements

To analyze at which S-phase stage the respective repetitive elements are replicated, the cells were categorized into early, mid or late replication patterns using the pattern of the EdU signal. For quantification of the degree of colocalization the H_{coeff} was used as described by Herce et al., 2013. Therefore, a nucleus mask was created based on the DAPI channel using ImageJ (Gaussian blur with sigma=2-10, autothreshold with method=Otsu, erode with 10 iterations, dilate with 10 iterations, Gaussian blur with sigma=1). Then, using Priithon a local median filter was applied to the channels that are to be compared. This removes background. Afterwards the H_{coeff} is calculated for each plane. For the graphs a mid-nuclear section of each image was selected. The steps with example images are shown in Figure 14A.

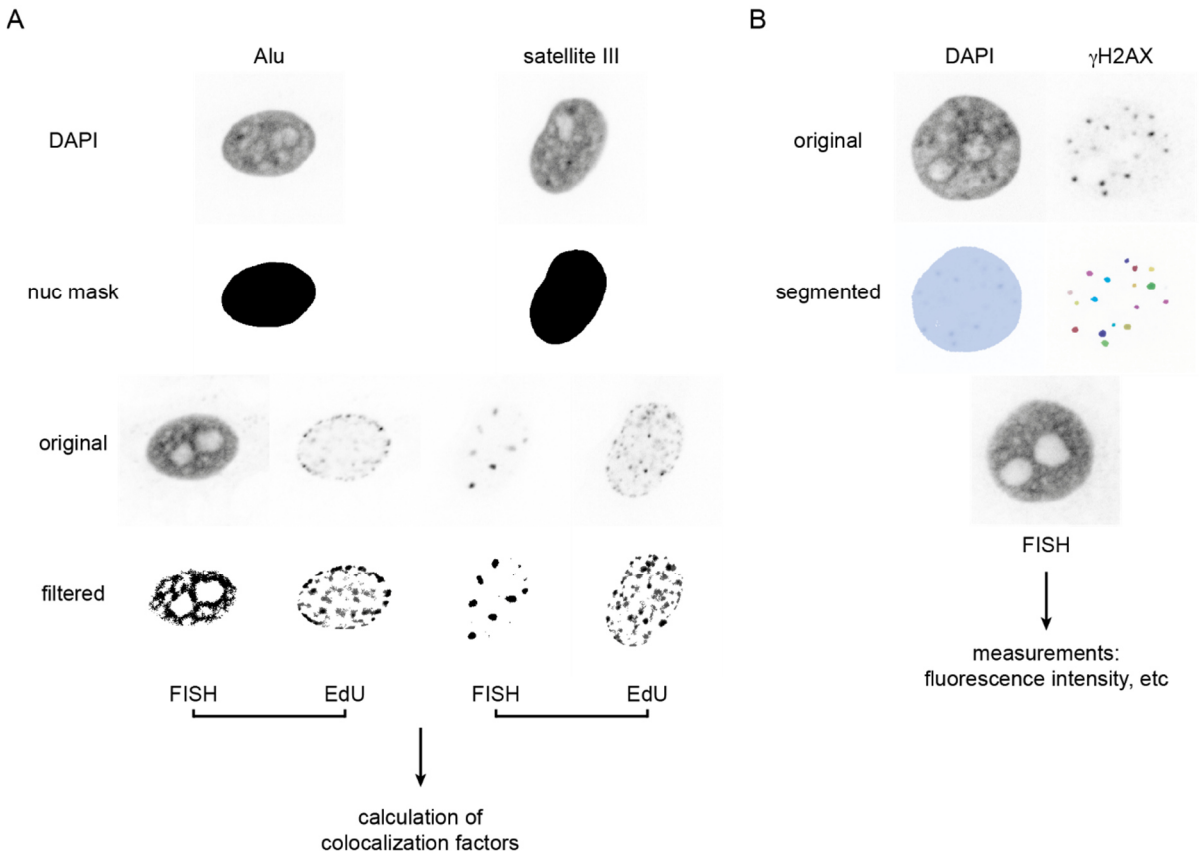

Figure 14: H_{coeff} analysis and segmentation of γH2AX foci. A) steps of the colocalization analysis with example images for replication studies. The DAPI channel is used to generate the nuc(leus) mask. Only within the nuc mask the other channels are filtered while maintaining the original intensities, everything outside the nuc mask is set to zero. Colocalization factors are then calculated from the filtered images. B) steps of the segmentation of γH2AX foci. The DAPI channel is used to segment the nucleus, γH2AX foci are segmented (different colors refer to different objects). Objects outside the nucleus are excluded. Intensities etc. from all channels are then measured within the segmented focus/nucleus.

6.4. Results & Discussion

6.4.1. Repetitive elements and their localization in chromatin

First, we verified that our probes were specific to the respective repetitive elements and visualized their chromatin association by hybridizing the probes to metaphase chromosomes of human HeLa and mouse C2C12 cells.

Alu elements are associated with gene-rich, euchromatic regions, R banding and DAPI-poor banding. Alu banding patterns can be used to identify chromosomes, since the pattern is individual for every chromosome (Korenberg and Rykowski, 1988). Hybridization of the Alu probe (Figure 15) showed the FISH signal in distinct bands as expected, which would allow the identification of individual chromosomes. Line profiles showed a drop in DAPI intensity when the Alu intensity increased. Alu was therefore anticorrelated to DAPI banding in chromosomes as it is described in the literature. In contrast to Alu elements, LINE1 elements are located in AT-rich (hetero)chromatin and therefore related to G banding and DAPI-bright regions (Korenberg and Rykowski, 1988). As expected the LINE1 signal in Figure 15 exhibited a banding pattern and the line profiles showed that major increases in DAPI intensity correlated to increases in LINE1 intensities except for centromeric regions.

Satellite III DNA in humans and major satellite DNA in mice belong to constitutive heterochromatin. Both satellites are pericentromerically located. The pUC 1.77 probe is specific to the satellite III regions of human chromosome 1. In a diploid cell line 2 signals can be expected. HeLa cells however are aneuploid. SKY analysis (Natale et al., 2017, in press) showed that chromosome 1 can be expected approximately 4 times per cell. In our metaphase FISH, more than 4 hybridization sites were visible, which were located close to the centromere of the chromosomes as expected. The probe hybridized to a large chromosome, which was most likely chromosome 1 and to at least one smaller chromosome. Celeda et al., 1994 showed a similar result under similar hybridization conditions and suggested that the pUC 1.77 probe has additional minor binding sites to most likely chromosomes 9, 16 or Y as chromosome 9 and Y also have a satellite III repeat. Since the HeLa cell line was derived from a female patient this cell line does not have a Y chromosome. It can therefore be excluded. Chromosome 16 has not been reported to have a satellite III region, however, it contains a satellite II region. Satellite II has a consensus sequence, that is rather similar to satellite III, though with more sequence variations (Warburton et al., 2008), which could explain the pUC 1.77 probe binding to this region. Satellite II is, like satellite III, pericentromeric heterochromatin and will therefore not interfere with the quality of our analysis.

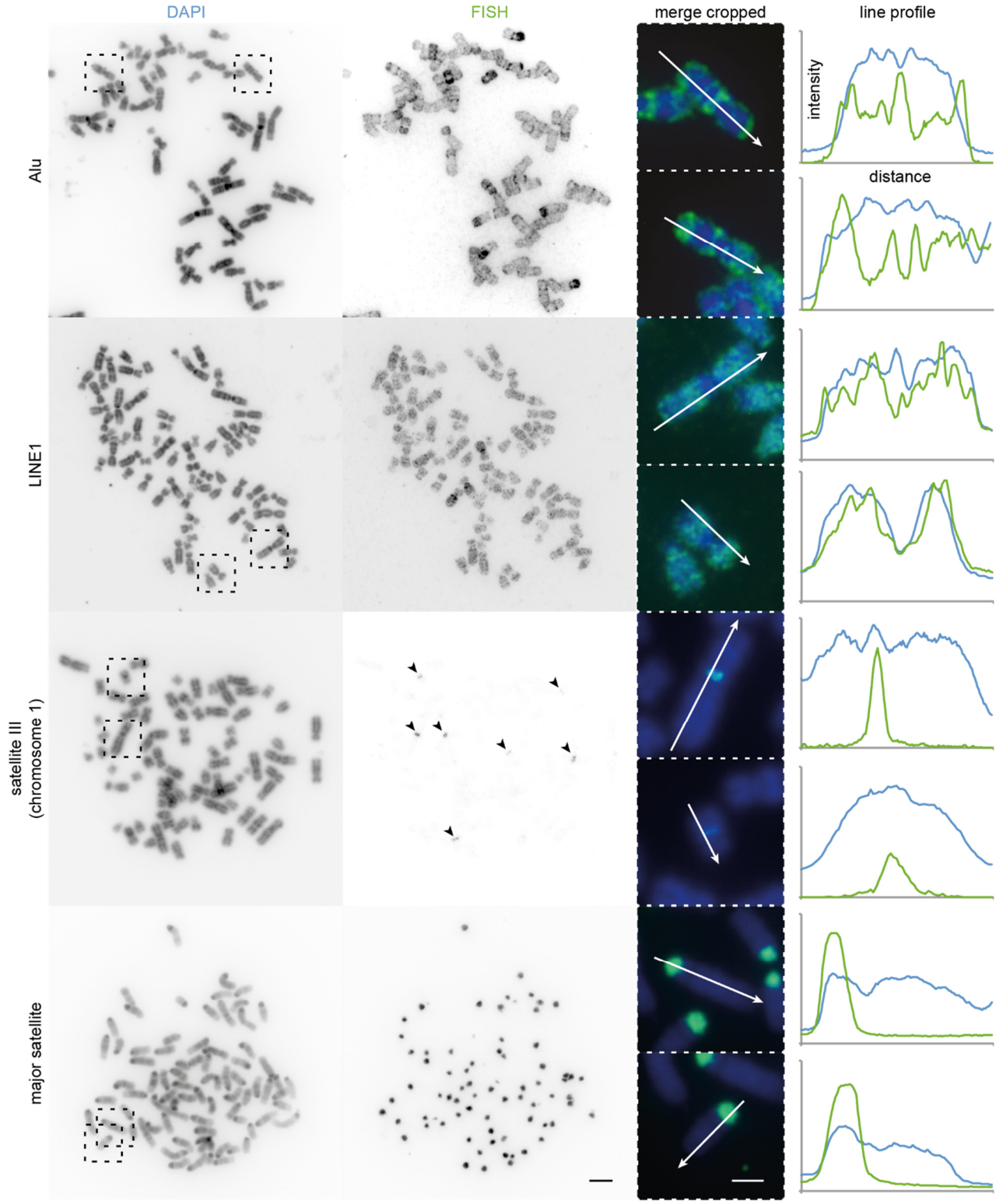

Figure 15: Metaphase FISH for Alu, LINE1 and satellite III (chromosome 1) in human cells and major satellite in mouse cells. Cell cultures (human HeLa and mouse C2C12) were enriched for mitotic cells by colcemid treatment and after metaphase preparation spread onto glass slides. FISH for Alu and LINE1 was performed under more stringent conditions (with formamide) whereas FISH for satellite III and major satellite was performed without formamide and therefore under less stringent conditions. Arrowheads point to the hybridized regions of the satellite III FISH. Merged images are enhanced from the regions surrounded by dashed squares. Arrows in the merged images show the position and direction of the line profiles (blue line = DAPI, green line = FISH). Scale bar in full images 5 µm, in cropped regions 2 µm.

Under more stringent conditions (hybridization with formamide) the probe might not hybridize to those minor binding sites. In contrast to satellite III regions in human chromosomes all telocentric

mouse chromosomes have a major satellite region (Broccoli et al., 1990, Kipling et al., 1991, Pertile et al., 2009, Kalitsis et al., 2006). FISH on C2C12 cells, which are female, showed a signal close to one edge in all chromosomes, where the mouse centromere is located, as expected.

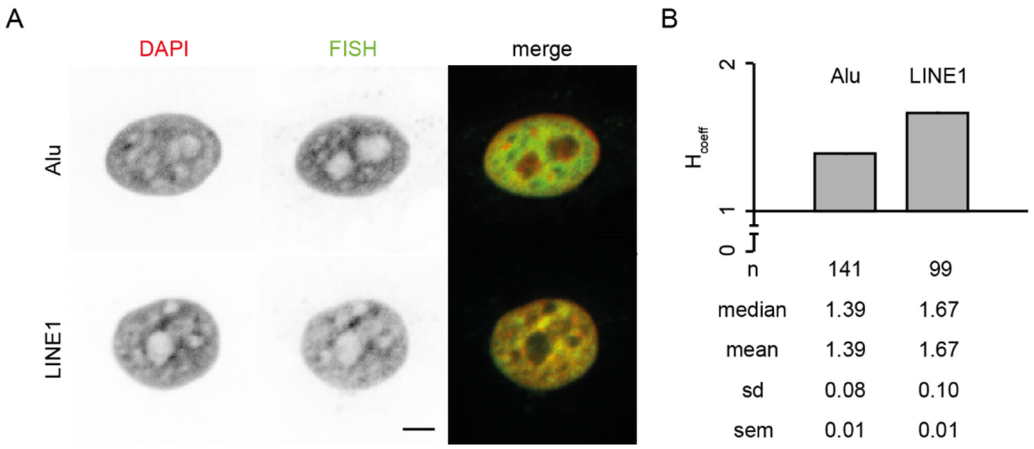

Figure 16: Colocalization of DAPI with Alu and LINE1 elements in human cells. A) Representative images of HeLa cells hybridized to FISH probes specific for Alu or LINE1 elements and the corresponding DAPI signal. Scale bar 5 µm. B) Colocalization analysis of FISH and DAPI signal at the three S-phase stages. Error bars show the standard error of the mean, which is extremely small (see table below graph). Data are from 2-3 independent experiments, n indicates the total number of cells analyzed, sd refers to the standard deviation and sem to standard error of the mean.

Both Alu and LINE1 make up a large percentage of the genome. With up to a million copies (Lander et al., 2001) the distribution in interphase nuclei is expected to be all over the nucleus. In order to determine how they correlate with DAPI stainings in a less condensed chromatin state than that of metaphase chromosomes we hybridized the Alu und LINE1 probes to interphase nuclei and measured the degree of colocalization using the H_{coeff} (Figure 16). A H_{coeff} value above 1 describes a colocalization between two signals, whereas a value below 1 is considered a more random distribution (for more details see 6.3.9). As expected both elements were found all over the nucleus but are excluded from the nucleoli. The Alu signal distribution showed a more homogenous signal with spots with low intensity. In contrast to that the LINE1 distribution in the nucleus was characterized by alternating patches of very bright and rather weak intensities. It seemed to correspond more to the DAPI signal distribution than Alu and colocalization analysis confirmed this observation. The mean H_{coeff} was 1.39 for Alu/DAPI and 1.67 for LINE1/DAPI indicating positive correlation. For Alu this seems different from the situation in metaphase chromosomes, where it is mostly excluded from DAPI bright regions but can be explained by the high copy number, extensive distribution and the less condensed chromatin state. For LINE1 the H_{coeff} was higher and thus showed a stronger colocalization as already suggested by visual inspection. Therefore, the chromatin association of Alu and LINE1 observed in metaphase chromosomes can to some degree be observed also in interphase nuclei.

6.4.2. DNA replication timing of repetitive elements

Different chromatin types are usually replicated during different times of S-phase. The repetitive elements we analyzed are located in different chromatin types, which led to the question whether we can observe differences in their replication timing. To address this question human HeLa and mouse C2C12 cells were incubated with EdU to label replication. After EdU detection and FISH for the respective repetitive elements, the degree of colocalization between the repetitive element and EdU was determined by H_{coeff} analysis (for details see Figure 14). For the euchromatic Alu element a replication during early S-phase would be expected. The rather homogenous distribution in the nucleus corresponded best to the early replication pattern, while the more peripheral mid and late S-phase patterns seemed to surround the Alu signal (Figure 17). In fact, the colocalization analysis showed a mean H_{coeff} of 1.59 for early S-phase, which indicates positive correlation. For mid and late S-phase, the H_{coeff} was below 1. This suggested that Alu is replicated during early S-phase.

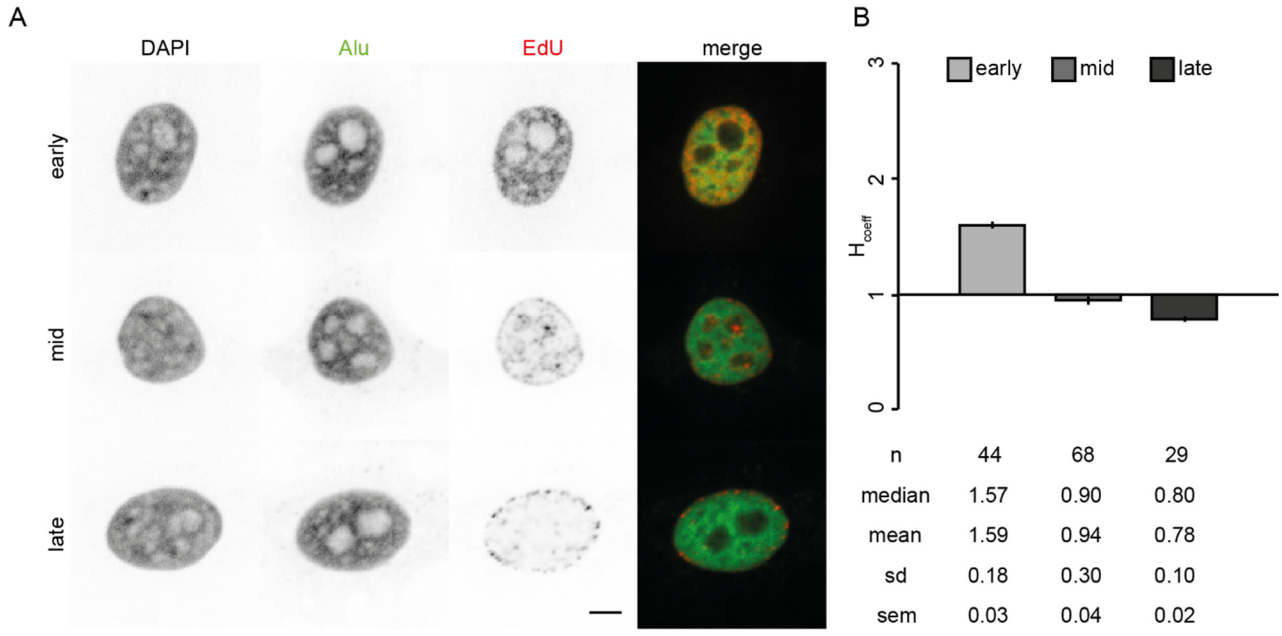

Figure 17: DNA replication timing of human Alu elements. HeLa cells were pulse labeled with EdU, fixed, stained for EdU and hybridized to the probe (FISH). A) Representative images of the cells at the three S-phase stages. Scale bar 5 µm. B) Colocalization analysis of FISH and EdU signal at the three S-phase stages. Error bars show the sem. Data are from 3 independent experiments, n indicates the total number of cells analyzed, sd refers to the standard deviation and sem to standard error of the mean.

LINE1 is associated with heterochromatic regions and therefore expected to replicate later than Alu, possibly in mid or even late S-phase, where heterochromatin is usually replicated. When comparing the replication patterns with the corresponding LINE1 signal we observed that the LINE1 signal surrounded early S-phase patterns (Figure 18A). When the early pattern progressed to less homogeneous signal the overlap with LINE1 increased, but with further progression towards the end of mid S-phase the overlap seemed to be reduced. This trend was also reflected in the H_{coeff} quantifications (Figure 18B). The strongest colocalization was measured in both early and mid S-phase

while the colocalization with late S-phase patterns was lowest. For late S-phase the value was still indicating a weak correlation, so there might be a proportion of LINE1 replication also during late S-phase. This led to the conclusion that LINE1 elements are mainly replicated during the early to mid S-phase transition.

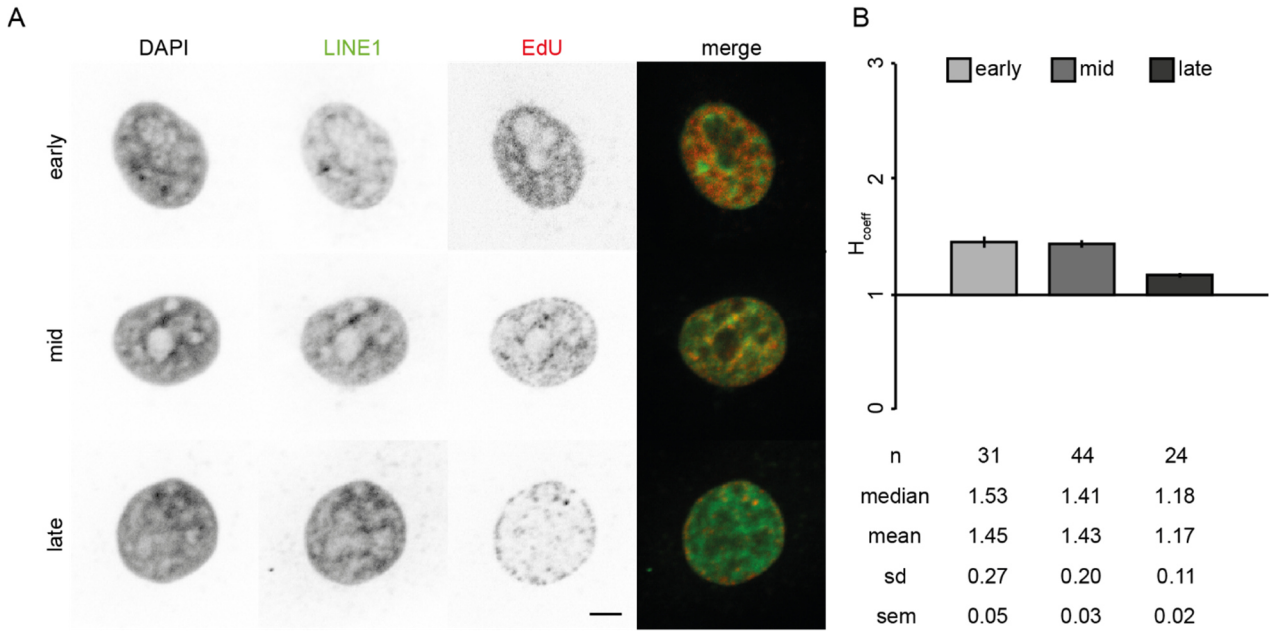

Figure 18: DNA replication timing of human LINE1 elements. HeLa cells were pulse labeled with EdU, fixed, stained for EdU and hybridized to the probe (FISH). A) Representative images of the cells at the three S-phase stages. Scale bar 5 µm. B) Colocalization analysis of FISH and EdU signal at the three S-phase stages. Error bars show the sem. Data are from 3 independent experiments, n indicates the total number of cells analyzed, sd refers to the standard deviation and sem to standard error of the mean.

Human satellite III and mouse major satellite DNA is strongly heterochromatic and major satellite DNA is known to be replicated in the second half of S-phase (late S-phase, Guenatri et al., 2004; Wu et al., 2005). The late S-phase pattern in mouse is characterized by large, horse-shoe shaped spots in the nucleus, that colocalize with the DAPI-rich chromocenters and major satellite DNA. Our results (Figure 19) are in good agreement with these previous findings, as the H_{coeff} shows the highest colocalization between major satellite DNA and the late replication pattern whereas for major satellite DNA and the early pattern the H_{coeff} indicates no correlation.

The FISH signal of human satellite III in interphase nuclei (Figure 20 and Figure 23) was detected as a spot pattern. As described already in the metaphase FISH more than 4 spots per nucleus were observed. As already mentioned we can assume that the minor binding sites described by Celeda et al., 1994 are located in pericentromeric satellites of chromosomes, they do not interfere with our analysis. We observed that the satellite III signal overlapped with the larger spots of replication signal already at the end of mid but also in late S-phase. The same trend is reflected in the colocalization measurement. There was no colocalization with the early replication pattern, but a clear colocalization with mid and

late replication patterns (Figure 20). We can therefore assume that the human satellite III is replicated at the mid to late S-phase transition.

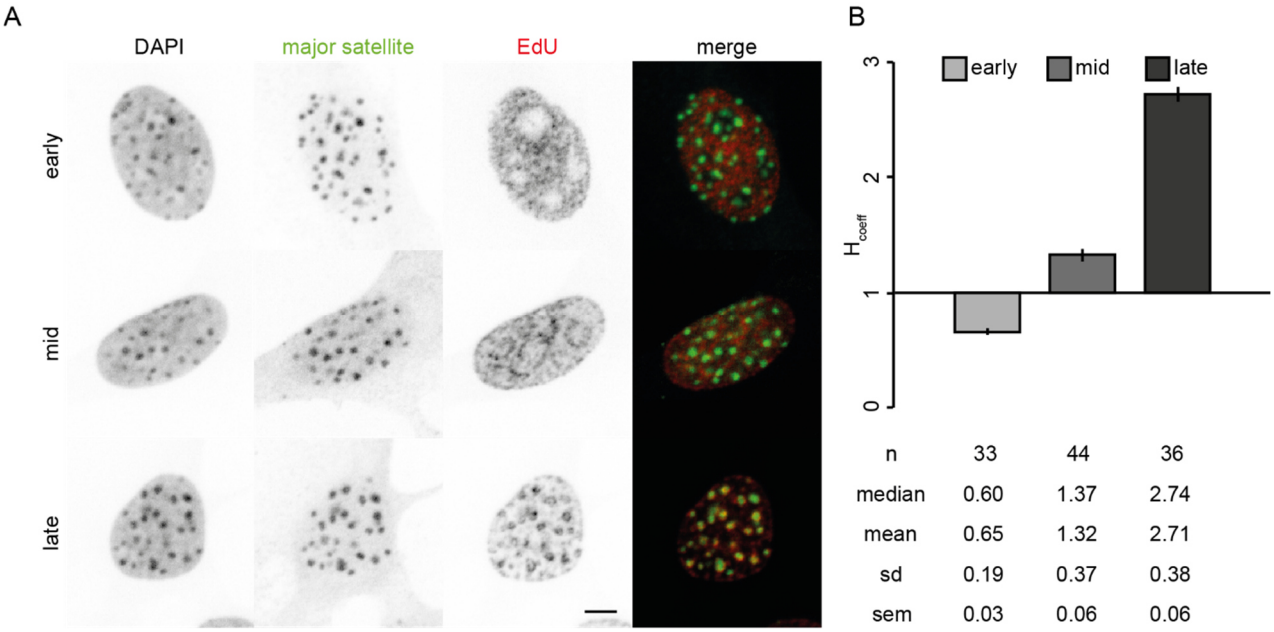

Figure 19:DNA replication timing of mouse major satellite DNA. C2C12 cells were pulse labeled with EdU, fixed, stained for EdU and hybridized to the probe (FISH). A) representative images of the cells at the three S-phase stages. Scale bar 5 µm. B) Colocalization analysis of FISH and EdU signal at the three S-phase stages. Error bars show the sem. Data are from 3 independent experiments, n indicates the total number of cells analyzed, sd refers to the standard deviation and sem to standard error of the mean.

It is generally believed that transcriptionally active (eu)chromatin is replicated during early S-phase, facultative chromatin in mid S-phase and constitutive heterochromatin during late S-phase (Okeefe et al., 1992). While this view is fundamentally true for most parts, it cannot be seen as a strict fact. Centromeric DNA (mouse minor satellite and α-satellite), which is considered constitutive heterochromatin, has been shown to replicate throughout S-phase (Weidtkamp-Peters et al., 2006, Erliandri et al., 2014). A similar observation has been made for human telomers (Arnoult et al., 2010). In replication timing studies on the human genome (Woodfine et al., 2004) a positive correlation between early replicating regions with high GC and Alu content could be found. Similarly, regions with a high LINE1 and low GC density corresponded to late replicating timing. In our findings, Alu replicates during early S-phase, which is in good agreement with these findings. However, we found that LINE1 is replicated mostly during the early to mid S-phase transition. At first glance this stands in contrast to the above described findings. LINE1 is an interspersed element meaning it occurs here and there, but with preference to AT rich regions, based on the preferential cleavage site TTTT/A of the LINE1 endonuclease (Feng et al., 1996), and hence heterochromatin. A small proportion of LINE1 can probably also be found in euchromatin, leading to overlap of the LINE1 signal with the early replication pattern. However, this small proportion cannot outcompete the heterochromatic LINE1 and plays only a minor role in replication timing. Another aspect that could bias our results is that the

LINE1 signal, due to high LINE1 abundancy, is to be found basically all over interphase nuclei. An abundant signal will naturally show higher correlations with another abundant signal, like the early S-phase pattern, than with a more focal signal, like the late S-phase pattern. Nevertheless, we see a clear difference between Alu, which is also quite extensively distributed, and LINE1 replication timing.

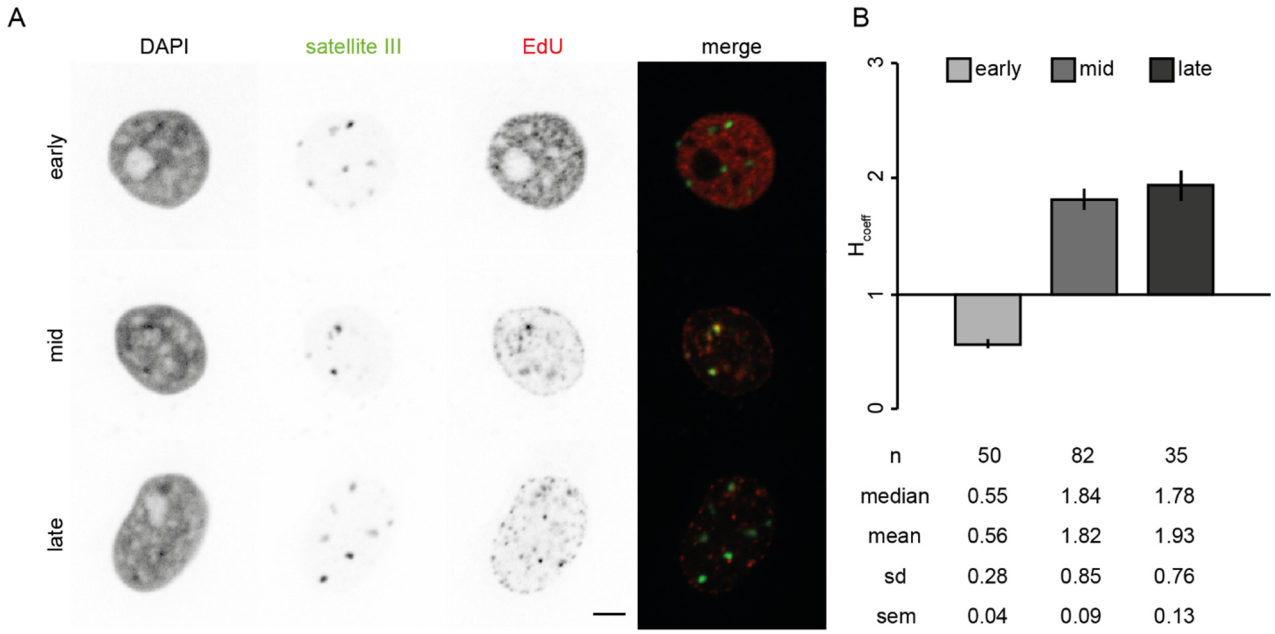

Figure 20: DNA replication timing of human satellite III DNA. HeLa cells were pulse labeled with EdU, fixed, stained for EdU and hybridized to the probe (FISH). The probe is specific for human satellite III of chromosome 1. A) representative images of the cells at the three S-phase stages. Scale bar 5 µm. B) Colocalization analysis of FISH and EdU signal at the three S-phase stages. Error bars show the sem. Data are from 3 independent experiments, n indicates the total number of cells analyzed, sd refers to the standard deviation and sem to standard error of the mean.

Woodfine et al., 2004 studied the replication timing in a genome-wide microarray approach, then examined chromosome 22 in more detail and compared their data with genome-wide sequencing information to assess among others GC content, Alu or LINE1 density. They found that early replication timing correlates with high GC content and enrichment in Alu elements, while sequences with high LINE1 density replicate late. Chromosome 22 is a chromosome, which, according to their own data and other studies (Lob et al., 2016), replicates rather early. Additionally, they concentrate on the long arm of the chromosome, missing the (peri)centromeric region, which also contains a satellite III region. In genome-wide approaches repetitive elements, especially tandem-repeats like satellites, can be challenging and are not always well represented. This was one of the reasons why we chose a microscopic approach to study replication timing specifically in repetitive elements. We observed that satellite III regions replicate after LINE1 during mid to late S-phase. Considering Woodfine et al., 2004 (and many other genome-wide studies) - for technical reasons - lack the satellites, they also lack regions, replicating later than LINE1. Although of course there might be other sequences outside the satellites replicating after LINE1, their definition of “late” replication timing might be biased and early and late replication timing should be interpreted in relative and not absolute terms. Taking all of this

into account, our microscopy data and the above-mentioned genome-wide data complement each other, agreeing that - in relative terms - Alu rich sequences (or Alu itself) replicate earlier than LINE1 rich sequences (or LINE1 itself). While for highly repetitive sequences like satellites microscopic approaches have an advantage over genome-wide studies, the genome-wide studies have a better resolution and information on the sequence identity.

We could show that human satellite III is replicated at the mid to late S-phase transition and reproduce that major satellite replicates during late S-phase. Although replication patterns in both humans and in mice are separated in early, mid and late S-phase, the definition of the respective patterns is not exactly the same. Notably the chromatin structure in human and mouse cells is different, which becomes very clear by the absence of chromocenters in human cells. Late replication in mice (here and in other studies for example Casas-Delucchi and Cardoso, 2011) is defined by huge spots, that colocalize with the pericentromeric major satellite DNA. Late replication in humans however is defined by larger spots (though clearly smaller than in mice) that are more disperse and smaller in numbers compared to early and mid S-phase patterns. This late replication pattern is very similar to the one observed in mouse cells at the very end of S-phase after the replication of chromocenters (Weidtkamp-Peters et al., 2006). The “late” replication pattern in mice from this study is hence more comparable to a transition pattern from mid to late S-phase in the human cells. In this context, we observe that pericentric heterochromatin, such as human satellite III and mouse major satellite, is replicated at a similar time (relative to the remaining chromatin) and therefore conserved throughout these two species. We observed that the human satellite III colocalizes also with some of the larger spots in late replication patterns. However, the spots in late S-phase are not all covered by satellite III, which raises the question what else is replicated at this time-point. Since satellite III is not present in all chromosomes, but only a subset of 7 autosomes plus the Y chromosome and we use a probe specific to chromosome 1, it might be that other satellite (types) replicate at the same time or shortly after the satellite III regions. To address this matter pericentromeric regions of all chromosomes should be analyzed for their replication timing. It is also possible that the very late replicating chromatin is not a single chromatin type but rather consists of a mixture of different heterochromatin types, like centromeric, pericentromeric satellites or even telomers from different chromosomes.

Assuming a domino-like activation of origins combined with origin firing probabilities and different chromatin types replication patterns observed in microscopy could be reproduced in simulations (Lob et al., 2016). They compare experimental data with their simulation and could show that stochastic origin activation in combination with the domino-model lead to the replication patterns commonly observed. If we follow this model and combine it with our data on repetitive elements, replication could progress like this: replication starts at origins in euchromatin. Replication forks progress and neighboring origins are activated in a “domino-like” fashion, Alu elements are being replicated within the euchromatic fractions of the cells, as observed. Activation of the neighboring origins can also

promote replication of centromeric regions as observed in experimental data (Weidtkamp-Peters et al., 2006) to a small part already in early S-phase, if their respective origins are close enough to euchromatic origins. A part of LINE1 is replicated now as well. Progressing origin activation gets closer to more heterochromatic regions. Facultative heterochromatin is replicated, along with it more LINE1 elements and other centromeric and telomeric regions. Finally, origins in pericentromeric heterochromatin are activated, facilitating replication of major satellite and satellite III DNA, like we and others could show (Guenatri et al., 2004; Wu et al., 2005). There might still be parts of the DNA that have not been replicated yet. Possibly their firing probability is very low, which leads to a very late replication. They might need to be enhanced by active neighboring origins to fire at all.

In context of the loop structure described in the first part of this thesis only a single origin of replication will be activated per loop. Due to their size, it is unlikely that Alu and LINE1 elements have their own origins of replication and their own replication timing. Despite their abundancy Alu and LINE1 elements will always be accompanied by other sequences on a loop structure. It is therefore much more likely that their replication timing is dictated by the activation of the individual origin on the loop and the associated chromatin type, which is what we observed. However, there are stretches of DNA with an extremely high density of LINE1 elements, for example a 100 kbp long region on the human X chromosome consists to 89% of LINE1 sequences (Lander et al., 2001). These regions might be worth further investigations towards replication timing. Pericentromeric satellites on the other hand can occupy stretches of several Mbp (Vissel and Choo, 1989). Hence, they are likely to occupy their own loops with their own replication origins. This would explain the distinct replication pattern and the rather synchronized replication timing within one satellite, when origins of adjacent loops are activated within a short time-frame. Theoretically it is possible that loops containing pericentromeric satellite sequences are larger and therefore would be replicated by fewer origins, but we saw no indication that replicons are larger in size at the late S-phase stage.

6.4.3. DNA repair kinetics of repetitive elements

To analyze DNA repair kinetics in repetitive elements the cells were irradiated with ionizing radiation (X-ray) and fixed at an early (0.5 h), an intermediate (3 h) and a late (24 h) time-point with subsequent γH2AX immuno-FISH staining under formamide-free conditions. Omitting the use of formamide improved the γH2AX staining quality dramatically, while still maintaining specific in situ hybridization. However, formamide free conditions are less stringent and allow more unspecific binding, as observed for the satellite III FISH on metaphases (Figure 15) and on interphases (Figure 23). For Alu, LINE1 and major satellite DNA FISH no difference in specificity could be observed with or without formamide.

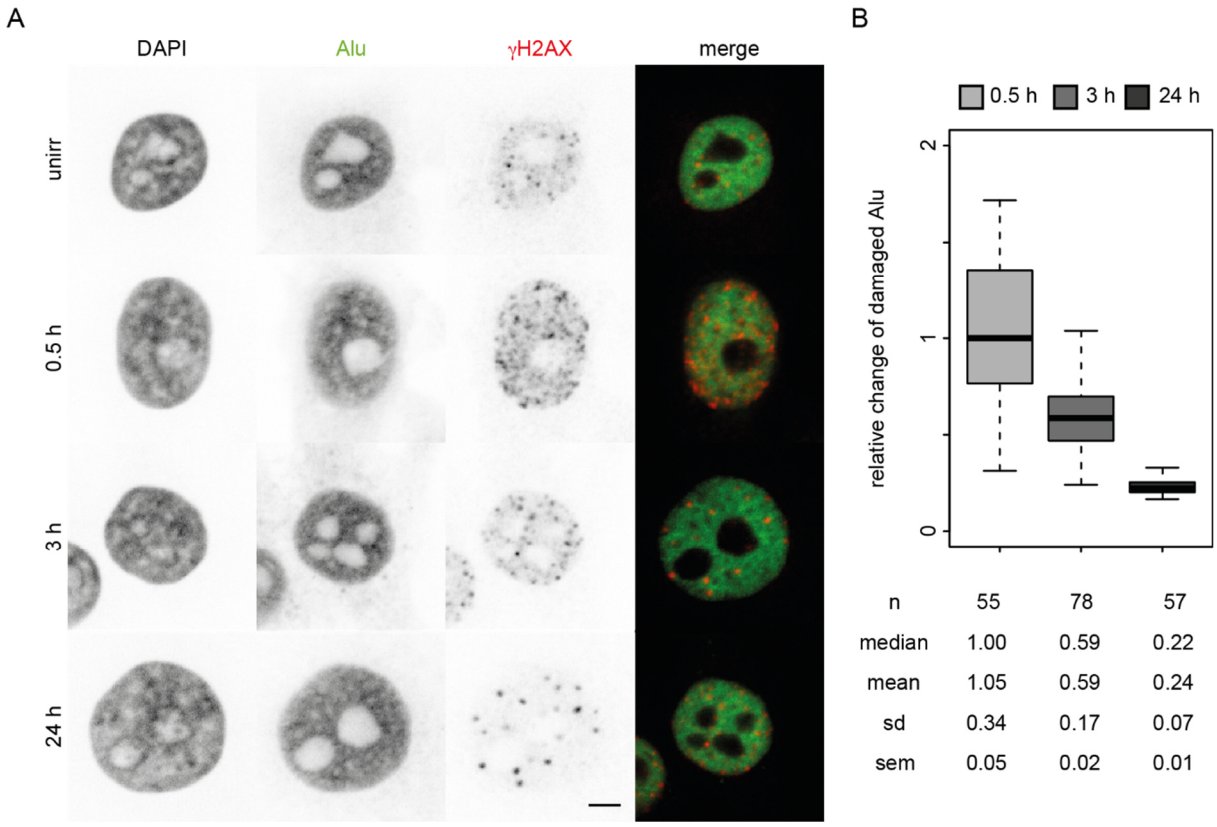

Figure 21: DNA repair kinetics of human Alu elements. HeLa cells were irradiated with 2 Gy X-ray, fixed after the time indicated and then stained for γH2AX and hybridized to the probe (FISH). A) representative images of the cells at different time-points post irradiation. Scale bar 5 µm. B) relative change of percentage of total Alu in γH2AX foci. Data are normalized to the median of the 0.5 h time-point. Data are from 3 independent experiments, n indicates the total number of cells analyzed, sd refers to the standard deviation and sem to standard error of the mean.

For the analysis of repair kinetics, the focal γH2AX pattern was segmented and the fraction of the respective repetitive element within those foci was calculated for every time-point. Data were normalized to the median of the 0.5 h time-point and are displayed as x-fold change in "damaged" fraction (sum of all repetitive element fractions within γH2AX foci per cell and time-point divided by median of the 0.5 h time-point). Unirradiated cells showed a weaker γH2AX signal than irradiated cells, the signal is most likely a byproduct of S-phase and not radiation induced. For this reason, γH2AX in unirradiated cells was not segmented and not shown in the analysis. We also analyzed global DNA repair kinetics by determining the fraction of the DAPI signal within the segmented γH2AX foci instead of the FISH signal. We will first examine our results on the repair kinetics of repetitive elements alone before we compare them with each other and with global repair kinetics.

The highest fraction of damaged DNA, total DNA or repetitive element DNA, would be expected at 0.5 h post irradiation and should then decrease, as the damage is repaired and the γH2AX signal decreases with only few but distinct foci left as described in Figure 6. This was observed for all elements. The total fraction of Alu or LINE1 in γH2AX foci was highest at 0.5 h post irradiation (Figure 21 and Figure 22). It then decreased to 50-60% of the original damaged fraction at 3 h and was lowest

with 22% at 24 h post irradiation. A general trend that γH2AX foci could be found for example particularly in LINE1 rich regions at a certain time-point could not be observed.

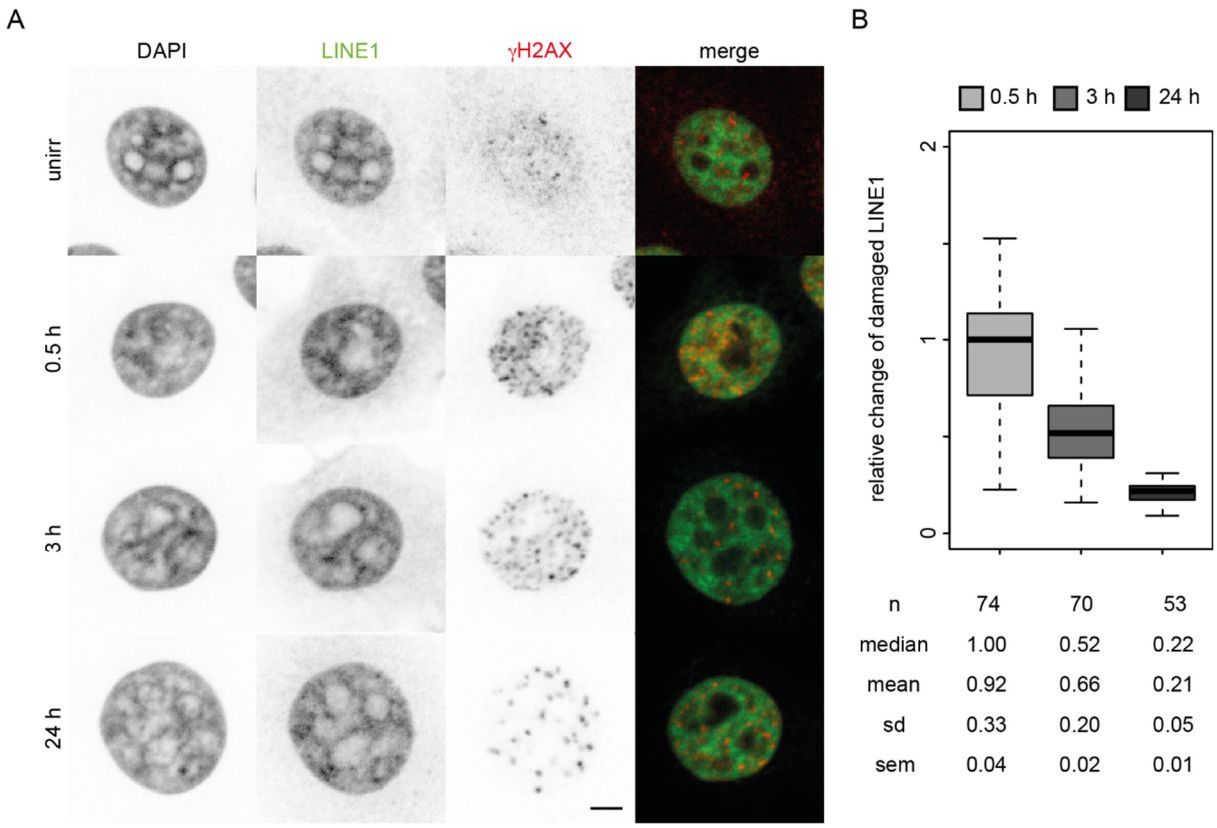

Figure 22: DNA repair kinetics of human LINE1 elements. HeLa cells were irradiated with 2 Gy X-ray, fixed after the time indicated and then stained for γH2AX and hybridized to the probe (FISH). A) representative images of the cells at different time-points post irradiation. Scale bar 5 µm. B) relative change of percentage of total LINE1 in γH2AX foci. Data are normalized to the median of the 0.5 h time-point. Data are from 3 independent experiments, n indicates the total number of cells analyzed, sd refers to the standard deviation and sem to standard error of the mean.

The fraction of satellite DNA labeled by γH2AX was highest at 0.5 h post irradiation and then decreased slowly to 81% of the original damaged fraction until it reached its minimum with 29% of the damaged fraction at 24 h. In case of spot-like FISH patterns (satellite III and major satellite) we also segmented the satellite regions and determined the fraction of total γH2AX signal within the satellites (Figure 23 C+D and Figure 24 C+D) to see if this would change over time. The fraction of γH2AX in satellite III regions stayed constant between 0.5 h and 3 h and only decreased at 24 h. Visual inspection of the images revealed that in many cells the satellite III regions contain only few γH2AX foci (with partial overlap) or vice versa the majority of γH2AX foci did contain only few satellite III regions with partial overlap. Since the lowest amount of γH2AX in our time-frame can be found at 24 h post irradiation it is natural that the amount of γH2AX in satellite III reaches also a minimum.

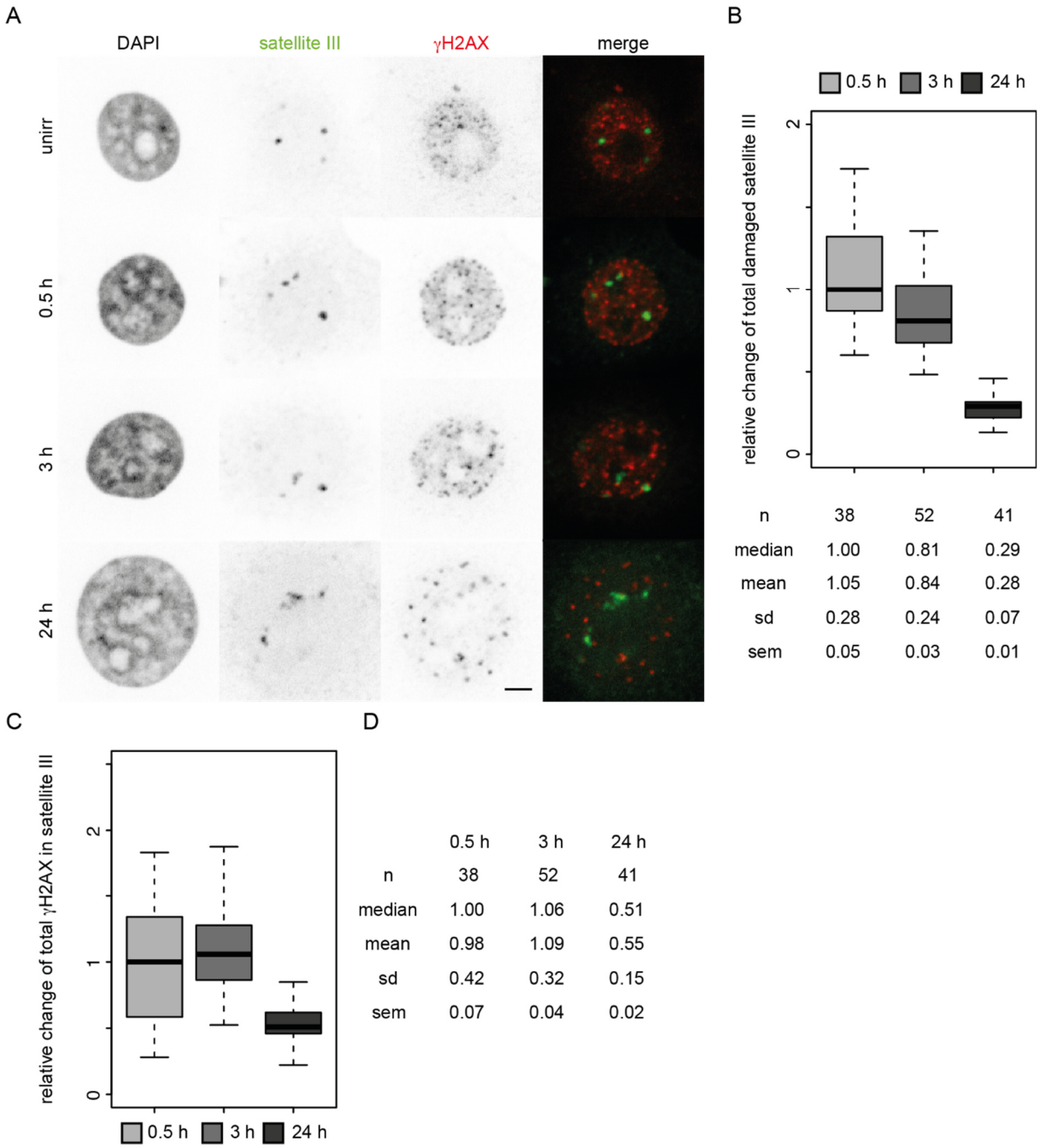

Figure 23: DNA repair kinetics of human satellite III. HeLa cells were irradiated with 2 Gy X-ray, fixed after the time indicated and then stained for γH2AX and hybridized to the probe (FISH). The probe is specific for the satellite III of chromosome 1. A) representative images of the cells at different time-points post irradiation. Scale bar 5 µm. B) relative change of percentage of total satellite III in γH2AX foci. Data are normalized to the median of the 0.5 h time-point. C) relative change of percentage of γH2AX intensity in satellite III regions. Data are normalized to the median of 0.5 h time-point. D) numbers to C. Data are from 3 independent experiments, n indicates the total number of cells analyzed, sd refers to the standard deviation and sem to standard error of the mean.

The fraction of major satellite DNA in γH2AX foci decreased with increasing time and reaches its minimum at 24 h post irradiation (Figure 24). When looking at the γH2AX signal of the cells the major satellite DNA mostly was localized in regions where there is no or little γH2AX signal, similar to satellite III. The change of γH2AX signal in major satellite DNA does not decrease dramatically, although it is lowest at the 24 h time-point.

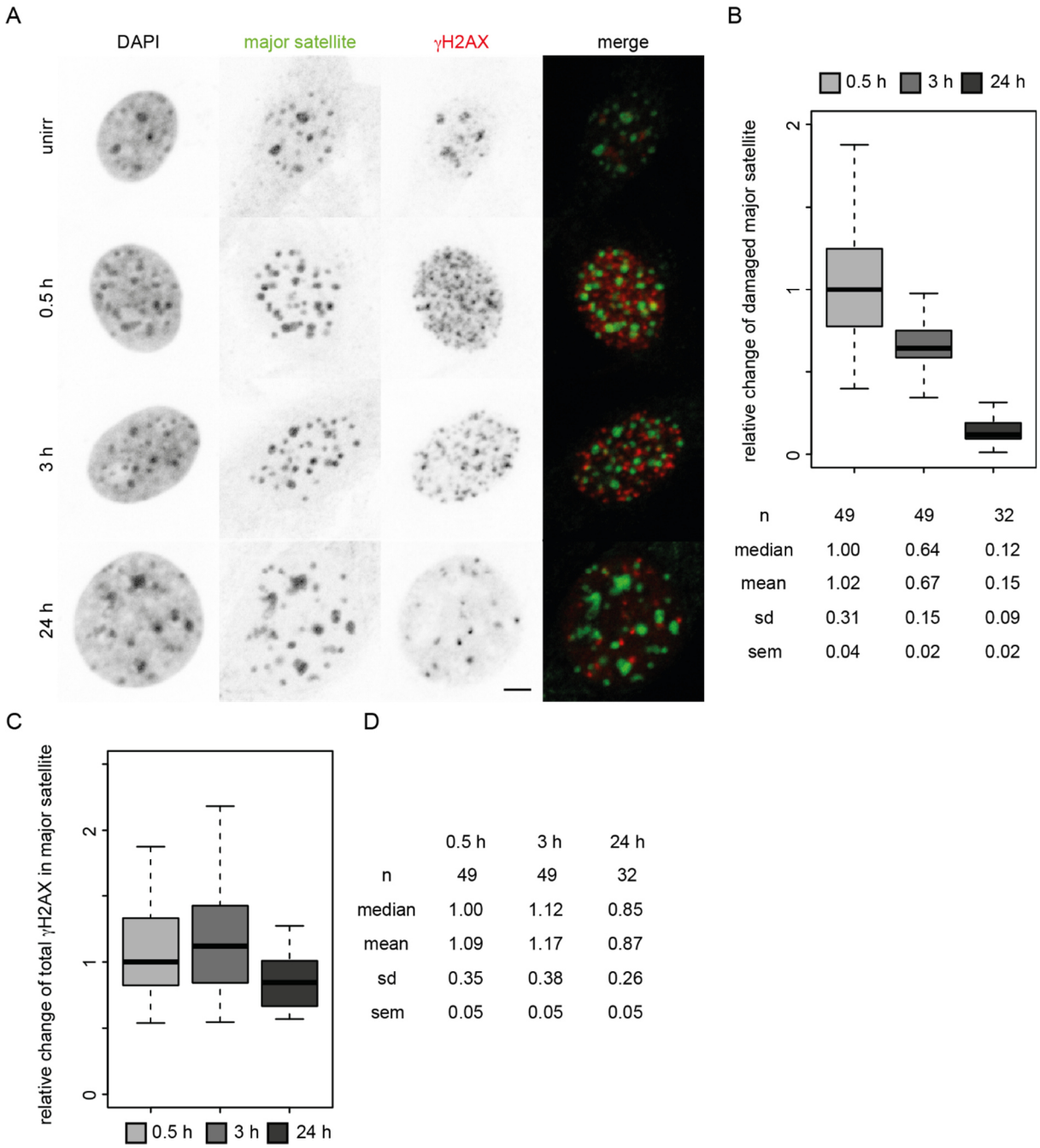

Figure 24: DNA repair kinetics of mouse major satellite DNA. C2C12 cells were irradiated with 2 Gy X-ray, fixed after the time indicated and then stained for γH2AX and hybridized to the probe (FISH). A) representative images of the cells at different time-points post irradiation. Scale bar 5 µm. B) relative change of percentage of total major satellite in γH2AX foci. Data are normalized to the median of the 0.5 h time-point. C) relative change of percentage of γH2AX intensity in major satellite regions. Data are normalized to the median of 0.5 h time-point. D) numbers to C. Data are from 3 independent experiments, n indicates the total number of cells analyzed, sd refers to the standard deviation and sem to standard error of the mean.

The minor overlap of γH2AX with pericentromeric satellite DNA raised the question if the histone H2AX is at all located in these regions. In previous studies a similar observation was made with "bending" of the γH2AX signal around heterochromatic regions in human and mouse cells upon irradiation with a heavy ion beam, that induces a linear track of DNA damage, suggesting a relocation of the damaged site from the originally hit site towards the periphery of the heterochromatin (Jakob et al., 2011). They targeted single chromocenters with the heavy ion beam and were able to show that

the initial phosphorylation of H2AX is taking place within the chromocenter but the signal is then moved to the periphery within the first 20 min after irradiation. This means that the low amount of γH2AX overlapping with the satellite, that we could observe, is due to the γH2AX signal having moved already to the periphery of the satellite after 30 min. Nevertheless, the signals are overlapping and γH2AX signal from the damaged satellite contributes to the measurements and we could observe differences in repair kinetics between the satellite regions and other elements. The comparison between the repair kinetics of the repetitive elements and the global DNA repair kinetics are shown in Figure 25. Global DNA repair kinetics were determined by analyzing the fraction of the DAPI signal within the segmented γH2AX foci instead of the FISH signal. Data were normalized to the median of the 0.5 h time-point. In human cells (Figure 25A) Alu and LINE1 elements were repaired with a similar speed as the global DNA. In comparison to the interspersed elements the damage in satellite III regions persisted longer especially at the intermediate time-point (3 h). Major satellite DNA in mouse cells (Figure 25B) however seems to be repaired according to the global DNA repair speed.

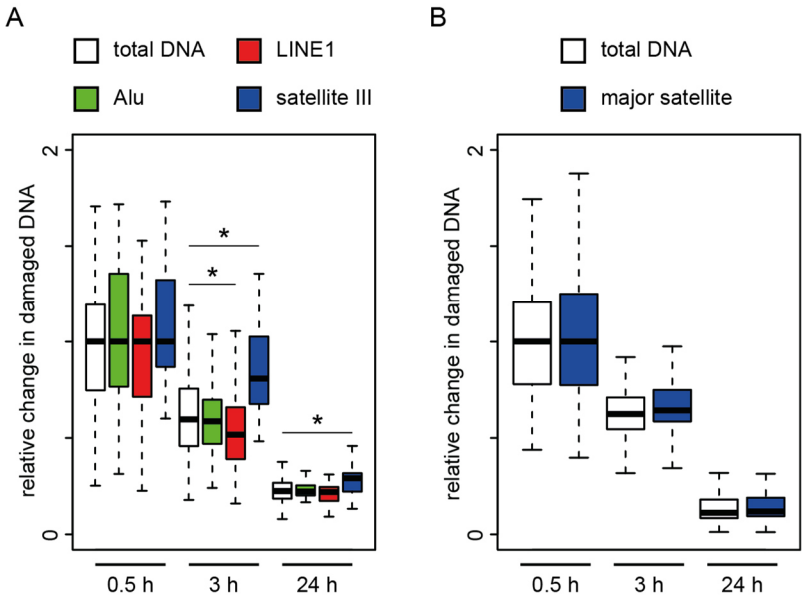

Figure 25: Comparison of DNA repair kinetics of repetitive elements in human and mouse cells. Summary of data from Figure 21 to Figure 24 B. A) relative change of damaged DNA fraction for total DNA, Alu elements, LINE1 elements and satellite III DNA in human HeLa cells. B) relative change of damaged DNA fraction for total DNA and major satellite DNA in mouse C2C12 cells. Data are normalized to the median of the 0.5 h time-point. Asterisks indicate significant differences ($p < 0.05$).

This suggests that the interspersed repetitive elements Alu and LINE1 are repaired along with the surrounding chromatin. Although Alu is more euchromatic than LINE1 we see no difference in their repair kinetic. It is possible that in the context of their small size and their dispersed distribution they do not have their own repair kinetics. On the other hand, the distinct association of LINE1 with AT-rich and rather heterochromatic regions (Korenberg and Rykowski, 1988) would have suggested that LINE1 is repaired more slowly like other heterochromatic regions. It is possible that the slow repair of heterochromatin is restricted only to the most condensed regions such as the pericentromeric satellites.

With our approach, we cannot confirm whether Alus and LINE1 are repaired correctly. During NHEJ DSB ends are, if necessary, partially resected leading to loss of sequence information. Since Alu and LINE1 elements are not coding in the sense of essential proteins loss of sequence can probably be better tolerated than in other sequences. In fact, the majority of Alus and LINEs in the genome are truncated and therefore inactive as a result of millions of years of evolution (Lander et al., 2001). On the other hand, since Alu and LINE1 sequences occur in high frequencies in the genome, it is also possible that they are found as homologous sequences during homology search in HR possibly at the wrong position of the sister chromatid, if additional Alus or LINE1s are in close proximity. Even a different chromosome could be recognized as a homolog. This might lead to the use of an illegitimate repair template and hence incorrect DNA repair (Burwinkel and Kilimann, 1998, White et al., 2015). In contrast to the interspersed elements, we observed that pericentromeric, tandemly repeated satellite III seemed to be repaired considerably slower in comparison to the remaining chromatin, similar to heterochromatic regions and mouse chromocenters (Goodarzi et al., 2008). We do not see a clear difference in repair kinetics of mouse major satellite DNA in comparison to global DNA repair. For our analysis, we used the DAPI signal within γH2AX foci to measure global DNA repair, which might be problematic in the context of mouse chromocenters. The relocation of γH2AX to the periphery of mouse chromocenters might be too strong (possibly stronger than in human satellite III) to observe a difference in repair kinetics. It has been proposed that heterochromatin in general is less accessible to the repair machinery due to the high condensation level (Cowell et al., 2007, Goodarzi et al., 2008). On the other hand Jakob et al., 2011 could show that repair factors can enter condensed heterochromatin in the form of mouse chromocenters, including the large kinase (p)ATM (350 kDa, UniProtKB entry Q62388, The UniProt, 2017) and that H2AX is initially phosphorylated within chromocenters, before being moved to the periphery. Apparently, this slower repair kinetic involves ATM and Artemis, suggesting that DSBs in heterochromatin are at least partially repaired with end resection (Goodarzi et al., 2010). In absence of ATM, DSBs associated with heterochromatin mostly remain unrepaired (Goodarzi et al., 2008). ATM is thought to phosphorylate KAP-1, a transcriptional silencer facilitating heterochromatin compaction (Ziv et al., 2006). Moreover, end resection seems to be a requirement for successful relocation, whereas repair of the DSB seems to take place outside of the heterochromatin, suggesting that chromatin complexity significantly contributes to slow repair kinetics (Goodarzi et al., 2010). The breaks move (probably a passive mechanism) to the periphery where they are stabilized and then repaired, in G2 phase preferentially by HR (Goodarzi et al., 2008, Goodarzi et al., 2010, Tsouroula et al., 2016). It has been suggested that the relocation of DSBs out of chromocenters serves the purpose of not using the wrong chromosome as a repair template within the clustered chromatin (Tsouroula et al., 2016). However, mouse chromocenters contain major satellite DNA from several chromosomes, this is not the case in humans. The damage is moved out of the

human satellite DNA as well, suggesting that the relocation is condensation driven and to avoid the use of the wrong template, not necessarily from another chromosome but also from the incorrect region on the sister chromatid/right chromosome. Most of these studies make use of mouse chromocenters as they are clearly distinct from mouse euchromatin and they do not analyze repair kinetics in human pericentromeric chromatin such as satellite III. Here we were able to show that human satellite III is repaired with slow kinetics and we assume that the repair mechanism might be very similar to what was observed in mice, despite the differences in (hetero)chromatin organization.

6.5. Conclusions

Taken together repetitive elements seem to be well integrated into chromatin and are preserved by DNA replication and repair processes with the same fidelity as the rest of the chromatin. While Alu and LINE1 are more integrated into the replication and repair processes along with the surrounding chromatin, probably due to their interspersed nature, pericentromeric chromatin, like mouse major satellite or human satellite III, are replicated in a more defined, focal pattern, and require a more specialized processing due to their highly condensed, heterochromatic characteristics before they can be efficiently repaired. We conclude that our results on replication timing and repair kinetics of repetitive elements can be embedded very well in what is known so far about S-phase progression and repair mechanisms. All three repetitive elements follow the general trend of early replication and repair of euchromatin and later replication and repair of heterochromatin (Okeefe et al., 1992, Goodarzi et al., 2008) except for LINE1, which is repaired at least with the same speed as Alu (Figure 26).

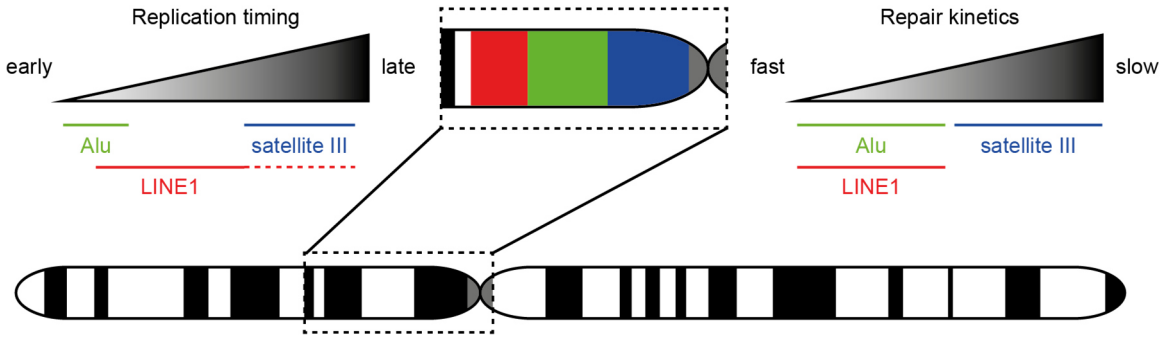

Figure 26: Distribution, replication timing and repair kinetics of human repetitive elements.

7. Conclusion & Outlook

The aim of this thesis was to gain insight into how chromatin and chromatin organization influences maintenance processes like DNA replication and repair. The two main aspects were structural chromatin organization and repetitive elements.

We took a rather unconventional approach to identify a basic unit of chromatin structure by analyzing single replicons and repair (nano)foci (γH2AX) using the super-resolution microscopy technique 3D-SIM. Both replicons and repair (nano)foci have been suggested to be constrained by an underlying chromatin structure (Chagin et al., 2016, Lob et al., 2016, Natale et al., 2017, in press) and we think that this structure is identical for both. We base this assumption on two aspects. First, they both appear as a focal pattern that exhibits a high degree of similarity by visual inspection. This visual observation alone however is not enough for the argument. We therefore went to analyze and quantitatively compare them, by staining replicons and repair (nano)foci within the same cell. This comparison provided us with the second aspect, which is that the DNA content and volume of replicons and repair (nano)foci was in the same range on a global scale and the majority of colocalizing foci had a surprisingly similar size. Hi-C data describe chromatin loops, formed by contact domains, with a size of ~ 185 kbp (Rao et al., 2014), which is only slightly larger than the DNA content of replicons and repair (nano)foci. While these types of experiments have the obvious advantage of knowing the sequence identity of the contact domains, they are only able to analyze those domains, that are enriched in the full cell population. The slight difference in sizes between the Hi-C data and our results might therefore be due to more transient loops, that we can possibly visualize by our approach. We therefore conclude, that there is a basic unit of chromatin structure, possibly in the form of loops, between the beads on a string and higher order organization levels like TADs, that dictates the sizes of replicons and repair (nano)foci. However, there are some aspects that need to be clarified. For example, if the DNA content of replicons is dependent on the nucleotide pulse length. For this, replicons should be labeled with different pulse lengths for example 15, 30 and 60 min. While a short pulse length might lead to underestimating the DNA content of replicons, an exceeded pulse length might lead to overestimation due to adjacent replicons merging into one structure. Depending on the outcome, it might make sense to repeat our experiment with an adjusted pulse length and a higher X-ray dose to increase the fraction of colocalizing replicons and repair (nano)foci. Another interesting aspect would be to find out how the loops are formed and how replicons and repair (nano)foci are constrained not to cross over to the next loop. If the boundary is formed by proteins, CTCF and the cohesin complex are promising candidates, as they have been observed to play a critical role in chromatin loop formation (Tark-Dame et al., 2014) and are associated with the majority of contact domains described by Rao et al., 2014 (short range contacts) and Dixon et al., 2012 (long range contacts). However, not all domains are accompanied by CTCF or cohesin binding sites and if CTCF

and cohesin are associated with more transient and dynamic loops is unknown. It is possible that also other factors play a role in loop formation. If they exist, who they are and how they coordinate loop formation would be additional interesting piece to solve the puzzle of structural chromatin organization.

The second part of this thesis focused on repetitive elements and their replication timing and repair kinetics using immuno-FISH to simultaneously label replication or repair and the respective repetitive element combined with microscopy. We were able to show that the euchromatic Alu element is replicated during early S-phase, LINE1, which is associated with AT-rich, heterochromatic regions seems to be replicated throughout S-phase, although the majority is replicated during the early to mid S-phase transition, while satellite III, which is pericentromeric heterochromatin, is replicated exclusively at the mid to late S-phase transition. This is consistent with the trend that euchromatin is replicated during early S-phase, facultative heterochromatin during mid S-phase and constitutive heterochromatin during late S-phase (Okeefe et al., 1992). There have also been genome wide approaches showing that early replicating regions are enriched for Alus, while late replicating regions are enriched in LINE1 (Woodfine et al., 2004), however these studies lack for technical reasons tandemly repeated DNA like the satellites, which replicate later than LINE1. Therefore, our data and genome wide studies complement each other. Since our probe for satellite III is specific for only one chromosome, although we observe additional minor binding sites, it might be interesting to study the replication timing of all pericentromeric satellites in humans. The question is if they would replicate as simultaneously as pericentromeric mouse major satellite DNA, which is present in almost all mouse chromosomes (Guenatri et al., 2004). For humans, it might not be as obvious if the different satellites do not occupy stretches of DNA as long as major satellite in mice or are not as clustered as in mouse chromocenters, which humans do not have. The repair kinetics of Alu and LINE1 are very similar to global repair kinetics, while damage in satellite III persists longer. This as well is consistent with the trend that euchromatin is repaired faster than heterochromatin (Goodarzi et al., 2008), although in this context LINE1 should as well be repaired more slowly. It is possible that only the most condensed heterochromatic regions like satellite III are repaired with slow kinetics. A similar observation has been made for mouse major satellite DNA, which is also pericentromeric heterochromatin (Goodarzi et al., 2008). All of these observations suggest that repetitive elements are well integrated into the genome. However, the high compaction level of satellite DNA apparently requires a more specialized processing prior to DNA repair, which seems to be performed by HR (Goodarzi et al., 2008). With our approach, we cannot analyze how efficiently repetitive elements are repaired. Due to their abundancy, they might be wrongfully recognized as repair templates during homologous recombination. The relocation of the damage outside of condensed heterochromatin has been proposed to also serve the purpose of not using the wrong chromosome as a template (Tsouroula et al., 2016). So, it would be interesting to see if repetitive elements are a hotspot for mutations and chromosomal aberrations.

8. References

Abbe, E. (1873). Beiträge zur Theorie des Mikroskops und der mikroskopischen Wahrnehmung. Archiv für mikroskopische Anatomie *9*, 413-418.

Arnoult, N., Schluth-Bolard, C., Letessier, A., Drascovic, I., Bouarich-Bourimi, R., Campisi, J., Kim, S.H., Boussouar, A., Ottaviani, A., Magdinier, F.*, et al.* (2010). Replication timing of human telomeres is chromosome arm-specific, influenced by subtelomeric structures and connected to nuclear localization. PLoS Genet *6*, e1000920.

Baddeley, D., Chagin, V.O., Schermelleh, L., Martin, S., Pombo, A., Carlton, P.M., Gahl, A., Domaing, P., Birk, U., Leonhardt, H.*, et al.* (2010). Measurement of replication structures at the nanometer scale using super-resolution light microscopy. Nucleic Acids Res *38*, e8.

Bannister, A.J., and Kouzarides, T. (2011). Regulation of chromatin by histone modifications. Cell Res *21*, 381-395.

Barau, J., Teissandier, A., Zamudio, N., Roy, S., Nalesso, V., Herault, Y., Guillou, F., and Bourc'his, D. (2016). The DNA methyltransferase DNMT3C protects male germ cells from transposon activity. Science *354*, 909-912.

Barton, O., Naumann, S.C., Diemer-Biehs, R., Kunzel, J., Steinlage, M., Conrad, S., Makharashvili, N., Wang, J., Feng, L., Lopez, B.S.*, et al.* (2014). Polo-like kinase 3 regulates CtIP during DNA double-strand break repair in G1. J Cell Biol *206*, 877-894.

Baumann, P., and West, S.C. (1998). Role of the human RAD51 protein in homologous recombination and double-stranded-break repair. Trends Biochem Sci *23*, 247-251.

Beck, C.R., Garcia-Perez, J.L., Badge, R.M., and Moran, J.V. (2011). LINE-1 elements in structural variation and disease. Annu Rev Genomics Hum Genet *12*, 187-215.

Beraldi, R., Pittoggi, C., Sciamanna, I., Mattei, E., and Spadafora, C. (2006). Expression of LINE-1 retroposons is essential for murine preimplantation development. Mol Reprod Dev *73*, 279-287.

Berezney, R., and Wei, X. (1998). The new paradigm: integrating genomic function and nuclear architecture. J Cell Biochem Suppl *30-31*, 238-242.

Berger, S.L. (2007). The complex language of chromatin regulation during transcription. Nature *447*, 407-412.

Beucher, A., Birraux, J., Tchouandong, L., Barton, O., Shibata, A., Conrad, S., Goodarzi, A.A., Krempler, A., Jeggo, P.A., and Lobrich, M. (2009). ATM and Artemis promote homologous recombination of radiation-induced DNA double-strand breaks in G2. EMBO J *28*, 3413-3427.

Biehs, R., Steinlage, M., Barton, O., Juhasz, S., Kunzel, J., Spies, J., Shibata, A., Jeggo, P.A., and Lobrich, M. (2017). DNA Double-Strand Break Resection Occurs during Non-homologous End Joining in G1 but Is Distinct from Resection during Homologous Recombination. Mol Cell *65*, 671-684 e675.

Bochman, M.L., and Schwacha, A. (2009). The Mcm complex: unwinding the mechanism of a replicative helicase. Microbiol Mol Biol Rev *73*, 652-683.

Bolzer, A., Kreth, G., Solovei, I., Koehler, D., Saracoglu, K., Fauth, C., Muller, S., Eils, R., Cremer, C., Speicher, M.R.*, et al.* (2005). Three-dimensional maps of all chromosomes in human male fibroblast nuclei and prometaphase rosettes. PLoS Biol *3*, e157.

Britton, S., Coates, J., and Jackson, S.P. (2013). A new method for high-resolution imaging of Ku foci to decipher mechanisms of DNA double-strand break repair. J Cell Biol *202*, 579-595.

Broccoli, D., Miller, O.J., and Miller, D.A. (1990). Relationship of Mouse Minor Satellite DNA to Centromere Activity. Cytogenet Cell Genet *54*, 182-186.

Brockdorff, N., Ashworth, A., Kay, G.F., Cooper, P., Smith, S., McCabe, V.M., Norris, D.P., Penny, G.D., Patel, D., and Rastan, S. (1991). Conservation of position and exclusive expression of mouse Xist from the inactive X chromosome. Nature *351*, 329-331.

Burma, S., Chen, B.P., Murphy, M., Kurimasa, A., and Chen, D.J. (2001). ATM phosphorylates histone H2AX in response to DNA double-strand breaks. J Biol Chem *276*, 42462-42467.

Burwinkel, B., and Kilimann, M.W. (1998). Unequal homologous recombination between LINE-1 elements as a mutational mechanism in human genetic disease. J Mol Biol *277*, 513-517.

Casas-Delucchi, C.S., Brero, A., Rahn, H.P., Solovei, I., Wutz, A., Cremer, T., Leonhardt, H., and Cardoso, M.C. (2011). Histone acetylation controls the inactive X chromosome replication dynamics. Nat Commun *2*, 222.
Casas-Delucchi, C.S., and Cardoso, M.C. (2011). Epigenetic control of DNA replication dynamics in mammals. Nucleus *2*, 370-382.
Caudron-Herger, M., Pankert, T., Seiler, J., Nemeth, A., Voit, R., Grummt, I., and Rippe, K. (2015). Alu element-containing RNAs maintain nucleolar structure and function. EMBO J *34*, 2758-2774.
Celeda, D., Aldinger, K., Haar, F.M., Hausmann, M., Durm, M., Ludwig, H., and Cremer, C. (1994). Rapid Fluorescence in-Situ Hybridization with Repetitive DNA Probes - Quantification by Digital Image-Analysis. Cytometry *17*, 13-25.
Celeda, D., Bettag, U., and Cremer, C. (1992). A Simplified Combination of DNA Probe Preparation and Fluorescence Insitu Hybridization. Z Naturforsch C *47*, 739-747.
Chagin, V.O., Casas-Delucchi, C.S., Reinhart, M., Schermelleh, L., Markaki, Y., Maiser, A., Bolius, J.J., Bensimon, A., Fillies, M., Domaing, P., *et al.* (2016). 4D Visualization of replication foci in mammalian cells corresponding to individual replicons. Nat Commun *7*, 11231.
Chagin, V.O., Reinhart, M., and Cardoso, M.C. (2015). High-resolution analysis of Mammalian DNA replication units. Methods Mol Biol *1300*, 43-65.
Chagin, V.O., Stear, J.H., and Cardoso, M.C. (2010). Organization of DNA replication. Cold Spring Harb Perspect Biol *2*, a000737.
Clemson, C.M., McNeil, J.A., Willard, H.F., and Lawrence, J.B. (1996). XIST RNA paints the inactive X chromosome at interphase: evidence for a novel RNA involved in nuclear/chromosome structure. J Cell Biol *132*, 259-275.
Cooke, H.J., and Hindley, J. (1979). Cloning of Human Satellite-Iii DNA - Different Components Are on Different Chromosomes. Nucleic Acids Research *6*, 3177-3197.
Cordaux, R., and Batzer, M.A. (2009). The impact of retrotransposons on human genome evolution. Nat Rev Genet *10*, 691-703.
Cowell, I.G., Sunter, N.J., Singh, P.B., Austin, C.A., Durkacz, B.W., and Tilby, M.J. (2007). gammaH2AX foci form preferentially in euchromatin after ionising-radiation. PLoS One *2*, e1057.
Cremer, T., and Cremer, M. (2010). Chromosome territories. Cold Spring Harb Perspect Biol *2*, a003889.
Cremer, T., Kreth, G., Koester, H., Fink, R.H., Heintzmann, R., Cremer, M., Solovei, I., Zink, D., and Cremer, C. (2000). Chromosome territories, interchromatin domain compartment, and nuclear matrix: an integrated view of the functional nuclear architecture. Crit Rev Eukaryot Gene Expr *10*, 179-212.
D'Amours, D., and Jackson, S.P. (2002). The Mre11 complex: at the crossroads of dna repair and checkpoint signalling. Nat Rev Mol Cell Biol *3*, 317-327.
Dekker, J., and Mirny, L. (2016). The 3D Genome as Moderator of Chromosomal Communication. Cell *164*, 1110-1121.
Dekker, J., and Misteli, T. (2015). Long-Range Chromatin Interactions. Cold Spring Harb Perspect Biol *7*, a019356.
Dellino, G.I., Cittaro, D., Piccioni, R., Luzi, L., Banfi, S., Segalla, S., Cesaroni, M., Mendoza-Maldonado, R., Giacca, M., and Pelicci, P.G. (2013). Genome-wide mapping of human DNA-replication origins: levels of transcription at ORC1 sites regulate origin selection and replication timing. Genome Res *23*, 1-11.
Dewannieux, M., Esnault, C., and Heidmann, T. (2003). LINE-mediated retrotransposition of marked Alu sequences. Nat Genet *35*, 41-48.
DiBiase, S.J., Zeng, Z.C., Chen, R., Hyslop, T., Curran, W.J., Jr., and Iliakis, G. (2000). DNA-dependent protein kinase stimulates an independently active, nonhomologous, end-joining apparatus. Cancer Res *60*, 1245-1253.
Dixon, J.R., Selvaraj, S., Yue, F., Kim, A., Li, Y., Shen, Y., Hu, M., Liu, J.S., and Ren, B. (2012). Topological domains in mammalian genomes identified by analysis of chromatin interactions. Nature *485*, 376-380.
Donaldson, A.D. (2005). Shaping time: chromatin structure and the DNA replication programme. Trends Genet *21*, 444-449.

Doolittle, W.F., and Sapienza, C. (1980). Selfish genes, the phenotype paradigm and genome evolution. Nature *284*, 601-603.
Erfle, H., Neumann, B., Liebel, U., Rogers, P., Held, M., Walter, T., Ellenberg, J., and Pepperkok, R. (2007). Reverse transfection on cell arrays for high content screening microscopy. Nat Protoc *2*, 392-399.
Erliandri, I., Fu, H.Q., Nakano, M., Kim, J.H., Miga, K.H., Liskovykh, M., Earnshaw, W.C., Masumoto, H., Kouprina, N., Aladjem, M.I., *et al.* (2014). Replication of alpha-satellite DNA arrays in endogenous human centromeric regions and in human artificial chromosome. Nucleic Acids Research *42*, 11502-11516.
Fanning, E., Klimovich, V., and Nager, A.R. (2006). A dynamic model for replication protein A (RPA) function in DNA processing pathways. Nucleic Acids Res *34*, 4126-4137.
Feng, Q., Moran, J.V., Kazazian, H.H., Jr., and Boeke, J.D. (1996). Human L1 retrotransposon encodes a conserved endonuclease required for retrotransposition. Cell *87*, 905-916.
Francke, U. (1994). Digitized and differentially shaded human chromosome ideograms for genomic applications. Cytogenet Cell Genet *65*, 206-218.
Frauer, C., Rottach, A., Meilinger, D., Bultmann, S., Fellinger, K., Hasenoder, S., Wang, M., Qin, W., Soding, J., Spada, F., *et al.* (2011). Different binding properties and function of CXXC zinc finger domains in Dnmt1 and Tet1. PLoS One *6*, e16627.
Fudenberg, G., Imakaev, M., Lu, C., Goloborodko, A., Abdennur, N., and Mirny, L.A. (2016). Formation of Chromosomal Domains by Loop Extrusion. Cell Rep *15*, 2038-2049.
Fuller, R.S., Funnell, B.E., and Kornberg, A. (1984). The dnaA protein complex with the E. coli chromosomal replication origin (oriC) and other DNA sites. Cell *38*, 889-900.
Garcia-Perez, J.L., Morell, M., Scheys, J.O., Kulpa, D.A., Morell, S., Carter, C.C., Hammer, G.D., Collins, K.L., O'Shea, K.S., Menendez, P., *et al.* (2010). Epigenetic silencing of engineered L1 retrotransposition events in human embryonic carcinoma cells. Nature *466*, 769-773.
Gilbert, D.M. (2001). Making sense of eukaryotic DNA replication origins. Science *294*, 96-100.
Goodarzi, A.A., Jeggo, P., and Lobrich, M. (2010). The influence of heterochromatin on DNA double strand break repair: Getting the strong, silent type to relax. DNA Repair (Amst) *9*, 1273-1282.
Goodarzi, A.A., Noon, A.T., Deckbar, D., Ziv, Y., Shiloh, Y., Lobrich, M., and Jeggo, P.A. (2008). ATM signaling facilitates repair of DNA double-strand breaks associated with heterochromatin. Mol Cell *31*, 167-177.
Gottlieb, T.M., and Jackson, S.P. (1993). The DNA-dependent protein kinase: requirement for DNA ends and association with Ku antigen. Cell *72*, 131-142.
Gratzner, H.G. (1982). Monoclonal antibody to 5-bromo- and 5-iododeoxyuridine: A new reagent for detection of DNA replication. Science *218*, 474-475.
Grawunder, U., Wilm, M., Wu, X., Kulesza, P., Wilson, T.E., Mann, M., and Lieber, M.R. (1997). Activity of DNA ligase IV stimulated by complex formation with XRCC4 protein in mammalian cells. Nature *388*, 492-495.
Guenatri, M., Bailly, D., Maison, C., and Almouzni, G. (2004). Mouse centric and pericentric satellite repeats form distinct functional heterochromatin. J Cell Biol *166*, 493-505.
Gustafsson, M.G., Shao, L., Carlton, P.M., Wang, C.J., Golubovskaya, I.N., Cande, W.Z., Agard, D.A., and Sedat, J.W. (2008). Three-dimensional resolution doubling in wide-field fluorescence microscopy by structured illumination. Biophys J *94*, 4957-4970.
Herce, H.D., Casas-Delucchi, C.S., and Cardoso, M.C. (2013). New image colocalization coefficient for fluorescence microscopy to quantify (bio-)molecular interactions. J Microsc *249*, 184-194.
Howes, T.R., and Tomkinson, A.E. (2012). DNA ligase I, the replicative DNA ligase. Subcell Biochem *62*, 327-341.
Huberman, J.A., and Riggs, A.D. (1968). On the mechanism of DNA replication in mammalian chromosomes. J Mol Biol *32*, 327-341.
Hubscher, U., Maga, G., and Spadari, S. (2002). Eukaryotic DNA polymerases. Annu Rev Biochem *71*, 133-163.

Jackson, D.A., and Pombo, A. (1998). Replicon clusters are stable units of chromosome structure: evidence that nuclear organization contributes to the efficient activation and propagation of S phase in human cells. J Cell Biol *140*, 1285-1295.
Jackson, S.P., and Bartek, J. (2009). The DNA-damage response in human biology and disease. Nature *461*, 1071-1078.
Jakob, B., Splinter, J., Conrad, S., Voss, K.O., Zink, D., Durante, M., Lobrich, M., and Taucher-Scholz, G. (2011). DNA double-strand breaks in heterochromatin elicit fast repair protein recruitment, histone H2AX phosphorylation and relocation to euchromatin. Nucleic Acids Res *39*, 6489-6499.
Jarmuz, M., Glotzbach, C.D., Bailey, K.A., Bandyopadhyay, R., and Shaffer, L.G. (2007). The Evolution of satellite III DNA subfamilies among primates. Am J Hum Genet *80*, 495-501.
Jeppesen, P., and Turner, B.M. (1993). The inactive X chromosome in female mammals is distinguished by a lack of histone H4 acetylation, a cytogenetic marker for gene expression. Cell *74*, 281-289.
Jolly, C., Metz, A., Govin, J., Vigneron, M., Turner, B.M., Khochbin, S., and Vourc'h, C. (2004). Stress-induced transcription of satellite III repeats. J Cell Biol *164*, 25-33.
Jonsson, Z.O., and Hubscher, U. (1997). Proliferating cell nuclear antigen: more than a clamp for DNA polymerases. Bioessays *19*, 967-975.
Joseph, A., Mitchell, A.R., and Miller, O.J. (1989). The organization of the mouse satellite DNA at centromeres. Exp Cell Res *183*, 494-500.
Kalitsis, P., Griffiths, B., and Choo, K.H. (2006). Mouse telocentric sequences reveal a high rate of homogenization and possible role in Robertsonian translocation. Proc Natl Acad Sci U S A *103*, 8786-8791.
Khazina, E., Truffault, V., Buttner, R., Schmidt, S., Coles, M., and Weichenrieder, O. (2011). Trimeric structure and flexibility of the L1ORF1 protein in human L1 retrotransposition. Nat Struct Mol Biol *18*, 1006-1014.
Kinner, A., Wu, W., Staudt, C., and Iliakis, G. (2008). Gamma-H2AX in recognition and signaling of DNA double-strand breaks in the context of chromatin. Nucleic Acids Res *36*, 5678-5694.
Kipling, D., Ackford, H.E., Taylor, B.A., and Cooke, H.J. (1991). Mouse minor satellite DNA genetically maps to the centromere and is physically linked to the proximal telomere. Genomics *11*, 235-241.
Korenberg, J.R., and Rykowski, M.C. (1988). Human genome organization: Alu, lines, and the molecular structure of metaphase chromosome bands. Cell *53*, 391-400.
Lachner, M., O'Sullivan, R.J., and Jenuwein, T. (2003). An epigenetic road map for histone lysine methylation. J Cell Sci *116*, 2117-2124.
Lander, E.S., Linton, L.M., Birren, B., Nusbaum, C., Zody, M.C., Baldwin, J., Devon, K., Dewar, K., Doyle, M., FitzHugh, W.*, et al.* (2001). Initial sequencing and analysis of the human genome. Nature *409*, 860-921.
Lee, E., Iskow, R., Yang, L., Gokcumen, O., Haseley, P., Luquette, L.J., 3rd, Lohr, J.G., Harris, C.C., Ding, L., Wilson, R.K.*, et al.* (2012). Landscape of somatic retrotransposition in human cancers. Science *337*, 967-971.
Leonhardt, H., Rahn, H.P., Weinzierl, P., Sporbert, A., Cremer, T., Zink, D., and Cardoso, M.C. (2000). Dynamics of DNA replication factories in living cells. J Cell Biol *149*, 271-280.
Li, G., and Reinberg, D. (2011). Chromatin higher-order structures and gene regulation. Curr Opin Genet Dev *21*, 175-186.
Li, G., and Zhu, P. (2015). Structure and organization of chromatin fiber in the nucleus. FEBS Lett *589*, 2893-2904.
Liang, F., and Jasin, M. (1996). Ku80-deficient cells exhibit excess degradation of extrachromosomal DNA. J Biol Chem *271*, 14405-14411.
Lieberman-Aiden, E., van Berkum, N.L., Williams, L., Imakaev, M., Ragoczy, T., Telling, A., Amit, I., Lajoie, B.R., Sabo, P.J., Dorschner, M.O.*, et al.* (2009). Comprehensive mapping of long-range interactions reveals folding principles of the human genome. Science *326*, 289-293.
Liu, P., Siciliano, J., Seong, D., Craig, J., Zhao, Y., de Jong, P.J., and Siciliano, M.J. (1993). Dual Alu polymerase chain reaction primers and conditions for isolation of human chromosome painting probes from hybrid cells. Cancer Genet Cytogenet *65*, 93-99.

Lob, D., Lengert, N., Chagin, V.O., Reinhart, M., Casas-Delucchi, C.S., Cardoso, M.C., and Drossel, B. (2016). 3D replicon distributions arise from stochastic initiation and domino-like DNA replication progression. Nat Commun *7*, 11207.
Lopez Perez, R., Best, G., Nicolay, N.H., Greubel, C., Rossberger, S., Reindl, J., Dollinger, G., Weber, K.J., Cremer, C., and Huber, P.E. (2016). Superresolution light microscopy shows nanostructure of carbon ion radiation-induced DNA double-strand break repair foci. FASEB J *30*, 2767-2776.
Luger, K., Mader, A.W., Richmond, R.K., Sargent, D.F., and Richmond, T.J. (1997). Crystal structure of the nucleosome core particle at 2.8 A resolution. Nature *389*, 251-260.
Ma, H., Samarabandu, J., Devdhar, R.S., Acharya, R., Cheng, P.C., Meng, C., and Berezney, R. (1998). Spatial and temporal dynamics of DNA replication sites in mammalian cells. J Cell Biol *143*, 1415-1425.
Mahaney, B.L., Meek, K., and Lees-Miller, S.P. (2009). Repair of ionizing radiation-induced DNA double-strand breaks by non-homologous end-joining. Biochem J *417*, 639-650.
Martin, S.L., Branciforte, D., Keller, D., and Bain, D.L. (2003). Trimeric structure for an essential protein in L1 retrotransposition. Proc Natl Acad Sci U S A *100*, 13815-13820.
Mathias, S.L., Scott, A.F., Kazazian, H.H., Jr., Boeke, J.D., and Gabriel, A. (1991). Reverse transcriptase encoded by a human transposable element. Science *254*, 1808-1810.
Matos, J., and West, S.C. (2014). Holliday junction resolution: regulation in space and time. DNA Repair (Amst) *19*, 176-181.
Meijer, M., Beck, E., Hansen, F.G., Bergmans, H.E., Messer, W., von Meyenburg, K., and Schaller, H. (1979). Nucleotide sequence of the origin of replication of the Escherichia coli K-12 chromosome. Proc Natl Acad Sci U S A *76*, 580-584.
Moore, J.M., Rabaia, N.A., Smith, L.E., Fagerlie, S., Gurley, K., Loukinov, D., Disteche, C.M., Collins, S.J., Kemp, C.J., Lobanenkov, V.V.*, et al.* (2012). Loss of maternal CTCF is associated with peri-implantation lethality of Ctcf null embryos. PLoS One *7*, e34915.
Morishima, A., Grumbach, M.M., and Taylor, J.H. (1962). Asynchronous duplication of human chromosomes and the origin of sex chromatin. Proc Natl Acad Sci U S A *48*, 756-763.
Mouse Genome Sequencing, C., Waterston, R.H., Lindblad-Toh, K., Birney, E., Rogers, J., Abril, J.F., Agarwal, P., Agarwala, R., Ainscough, R., Alexandersson, M.*, et al.* (2002). Initial sequencing and comparative analysis of the mouse genome. Nature *420*, 520-562.
Murga, M., Jaco, I., Fan, Y., Soria, R., Martinez-Pastor, B., Cuadrado, M., Yang, S.M., Blasco, M.A., Skoultchi, A.I., and Fernandez-Capetillo, O. (2007). Global chromatin compaction limits the strength of the DNA damage response. J Cell Biol *178*, 1101-1108.
Nakamura, H., Morita, T., and Sato, C. (1986). Structural organizations of replicon domains during DNA synthetic phase in the mammalian nucleus. Exp Cell Res *165*, 291-297.
Nakayasu, H., and Berezney, R. (1989). Mapping replicational sites in the eucaryotic cell nucleus. J Cell Biol *108*, 1-11.
Nick McElhinny, S.A., Snowden, C.M., McCarville, J., and Ramsden, D.A. (2000). Ku recruits the XRCC4-ligase IV complex to DNA ends. Mol Cell Biol *20*, 2996-3003.
Norris, D.P., Brockdorff, N., and Rastan, S. (1991). Methylation status of CpG-rich islands on active and inactive mouse X chromosomes. Mamm Genome *1*, 78-83.
Okazaki, R., Okazaki, T., Sakabe, K., Sugimoto, K., and Sugino, A. (1968). Mechanism of DNA chain growth. I. Possible discontinuity and unusual secondary structure of newly synthesized chains. Proc Natl Acad Sci U S A *59*, 598-605.
Okeefe, R.T., Henderson, S.C., and Spector, D.L. (1992). Dynamic Organization of DNA-Replication in Mammalian-Cell Nuclei - Spatially and Temporally Defined Replication of Chromosome-Specific Alpha-Satellite DNA-Sequences. Journal of Cell Biology *116*, 1095-1110.
Orgel, L.E., and Crick, F.H. (1980). Selfish DNA: the ultimate parasite. Nature *284*, 604-607.
Paull, T.T., Rogakou, E.P., Yamazaki, V., Kirchgessner, C.U., Gellert, M., and Bonner, W.M. (2000). A critical role for histone H2AX in recruitment of repair factors to nuclear foci after DNA damage. Current Biology *10*, 886-895.
Pertile, M.D., Graham, A.N., Choo, K.H., and Kalitsis, P. (2009). Rapid evolution of mouse Y centromere repeat DNA belies recent sequence stability. Genome Res *19*, 2202-2213.

Plath, K., Fang, J., Mlynarczyk-Evans, S.K., Cao, R., Worringer, K.A., Wang, H., de la Cruz, C.C., Otte, A.P., Panning, B., and Zhang, Y. (2003). Role of histone H3 lysine 27 methylation in X inactivation. Science *300*, 131-135.
Pope, B.D., Ryba, T., Dileep, V., Yue, F., Wu, W., Denas, O., Vera, D.L., Wang, Y., Hansen, R.S., Canfield, T.K., *et al.* (2014). Topologically associating domains are stable units of replication-timing regulation. Nature *515*, 402-405.
Prak, E.T., and Kazazian, H.H., Jr. (2000). Mobile elements and the human genome. Nat Rev Genet *1*, 134-144.
Probst, A.V., Okamoto, I., Casanova, M., El Marjou, F., Le Baccon, P., and Almouzni, G. (2010). A strand-specific burst in transcription of pericentric satellites is required for chromocenter formation and early mouse development. Dev Cell *19*, 625-638.
Quentin, Y. (1994). A master sequence related to a free left Alu monomer (FLAM) at the origin of the B1 family in rodent genomes. Nucleic Acids Res *22*, 2222-2227.
Rao, S.S., Huntley, M.H., Durand, N.C., Stamenova, E.K., Bochkov, I.D., Robinson, J.T., Sanborn, A.L., Machol, I., Omer, A.D., Lander, E.S., *et al.* (2014). A 3D map of the human genome at kilobase resolution reveals principles of chromatin looping. Cell *159*, 1665-1680.
Rayleigh (1896). XV. On the theory of optical images, with special reference to the microscope. Philosophical Magazine Series 5 *42*, 167-195.
Riballo, E., Critchlow, S.E., Teo, S.H., Doherty, A.J., Priestley, A., Broughton, B., Kysela, B., Beamish, H., Plowman, N., Arlett, C.F., *et al.* (1999). Identification of a defect in DNA ligase IV in a radiosensitive leukaemia patient. Curr Biol *9*, 699-702.
Riballo, E., Kuhne, M., Rief, N., Doherty, A., Smith, G.C., Recio, M.J., Reis, C., Dahm, K., Fricke, A., Krempler, A., *et al.* (2004). A pathway of double-strand break rejoining dependent upon ATM, Artemis, and proteins locating to gamma-H2AX foci. Mol Cell *16*, 715-724.
Robinson, N.P., and Bell, S.D. (2005). Origins of DNA replication in the three domains of life. FEBS J *272*, 3757-3766.
Rogakou, E.P., Boon, C., Redon, C., and Bonner, W.M. (1999). Megabase chromatin domains involved in DNA double-strand breaks in vivo. J Cell Biol *146*, 905-916.
Rogakou, E.P., Pilch, D.R., Orr, A.H., Ivanova, V.S., and Bonner, W.M. (1998). DNA double-stranded breaks induce histone H2AX phosphorylation on serine 139. J Biol Chem *273*, 5858-5868.
Rothkamm, K., Kruger, I., Thompson, L.H., and Lobrich, M. (2003). Pathways of DNA double-strand break repair during the mammalian cell cycle. Mol Cell Biol *23*, 5706-5715.
Sadoni, N., Cardoso, M.C., Stelzer, E.H., Leonhardt, H., and Zink, D. (2004). Stable chromosomal units determine the spatial and temporal organization of DNA replication. J Cell Sci *117*, 5353-5365.
Saksouk, N., Simboeck, E., and Dejardin, J. (2015). Constitutive heterochromatin formation and transcription in mammals. Epigenetics Chromatin *8*, 3.
Salic, A., and Mitchison, T.J. (2008). A chemical method for fast and sensitive detection of DNA synthesis in vivo. Proc Natl Acad Sci U S A *105*, 2415-2420.
Sanborn, A.L., Rao, S.S., Huang, S.C., Durand, N.C., Huntley, M.H., Jewett, A.I., Bochkov, I.D., Chinnappan, D., Cutkosky, A., Li, J., *et al.* (2015). Chromatin extrusion explains key features of loop and domain formation in wild-type and engineered genomes. Proc Natl Acad Sci U S A *112*, E6456-6465.
Santos-Rosa, H., Schneider, R., Bannister, A.J., Sherriff, J., Bernstein, B.E., Emre, N.C., Schreiber, S.L., Mellor, J., and Kouzarides, T. (2002). Active genes are tri-methylated at K4 of histone H3. Nature *419*, 407-411.
Sartori, A.A., Lukas, C., Coates, J., Mistrik, M., Fu, S., Bartek, J., Baer, R., Lukas, J., and Jackson, S.P. (2007). Human CtIP promotes DNA end resection. Nature *450*, 509-514.
Sayah, D.M., Sokolskaja, E., Berthoux, L., and Luban, J. (2004). Cyclophilin A retrotransposition into TRIM5 explains owl monkey resistance to HIV-1. Nature *430*, 569-573.
Schermelleh, L., Heintzmann, R., and Leonhardt, H. (2010). A guide to super-resolution fluorescence microscopy. J Cell Biol *190*, 165-175.
Schleif, R. (1992). DNA looping. Annu Rev Biochem *61*, 199-223.

Schmidt, R., Wurm, C.A., Jakobs, S., Engelhardt, J., Egner, A., and Hell, S.W. (2008). Spherical nanosized focal spot unravels the interior of cells. Nat Methods *5*, 539-544.
Shapiro, J.A., and von Sternberg, R. (2005). Why repetitive DNA is essential to genome function. Biol Rev Camb Philos Soc *80*, 227-250.
Silva, J., Mak, W., Zvetkova, I., Appanah, R., Nesterova, T.B., Webster, Z., Peters, A.H., Jenuwein, T., Otte, A.P., and Brockdorff, N. (2003). Establishment of histone h3 methylation on the inactive X chromosome requires transient recruitment of Eed-Enx1 polycomb group complexes. Dev Cell *4*, 481-495.
Smith, G.C., and Jackson, S.P. (1999). The DNA-dependent protein kinase. Genes Dev *13*, 916-934.
Sneeden, J.L., Grossi, S.M., Tappin, I., Hurwitz, J., and Heyer, W.D. (2013). Reconstitution of recombination-associated DNA synthesis with human proteins. Nucleic Acids Res *41*, 4913-4925.
Solovei, I., and Cremer, M. (2010). 3D-FISH on cultured cells combined with immunostaining. Methods Mol Biol *659*, 117-126.
Sporbert, A., Gahl, A., Ankerhold, R., Leonhardt, H., and Cardoso, M.C. (2002). DNA polymerase clamp shows little turnover at established replication sites but sequential de novo assembly at adjacent origin clusters. Mol Cell *10*, 1355-1365.
Sung, P., Krejci, L., Van Komen, S., and Sehorn, M.G. (2003). Rad51 recombinase and recombination mediators. J Biol Chem *278*, 42729-42732.
Tark-Dame, M., Jerabek, H., Manders, E.M., van der Wateren, I.M., Heermann, D.W., and van Driel, R. (2014). Depletion of the chromatin looping proteins CTCF and cohesin causes chromatin compaction: insight into chromatin folding by polymer modelling. PLoS Comput Biol *10*, e1003877.
Tark-Dame, M., van Driel, R., and Heermann, D.W. (2011). Chromatin folding--from biology to polymer models and back. J Cell Sci *124*, 839-845.
The UniProt, C. (2017). UniProt: the universal protein knowledgebase. Nucleic Acids Res *45*, D158-D169.
Tolhuis, B., Palstra, R.J., Splinter, E., Grosveld, F., and de Laat, W. (2002). Looping and interaction between hypersensitive sites in the active beta-globin locus. Mol Cell *10*, 1453-1465.
Trojer, P., and Reinberg, D. (2007). Facultative heterochromatin: is there a distinctive molecular signature? Mol Cell *28*, 1-13.
Tsouroula, K., Furst, A., Rogier, M., Heyer, V., Maglott-Roth, A., Ferrand, A., Reina-San-Martin, B., and Soutoglou, E. (2016). Temporal and Spatial Uncoupling of DNA Double Strand Break Repair Pathways within Mammalian Heterochromatin. Mol Cell *63*, 293-305.
Turinetto, V., and Giachino, C. (2015). Multiple facets of histone variant H2AX: a DNA double-strand-break marker with several biological functions. Nucleic Acids Res *43*, 2489-2498.
Valgardsdottir, R., Chiodi, I., Giordano, M., Rossi, A., Bazzini, S., Ghigna, C., Riva, S., and Biamonti, G. (2008). Transcription of Satellite III non-coding RNAs is a general stress response in human cells. Nucleic Acids Res *36*, 423-434.
Vissel, B., and Choo, K.H. (1989). Mouse major (gamma) satellite DNA is highly conserved and organized into extremely long tandem arrays: implications for recombination between nonhomologous chromosomes. Genomics *5*, 407-414.
Warburton, P.E., Hasson, D., Guillem, F., Lescale, C., Jin, X., and Abrusan, G. (2008). Analysis of the largest tandemly repeated DNA families in the human genome. BMC Genomics *9*, 533.
Waye, J.S., and Willard, H.F. (1986). Structure, Organization, and Sequence of Alpha Satellite DNA from Human Chromosome-17 - Evidence for Evolution by Unequal Crossing-over and an Ancestral Pentamer Repeat Shared with the Human X-Chromosome. Mol Cell Biol *6*, 3156-3165.
Weidtkamp-Peters, S., Rahn, H.P., Cardoso, M.C., and Hemmerich, P. (2006). Replication of centromeric heterochromatin in mouse fibroblasts takes place in early, middle, and late S phase. Histochem Cell Biol *125*, 91-102.
White, T.B., Morales, M.E., and Deininger, P.L. (2015). Alu elements and DNA double-strand break repair. Mob Genet Elements *5*, 81-85.
Wong, A.K., and Rattner, J.B. (1988). Sequence organization and cytological localization of the minor satellite of mouse. Nucleic Acids Res *16*, 11645-11661.

Woodfine, K., Fiegler, H., Beare, D.M., Collins, J.E., McCann, O.T., Young, B.D., Debernardi, S., Mott, R., Dunham, I., and Carter, N.P. (2004). Replication timing of the human genome. Hum Mol Genet *13*, 191-202.
Wu, J.C., and Manuelidis, L. (1980). Sequence definition and organization of a human repeated DNA. J Mol Biol *142*, 363-386.
Wu, R., Terry, A.V., Singh, P.B., and Gilbert, D.M. (2005). Differential subnuclear localization and replication timing of histone H3 lysine 9 methylation states. Mol Biol Cell *16*, 2872-2881.
Zink, D., Bornfleth, H., Visser, A., Cremer, C., and Cremer, T. (1999). Organization of early and late replicating DNA in human chromosome territories. Exp Cell Res *247*, 176-188.
Ziv, Y., Bielopolski, D., Galanty, Y., Lukas, C., Taya, Y., Schultz, D.C., Lukas, J., Bekker-Jensen, S., Bartek, J., and Shiloh, Y. (2006). Chromatin relaxation in response to DNA double-strand breaks is modulated by a novel ATM- and KAP-1 dependent pathway. Nat Cell Biol *8*, 870-876.

9. Annex

9.1. Statistical analysis and data representation

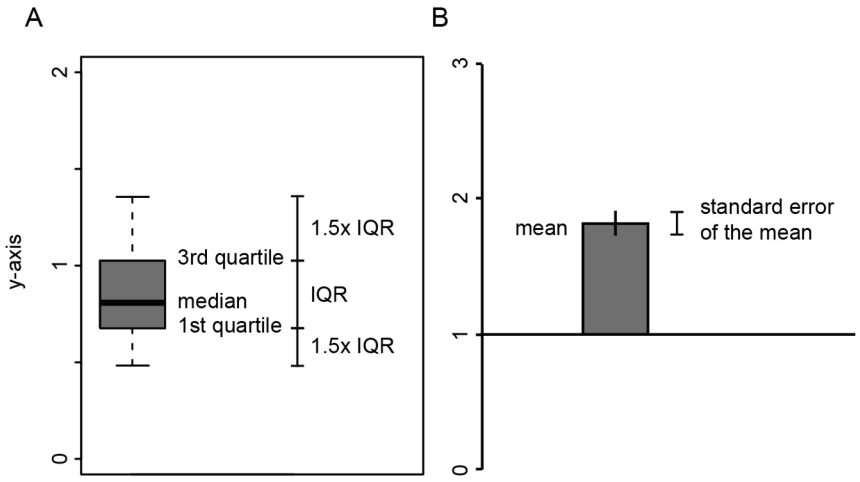

Figure S 1 Statistical analysis and data representation in boxplots (A) and barplots (B).

Numbers given in the text are median values unless otherwise indicated. Statistical analysis was performed with a Wilcoxon rank sum test using R ($p < 0.05$).

9.2. Supplementary material for Chapter 5

9.2.1. Summary of statistics

Table S 1: Repair kinetics by relative change in γH2AX intensity and nucleus area in HeLa, HeLa Kyoto and C2C12 cells after X-ray irradiation (Figure 6 and Figure 7).

relative change in γH2AX intensity

		unirr	2 Gy 0.5 h	2 Gy 3 h	2 Gy 24 h	5 Gy 0.5 h	5 Gy 3 h	5 Gy 24 h	10 Gy 0.5 h	10 Gy 3 h	10 Gy 24 h
HeLa	n	2015	790	760	1344	680	772	839	657	733	710
	median	1.00	1.41	1.43	1.05	2.69	1.97	1.10	4.26	3.10	1.80
	mean	1.02	1.45	1.46	1.09	2.74	2.04	1.18	4.39	3.22	1.82
	sd	0.23	0.29	0.40	0.50	0.69	0.58	0.42	1.20	1.07	0.61
	sem	0.01	0.01	0.01	0.01	0.03	0.02	0.01	0.05	0.04	0.02
HeLa Kyoto	n	1734	444	1278	1941	563	664	212	826	778	794
	median	1.00	1.39	1.03	1.19	1.85	1.46	0.78	2.89	2.32	1.29
	mean	1.00	1.41	1.07	1.20	1.89	1.46	0.83	2.94	2.35	1.39
	sd	0.19	0.24	0.29	0.23	0.31	0.36	0.23	0.58	0.49	0.40
	sem	0.00	0.01	0.01	0.01	0.01	0.01	0.02	0.02	0.02	0.01
C2C12	n	1018	246	436	724	243	299	218	394	569	236
	median	1.00	3.02	1.94	1.17	5.23	2.44	1.42	8.18	4.67	2.14
	mean	1.02	3.12	2.03	1.22	5.53	2.54	1.56	8.65	4.91	2.23
	sd	0.22	0.92	0.54	0.35	1.97	0.84	0.59	2.80	1.72	0.85
	sem	0.01	0.06	0.03	0.01	0.13	0.05	0.04	0.14	0.07	0.06

nucleus area in µm²

		unirr	2 Gy 0.5 h	2 Gy 3 h	2 Gy 24 h	5 Gy 0.5 h	5 Gy 3 h	5 Gy 24 h	10 Gy 0.5 h	10 Gy 3 h	10 Gy 24 h
HeLa	n	2015	790	760	1344	680	772	839	657	733	710
	median	153.15	133.55	144.09	178.99	130.25	124.05	236.57	121.09	127.81	277.76
	mean	158.35	137.88	146.83	189.42	133.85	128.81	234.54	126.64	132.50	279.58
	sd	46.81	39.70	38.71	66.68	39.12	37.00	85.62	37.90	38.01	68.99
	sem	1.04	1.41	1.40	1.82	1.50	1.33	2.96	1.48	1.40	2.59
HeLa Kyoto	n	1734	444	1278	1941	563	664	212	826	778	794
	median	153.65	112.52	116.50	186.57	105.68	119.92	130.22	108.18	132.47	263.89
	mean	156.59	119.23	120.82	194.04	113.19	127.24	148.96	112.89	136.84	271.74
	sd	43.81	39.27	31.60	58.46	35.44	38.38	66.87	30.51	38.35	73.46
	sem	1.05	1.86	0.88	1.33	1.49	1.49	4.59	1.06	1.37	2.61
C2C12	n	1018	246	436	724	243	299	218	394	569	236
	median	166.22	156.42	193.38	202.85	161.23	175.41	306.18	173.96	174.92	361.27
	mean	179.63	181.07	207.31	223.26	178.50	195.09	337.47	196.00	188.47	355.98
	sd	76.98	99.69	78.78	110.61	86.69	92.06	161.09	110.22	77.07	143.27
	sem	2.41	6.36	3.77	4.11	5.56	5.32	10.91	5.55	3.23	9.33

n = number of analyzed cells

Table S 2: Replicons and repair (nano)foci in HeLa, HeLa Kyoto and C2C12 cell images with 3D-SIM (Figure 8)

Number of replicons and repair (nano)foci per nucleus

		early	mid	late	2 Gy	5 Gy
HeLa	n	25	27	20	39	33
	median	4163	5492	3299.5	1260	2181
	mean	4245.88	5263.93	3457.75	1671.69	2298.30
	sd	1156.02	1319.74	1068.50	842.51	433.55
	sem	231.20	253.98	238.92	134.91	75.47
HeLa Kyoto	n	23	14	23	30	30
	median	5368	4879	4136	1701	2558
	mean	5668.52	4952.14	4113.96	1951.77	2763.40
	sd	977.78	757.76	912.81	729.14	874.30
	sem	203.88	202.52	190.33	133.12	159.62
C2C12	n	18	16	17	25	26
	median	4274.5	5801.5	4565	2443	3187
	mean	4127.33	5717.13	4555.88	2344.36	3017.19
	sd	645.39	630.43	746.90	706.11	627.86
	sem	152.12	157.61	181.15	141.22	123.13

n = number of analyzed cells

Table S 3: Control to define colocalization in super-resolution microscopy (Figure 10).

Number of red and green repair (nano)foci per nucleus

	2 Gy 488	2 Gy 594	5 Gy 488	5 Gy 594
n*	15	15	10	10
median	2076	2014	2971.5	3062.5
mean	2425.27	2430.67	2836.30	2866.50
sd	972.42	1063.52	669.76	707.30
sem	251.08	274.60	211.80	223.67

Max coloc distance

	2 Gy	5 Gy
n**	15974	12038
median	0.06	0.06
mean	0.06	0.06
sd	0.02	0.02
sem	0.00	0.00

ratio DNA content red/green repair (nano)foci

	2 Gy	5 Gy
n**	15974	12038
median	1.08	1.07
mean	1.32	1.36
sd	1.06	1.13
sem	0.01	0.01

ratio volume ratio red/green repair (nano)foci

	2 Gy	5 Gy
n**	15974	12038
median	1.08	1.08
mean	1.32	1.36
sd	1.06	1.13
sem	0.01	0.01

n* = number of analyzed cells

n** = number of analyzed red/green repair (nano)foci pairs

Table S 4: Percentage of the genome covered by replicons or repair (nano)foci

Percentage of genome covered by replicons/repair (nano)foci

		early	mid	late	2 Gy	5 Gy
HeLa	n	25	27	20	39	33
	median	3.48	4.26	2.71	1.63	3.10
	mean	3.59	4.44	2.64	1.84	3.29
	sd	0.94	1.71	0.66	0.67	0.81
	sem	0.19	0.33	0.15	0.11	0.14
HeLa Kyoto	n	23	14	23	30	30
	median	5.53	6.29	4.59	2.29	3.54
	mean	5.73	6.15	4.60	2.35	3.55
	sd	0.64	0.99	1.12	0.47	0.58
	sem	0.13	0.26	0.23	0.09	0.11
C2C12	n	18	16	17	25	26
	median	6.58	7.53	7.37	4.05	6.40
	mean	6.59	7.62	7.13	4.14	6.48
	sd	1.24	0.97	1.26	0.67	0.82
	sem	0.29	0.24	0.31	0.13	0.16

n = number of analyzed cells

Table S 5: Percentage of replicons colocalizing with repair (nano)foci (Figure 11).

% replicons with repair (nano)foci within 0.1 µm distance per nucleus

		2 Gy early	2 Gy mid	2 Gy late	5 Gy early	5 Gy mid	5 Gy late
HeLa	n	18	11	10	7	16	10
	median	0.92	1.10	0.83	1.49	1.33	1.47
	mean	0.97	1.19	0.88	1.33	1.47	1.45
	sd	0.33	0.39	0.23	0.28	0.41	0.17
	sem	0.08	0.12	0.07	0.11	0.10	0.05
HeLa Kyoto	n	11	6	13	12	8	10
	median	1.85	1.27	1.52	2.41	2.19	2.30
	mean	2.03	1.39	1.54	2.41	2.11	2.25
	sd	0.98	0.33	0.33	0.24	0.32	0.38
	sem	0.30	0.13	0.09	0.07	0.11	0.12
C2C12	n	8	10	7	10	6	10
	median	1.61	1.94	1.94	2.79	2.32	1.93
	mean	1.71	1.86	1.94	3.06	2.27	1.95
	sd	0.52	0.25	0.13	1.00	0.26	0.34
	sem	0.18	0.08	0.05	0.32	0.11	0.11

n= number of analyzed cells

Table S 6: DNA content of replicons and repair (nano)foci (Figure 12).

DNA content of replicons and repair (nano)foci in kbp

		early	mid	late	2 Gy	5 Gy
HeLa	n*	106147	142126	69155	65196	75844
	median	33501.08	38182.49	27481.47	71189.32	91233.01
	mean	85525.48	85396.84	77156.99	111433.59	144803.30
	sd	117140.27	113339.18	113984.05	137669.99	186564.06
	sem	359.54	300.64	433.44	539.17	677.43
HeLa Kyoto	n*	130376	69330	94621	58553	82902
	median	48229.08	55392.02	39354.13	83265.18	85788.33
	mean	98016.45	120507.93	108555.36	116954.39	124513.35
	sd	121532.70	161651.48	159974.31	129548.87	148132.61
	sem	336.58	613.93	520.06	535.38	514.48
C2C12	n*	74292	91474	77450	58609	78447
	median	105957.30	85935.59	61627.41	104569.25	118563.18
	mean	181972.91	151893.92	178478.12	201212.47	244664.25
	sd	225574.83	195060.93	367821.29	323422.66	383781.28
	sem	827.60	644.94	1321.68	1335.94	1370.24

ratio DNA content replicon/repair (nano)focus

		2 Gy early	2 Gy mid	2 Gy late	2 Gy Max coloc	5 Gy Max coloc	5 Gy early	5 Gy mid	5 Gy late
HeLa	n**	763	651	293	15974	12038	358	1352	541
	median	0.44	0.47	0.40	1.08	1.07	0.37	0.56	0.37
	mean	1.77	2.08	1.91	1.32	1.36	1.43	1.65	1.74
	sd	3.58	4.35	4.93	1.06	1.13	2.87	3.67	3.96
	sem	0.13	0.17	0.29	0.01	0.01	0.15	0.10	0.17
HeLa Kyoto	n**	1231	438	867	15974	12038	1647	807	880
	median	1.14	1.20	1.05	1.08	1.07	0.92	1.17	0.81
	mean	2.79	2.74	3.19	1.32	1.36	2.38	3.09	2.35
	sd	4.48	3.97	5.34	1.06	1.13	3.73	4.73	4.20
	sem	0.13	0.19	0.18	0.01	0.01	0.09	0.17	0.14
C2C12	n**	542	1062	651	15974	12038	1309	788	847
	median	0.67	0.95	0.63	1.08	1.07	1.02	0.60	0.42
	mean	2.30	2.52	2.34	1.32	1.36	2.57	2.21	2.89
	sd	4.03	4.38	4.32	1.06	1.13	4.03	3.89	10.14
	sem	0.17	0.13	0.17	0.01	0.01	0.11	0.14	0.35

n* = number of analyzed replicons or repair (nano)foci

n** = number of analyzed replicon/repair (nano)foci pairs

9.2.2. Volumes of replicons and repair (nano)foci

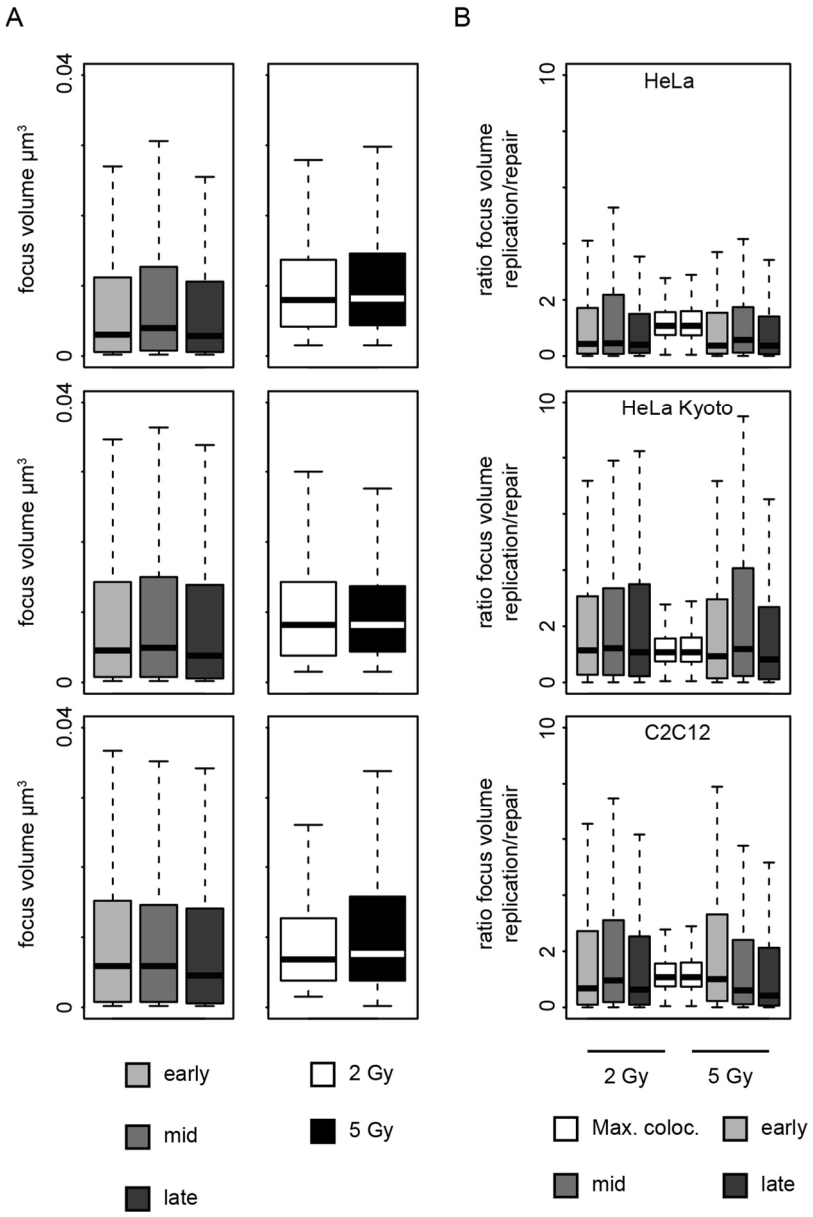

Figure S 2: Volume of replicons and repair (nano)foci. A) Volume of replicons and repair (nano)foci in HeLa, HeLa Kyoto and C2C12 cells. Significant differences in DNA content between replicons from different S-phase stages and between repair (nano)foci from different X-ray doses were detected ($p < 0.05$) due to extremely high n numbers ($n > 58500$). B) Ratio of volumes of replicons colocalizing with a repair (nano)focus in comparison to the control shown in Figure 10.

Table S 7: Volume of replicons and repair (nano)foci (Figure S 2)

Volume of replicons and repair (nano)foci in 10^{-3} µm^3

		early	mid	late	2 Gy	5 Gy
HeLa	n*	106147	142126	69155	65196	75844
	median	3.04	3.99	2.85	7.99	8.18
	mean	7.62	8.34	7.54	11.71	12.72
	sd	10.20	10.51	10.65	14.29	15.67
	sem	0.03	0.03	0.04	0.06	0.06
HeLa Kyoto	n*	130376	69330	94621	58553	82902
	median	4.56	4.94	3.80	8.18	8.18
	mean	8.89	9.84	9.32	10.92	11.22
	sd	10.70	12.63	12.99	11.44	12.60
	sem	0.03	0.05	0.04	0.05	0.04
C2C12	n*	74292	91474	77450	58609	78447
	median	5.89	5.89	4.56	6.84	7.61
	mean	9.71	9.73	9.96	12.16	14.71
	sd	11.44	11.57	14.69	17.27	21.32
	sem	0.04	0.04	0.05	0.07	0.08

ratio volume replicon/repair (nano)focus

		2 Gy early	2 Gy mid	2 Gy late	2 Gy Max coloc	5 Gy Max coloc	5 Gy early	5 Gy mid	5 Gy late
HeLa	n**	763	651	293	15974	12038	358	1352	541
	median	0.43	0.45	0.40	1.08	1.08	0.37	0.57	0.37
	mean	1.77	2.10	1.86	1.32	1.36	1.43	1.67	1.73
	sd	3.59	4.38	4.55	1.06	1.13	2.84	3.69	3.96
	sem	0.13	0.17	0.27	0.01	0.01	0.15	0.10	0.17
HeLa Kyoto	n**	1231	438	867	15974	12038	1647	807	880
	median	1.14	1.22	1.07	1.08	1.08	0.93	1.19	0.82
	mean	2.79	2.76	3.27	1.32	1.36	2.40	3.13	2.36
	sd	4.41	3.93	5.59	1.06	1.13	3.76	4.80	4.30
	sem	0.13	0.19	0.19	0.01	0.01	0.09	0.17	0.14
C2C12	n**	542	1062	651	15974	12038	1309	788	847
	median	0.68	0.96	0.63	1.08	1.08	1.00	0.61	0.42
	mean	2.32	2.55	2.37	1.32	1.36	2.60	2.21	2.85
	sd	4.23	4.36	4.42	1.06	1.13	3.99	3.95	8.70
	sem	0.18	0.13	0.17	0.01	0.01	0.11	0.14	0.30

n* = number of analyzed replicons or repair (nano)foci

n** = number of analyzed replicon/repair (nano)foci pairs

List of abbreviations

3D-SIM	3D structured illumination microscopy
3C	chromosome conformation capture
ATM	ataxia telangiectasia mutated
bp	base pairs
BrdU	5-bromo-2´-deoxyuridine
BSA	bovine serum albumin
CTCF	CCCTC-binding factor
CtIP	C-terminal binding protein-interacting protein
CypA	Cyclophilin A
DAPI	4´,6-diamidino-2-phenylindole
DNA-PK	DNA-dependent protein kinase
DSB	double strand break
EdU	5-ethynyl-2´-deoxyuridine
EDTA	ethylenediaminetetraacetic acid
FISH	fluorescence in situ hybridization
gDNA	genomic DNA
γH2AX	histone H2AX phosphorylated at Ser139
HIV-1	human immunodeficiency virus type 1
HR	homologous recombination
IQR	inter quartile range
kbp	kilo base pairs
LCR	locus control region
LINE	long interspersed nuclear element
LTR	long terminal repeat
max	maximum
MCM	mini chromosome maintenance complex
Mbp	Mega base pairs
min	minimum
MRN	Mre11/Rad50/Xrs2 complex
NHEJ	non-homologous end joining
PBS	phosphate buffered saline
PCR	polymerase chain reaction
PCNA	proliferating cell nuclear antigen
pol α/δ/ε	DNA polymerase α/δ/ε
RPA	replication protein A
sd	standard deviation
sem	standard error of the mean
SINE	short interspersed nuclear element
SSC	saline-sodium citrate buffer
STED	stimulated emission depletion (microscopy)
TAD	topologically associated domain
TRIM5-α	tripartite motif-containing protein 5 α
TUNEL	terminal desoxynucleotidyl transferase mediated dUTP nick end labeling
Xa	active X chromosome
Xi	inactive X chromosome
XRCC4	X-ray repair cross complementing 4
XLF	XRCC4 like factor
unirr	unirradiated

List of contributions

Correlating DNA replication & repair structures as elementary units of chromatin

Annina Scholl planned, performed*, analyzed the experiments, prepared the figures and wrote the text
Andreas Maiser did 3D SIM imaging
Cristina Cardoso conceived the project

*Repair kinetics of HeLa, HeLa Kyoto and C2C12 cells (Figure 6 and Figure 7)
Annina Scholl planned the experiment, imaged and analyzed and prepared the figures
Annina Scholl and Diana Imblan performed the experiment

DNA repair kinetics and replication timing of repetitive elements

Annina Scholl planned, performed, analyzed the experiments, prepared the figures and wrote the text
Cristina Cardoso and Francesco Natale conceived the project

List of figures

List of tables

Acknowledgements - Danksagung

First of all, I would like to thank Prof. Dr. M. Cristina Cardoso for giving me the great opportunity of working in her lab and for making the thesis possible, for always having an open door, her patience, providing great input and help. I am truly grateful for my time in her group and all the things I have learned.

I would also like to thank Prof. Dr. Bodo Laube for being the second advisor and giving helpful feedback. I´m grateful to the GRK 1657 and the DFG for funding my work and to the GRK members for all the discussions during retreats and meetings.

Thanks a million to Alexander Rapp and Francesco Natale for all their input, help, for great answers to stupid questions and for troubleshooting experiments, machines and analysis even if they did not have the time. Thank you also to Stephan who taught me how to use R without becoming desperate or angry upon error messages, who taught me how to write codes and who always has my back.

Special thanks goes to Andreas Maiser from the LMU in Munich for imaging my millions of samples with 3D-SIM. Without him the chromatin organization project would not have been possible.

I would also like to thank all the present and past members of the Cardoso lab, especially the replication group, for the great time and support, Anne Lehmkuhl for taking care of my cells, for always having an open ear and being the heart of our lab, to Diana for assisting me with some of my experiments and to my bench neighbors Cathia and Steffi for listening, assisting, giving feedback and more…

Thank you very much also to the people proofreading and revising my thesis: Alex, Cathia, Marius and Stephan.

And last but not least I would like to say thank you to my family. Vielen Dank für all eure Unterstützung während der Schulzeit, meinem Studium und während der Doktorarbeit, für euer Verständnis, wenn ich beschäftigt war und dafür, dass ihr mich in schlechten Zeiten wieder aufgebaut und euch in guten Zeiten mit mir gefreut habt. Ohne euch wäre ich nicht so weit gekommen. Vielen Dank!

Curriculum vitae

PERSONAL INFORMATION

Name:	Annina Scholl
Date of birth:	September 28, 1989
Place of birth:	Hardheim
Address:	TU Darmstadt Department Biology Cell Biology and Epigenetics Schnittspahnstraße 10 64287 Darmstadt, Germany

EDUCATION

since 08/2014	**PhD thesis** at TU Darmstadt “Interplay of DNA replication, repair and chromatin under radiation stress” in the group "Cell Biology and Epigenetics" of Prof. M. C. Cardoso
2012-2014	**Master of Science (M.Sc.) - Technical Biology** at TU Darmstadt grade: very good
02 – 08/2014	Master thesis (external) in marine science: "Photoperiodic time-measurement in Antarctic krill" at the Alfred Wegener Institute Helmholtz Centre for Polar and Marine research in the group “Antarctic krill” of Prof. Dr. B. Meyer, under supervision of Dr. M. Teschke
2009-2012	**Bachelor of Science (B.Sc.) - Biology** at TU Darmstadt grade: good
05. – 08/2012	Bachelor thesis in microbiology: "Construction of a gfp-based reporter-gene-system in *Halobacterium salinarum*" in the group “Microbiology and Archaea” of Prof. F. Pfeifer, under supervision of Dr. S. Fröls
2009	**Abitur** at Gymnasium Michelstadt grade: good majors: chemistry, mathematics

TEACHING/RESEARCH INTERNSHIPS

2011	Supervision of bachelor students during practical courses
2012	Supervision of bachelor students during advanced practical courses
2014-2016	Project planning and supervision of bachelor and master students during advanced practical courses
2013-2014	10 weeks internship in group “Antarctic krill” of Prof. Dr. B. Meyer at the Alfred Wegener Institute, Helmholtz Centre for Polar and Marine research
2012	6 weeks internship in group “Antarctic krill” of Prof. Dr. B. Meyer at the Alfred Wegener Institute, Helmholtz Centre for Polar and Marine research

CONFERENCE CONTRIBUTIONS

Poster at “Epigenetics & Chromatin”, September 13-17, 2016, Cold Spring Harbor Laboratories, USA
“Correlating DNA replication and repair structures as elementary units of chromatin organization”

PUBLICATIONS

in press “Identification of the elementary structural units of the DNA damage response”

Francesco Natale*, Alexander Rapp*, Wei Yu, Andreas Maiser, Hartmann Harz, Annina Scholl, Stephan Grulich, Tobias Anton, David Hörl, Wei Chen, Marco Durante, Gisela Taucher-Scholz, Heinrich Leonhardt, and M. Cristina Cardoso
*equally contributing authors
Nature Communications